Gap Size Effect on Low Reynolds Number Wind Tunnel Experiments.

Nilanjan Saha

Thesis submitted to the Faculty of Virginia Polytechnic Institute and State University in partial fulfillment of the requirements for the degree of

Master of Science
In
Aerospace Engineering

Dr. James F. Marchman, Chair
Dr. William J. Devenport
Dr. William H. Mason

December 3rd , 1999
Blacksburg, Virginia

Gap Size Effect on Low Reynolds Number Wind Tunnel Experiments.

Nilanjan Saha (Abstract)

A system was designed to measure the effect of gap size on semi-span low Reynolds number wind tunnel experiments. The lift forces on NACA 1412, NACA 2412 and NACA 4412 half wings were measured using a strain gauge balance at chord Reynolds numbers of 100,000 and 200,000 and three different gap sizes including sealed gap. Pressure distributions on both airfoil top and bottom surfaces in the chord-wise direction near the gap were recorded for these airfoils. Also recorded was the span wise pressure distribution on both the airfoil surfaces at the quarter chord section. The results revealed that the presence of the gap, however small, affects the measurements. These effects were mainly observed in drop of lift and change in zero lift angle of attack and change in stall angle for the airfoil. The size of the gap is not linearly related to these changes, which also depend on the camber of the airfoil. These changes occur due to the flow through the gap from the lower surface to the upper surface of the model. The wing/end plate gap effect reduces along the span but is not fully restricted to the base of the model and the model behaves more like a full three-dimensional wing than a semi-span model. This study was made possible with the support of Department of Aerospace and Ocean Engineering, Virginia Polytechnic Institute and State University under the supervision of Dr. James Marchman.

Acknowledgements

First and foremost I would like to take this opportunity to thank my advisor Dr. James Marchman for his valuable advice, guidance, patience and for giving me this opportunity. I am honored to be associated with him on both academic and non-academic areas throughout my stay in Blacksburg. I would like to mention my special thanks to my parents and my brother and sister-in-law for their continuous encouragement and support in my life. I am forever grateful to them for that.

I would like to thank Jacob George for his help in scanivalve pressure measurement system, Troy Jones for helping me by developing the data acquisition system for the experiment and Matt Orr for the construction of the models. My special thanks for Mr. Greg Bandy who worked hand in hand with me in the tunnel. I would also like to thank Greg Dudding, Bruce Stanger, Kent Morris and Gary Stafford in the Aerospace shop who have always been exceptionally helpful whenever I faced any problem in developing the experimental set up.

My special thanks goes to Dr. William Devenport and Dr. William Mason for agreeing to be in my Graduate committee in spite of their busy schedules.

I am grateful to my roommate Amit, without whose help I would be still taking data. Last but no the least to my friends Vijay and Pankaj for just being there in my difficult times.

Nilanjan

Table of content

List of Tables

List of Figures

Nomenclatures

α	Angle of attack
C	Wing chord
C_L	Lift Coefficient
$C_{L\max}$	Maximum lift coefficient

C_P	Coefficient of pressure
C_{Di}	Induced drag coefficient
FS	Full scale
P_{ref}	Reference pressure
P_{meas}	Pressure measured
Re	Reynolds number
T	Flow temperature
"	Inch
’	Foot

Chapter 1

Introduction

1.1 Perspective of the Present Study

Low Reynolds number wind tunnel experiments have been conducted for nearly a century. The history of such experiments dates back to the era of the Wright brothers. Early tunnels had poor acoustic conditions or high turbulence levels [(1)]. This made it difficult to conduct accurate experiments at the low Reynolds numbers ranging from 50,000 to 500,000. During the 1930s designers started conducting serious experiments on various phenomena which were being ignored previously as erroneous data or were overlooked completely [(1)].

The use of semi-span models has been one of the popular methods for testing airfoil aerodynamics. In this technique the model to be tested is generally mounted through a hole on the tunnel wall or an endplate as shown in figure 1.1 (pg. 59). The other end of the model is left free in the airflow. This is termed semi-span testing because all three-dimensional effects due to the finite span of the model are assumed to be taking place only at and near the free end. The other end, which is attached to the wall of the tunnel or an end plate is expected to behave similarly to a two dimensional model. However in any such experiment, which involves measurement of force, a small gap always exists

between the airfoil and the wind tunnel wall so that the forces acting on the airfoils, are not transferred to the tunnel wall degrading the reliability of the measurement. This gap is essential because any physical contact between the model and the end plate may transfer forces on the model and it would be extremely difficult to isolate and measure the forces acting only on the model. It can be noted that our interest lies only in the forces acting on the model. So it is necessary to maintain a small gap between the model and the wind tunnel side wall or the end plate. But presently no particular standard exists to size the gap, which is almost inevitable in semi-span tests even though such tests have been conducted for many years. This could cause serious discrepancies because as soon as a gap is introduced the model ceases to behave as a two-dimensional airfoil and some three-dimensional effects such as loss of lift creep in, as shown in the present research. There has previously been little controversy over the acceptable size of the gap to be used in semi-span tests. This problem will be discussed in more detail later in this chapter.

Another method of testing wing aerodynamics is with a full span model. In this arrangement the model is held at mid span as shown in figure 1.2 and mounted on a balance by some attachment. In this method both ends of the model are free and the tests give full three-dimensional results. The advantage of this method over the semi-span method is that one doesn’t need to consider the effect of gap on the results in order to estimate the characteristics of a full three-dimensional wing. However in this method the strut used to attach the wing sits in the flow and may affect the flow. To minimize this

effect the strut is usually covered with a streamlined shroud. But still one needs to evaluate the effect of strut interference. It can alter the zero lift angle of attack and also change the local flow angularity and can interfere with the wing boundary layer [(1)].

Even though at conventional Reynolds numbers there has been success at using the semi-span testing to examine 3-D wing behavior there have been contradictions in test results from apparently carefully conducted low Reynolds number studies by competent researchers causing much frustration [(2,3,4)]. An examination of previously published results to examine model-mounting influences indicates the complexity and uncertainty associated with low Reynolds number aerodynamic testing [(1)].

Figure 1.3 illustrates part of the problem of determining the accuracy of data for low Reynolds number wind tunnel tests [(1)]. Both sets of data [(2)] in this figure were taken for the same two-dimensional airfoil and using the same apparatus and at the same Reynolds number. Apparently there is no feasible explanation for the difference of results. It only points to the fact that it is extremely difficult to ascertain the accuracy of test data at low Reynolds numbers. Figure 1.4 shows the three dimensional lift coefficient data measured for the Wortmann FX63-137 airfoil at the Virginia Tech Stability Tunnel at Blacksburg and Notre Dame University in Indiana. The only noted difference in the tests was the level of turbulence apart from wing aspect ratio in some cases. But the data was corrected for the aspect ratio using standard correction methods and there still exist significant differences. Although it might lead one to conclude the free stream turbulence is

somehow responsible for the shift in lift curve it does not sound logical because an increase in turbulence would increase the $C_{L\,max}$ which is opposite to the effect seen as noted by Marchman [1]. The Virginia Tech Stability Tunnel has a lower turbulence level than the tunnel at Notre Dame, yet it produced higher C_{Lmax}. Upon investigation it was found that the difference in test data was primarily caused by different model-mounting techniques i.e. the use of full span tests versus semi-span tests and due to the size of gap used in semi-span tests.

Most reported data for the low Reynolds number aerodynamics of the Wortmann FX63-137 airfoil are for two-dimensional tests where the model was mounted between two end plates. However there is a difference in even how the plates were mounted. Mueller [2] used a small gap between the plates and the model to ensure forces are not transferred form the end plates to the model or vice versa although the size of the gap was not mentioned.

All finite wing tests by Marchman were conducted using full three dimensional models mounted on a single strut where as Render [4] used the traditional approach of an end plate attached to the semi-span models. In spite of all the precautions taken and the corrections made for the blockage and flow angularity and the induced incidence and the buoyancy effects on the experimental data there still existed a few discrepancies in the obtained data at different facilities for the same airfoil section.

Experiments were conducted on the Wortman FX 63-137airfoil at low Reynolds numbers (70,000-300,000) at Notre Dame by Bastedo and Mueller [2] and at VPI by Marchman and his associates [3] and at Cranfield by Render [4]. A comparison of data for the three dimensional test results was made by Marchman and Sumantran [5] and is shown in figures 1.5 to 1.8 along with the comparison of tunnel flow environments which is shown in table 1.1. These revealed some apparent discrepancies. Tests performed at VPI using an end plate, semi-span model technique, similar to that used in Notre Dame, showed that the gap between the model and the endplate could reduce lift causing a shift in the lift curve [5]. Data obtained at Notre Dame shows a shift in zero lift angle of attack and the lift curve shifts towards left (figure 1.6 and 1.7) with increasing Reynolds numbers. This is particularly interesting because a change in Reynolds number doesn't have any known effect on the linear portion of the lift curve. Renders's data is in good agreement with the VPI data for zero lift angle of attack but shows significantly higher lift curve slope. When the gap was open it was found that the VPI end plate measurements produced similar results to those from Notre Dame with an open gap for a model of effective aspect ratio of 4.

Marchman [1] noted that "Researchers are often at odds with other researchers regarding test data accuracy, data acquisition techniques, data measurement reliability, model accuracy, tunnel correction etc." Acoustic and tunnel turbulence level present in the tunnel may have caused some effects on the results. The reported turbulence level at VPI

was 0.018% whereas at Cranfield it was 0.1% [5]. There is a large difference in the stall hysteresis behavior between VPI and Notre Dame data. The low Reynolds number stall hysteresis loop is known to be very sensitive to the tunnel environment and acoustics. Level of surface smoothness of the model also alters the size of the stall hysteresis loop. Sumantran, Sun and Marchman [6] have shown that increasing free stream turbulence can decrease the size of the hysteresis loop as can exposing the model to sound of a particular frequencies. When the model was exposed to a noise of low frequency (1970 Hz) it abruptly changes to a gradual trailing edge stall form a leading edge type stall and also greatly reduce the size of the hysteresis loop. This type of stall with acoustic disturbance is similar to stall observed by Mueller at the same Reynolds numbers for a 2-D airfoil (figure 4, Ref 2). The turbulence and acoustic characteristics of a wind tunnel certainly affect low Reynolds number wind tunnel data and further investigation needs to be carried out in this area [5].

The present study establishes that some test result discrepancies may very well be caused by different gap test techniques such as a different size of gaps used for semi-span models. It is quite possible that the character of stall and size of the hysteresis loop are also influenced by degree of sealing of a model-plate gap where end mounted test procedures were used [5]. In the present research studies have been made to investigate this phenomenon which has not been investigated in great detail in the past.

1.2 Gap Effects at Low Reynolds Number

With semi-span tests using a gap at the base of the wing, no matter how small the gap is, there is always a possibility of air moving towards the upper surface causing a leakage effect as shown in fig 1.9. The sectional view of the airfoil and end plate is shown in figure 1.10. This flow from the lower surface to the upper surface through the gap helps the flow to remain attached to the upper surface at high angle of attack. This can change the stalling angle for the airfoil being tested and can shift the lift curve slope. For a small aspect ratio wing the result obtained from semi-span tests can vary significantly from full span testing because the gap size may not be of completely negligible magnitude to the span of the wing.

Pope [8] commented that gaps could significantly affect the result if its not kept small enough. He says that a gap will decrease effective aspect ratio and can give errors as high as 47% while measuring induced drag coefficient (C_{di}). According to Pope, viscous effects will reduce this effect but the viscous effect is not yet fully understood. He also noted that if the clearance is held to less than 0.005 span its effect will probably be negligible while few others believe gaps less than 0.02 span is acceptable [8]. However this area has not yet been explored fully and there is no experimental data to support this theory.

Previous studies have given a little insight into the flow structure present in such experiments as shown in figure 1.9. This flow through the gap can be dependent on many different phenomena such as the extent of the boundary layer generated by the end plate that was used to simulate the tunnel wall or the camber of the airfoil or angle of attack on the model or the flow Reynolds number. But few studies have been conducted in the past to investigate this phenomenon. Marchman and associates [1,3,5,6,9, 10] at VPI have made some studies regarding the effect of gap on semi-span tests.

Research conducted by Marchman et al [9] was to evaluate the effect of the end plate gap on the force data obtained on a semi-span wing model of aspect ratio 4. Tests were conducted on Wortmann FX63-137 airfoil at Reynolds numbers of 100,000 to 200,000 and the gap size was varied between 0.1mm and 0.2mm. He observed a definitive loss of lift in the presence of the wing/end plate gap causing a shift of zero lift angle of attack. The shift was of the same order of magnitude as the difference observed in the reported data for the same airfoil measured using a strut mounted full 3-D wing and there was no effect of Reynolds number on zero lift angle of attack. He commented [9] that there was an aspect ratio effect in presence of the gap i.e. the model behaves more like a finite aspect ratio wing in the presence of the gap.

Symmetrical aerofoil sections NACA 0012, 0015 and 0021 were also tested by Marchman et al [10]. These sections are commonly used on helicopter rotor blades, horizontal stabilizers, canards and submarine bow and stern planes. He observed that

unlike the Wortmann airfoil, there is no shift in the zero lift angle of attack with gap size for all these airfoil. It is to be noted that none of these airfoils are cambered. He concluded that this phenomenon is unique to the cambered airfoils. However the gap size influences the slope of the lift curve even for the symmetrical airfoil. Sealing the gap and variation in the gap size also influences the size and extent of stall hysteresis. It can be concluded from his observation that the "effective" aspect ratio of the wing and resulting lift curve slope decrease as gap size increases. All previous studies conducted by Marchman and associates [1,3,5,6,9,10] on gap size effect on semi-span low Reynolds number tests have shown that the test results always depend on the gap that exists between the wall of the tunnel and the model. He observed [9] that there is definitive loss of lift due to the presence of the gap and the zero lift angle of attack shifts with increasing gap sizes. Even with a very narrow gap the effect is evident and the flow through the gap changes the separation pattern near the stalling angle of attack. Mueller [2] and more recently Marchman [6] have examined the effect of stall hysteresis behavior although it can be quite difficult to measure the effect of this behavior accurately due to difference of turbulence level in the tunnel and the acoustic properties.

1.3 Objective of the Present Study

Low Reynolds number wind tunnel experiments have been conducted for almost a century. But even with a hundred years of experience in wind tunnel experiments some times the data were found to be not in agreement with the data taken for the same airfoil

at a different facility [2,3,4]. This disagreement of data was mostly attributed to the different tunnel environment and test techniques. Sidewall boundary layer also might have contributed to the difference in data obtained in different test condition and is discussed in section 2.6. But not much thought was given to investigate the effect of gaps on the results when semi-span testing methods were employed. Discussion in the present research mainly concentrates on the effect of gap size on semi-span wind tunnel experiments at low Reynolds number. There is a need to come up with a standard test condition with respect to gap sizes based on tunnel dimension and the aspect ratio of the wing and Reynolds number. This requires a series of wind tunnel experiments, on a variety of airfoils, with a wide range Reynolds numbers and gap sizes.

There are plans for several types of aircraft that will be operating in the range of 50,000 to 500,000 range of wing chord Reynolds number [6]. The effect of a gap can cause serious deviation of data obtained at different facilities. The implication of this effect and interpretation of wind tunnel test results in this range need to be examined [5]. Follow up study is required to support and further investigate the phenomenon and to generate a data set without any discrepancies due to this previously unexplored or very little explored event. The work done in this field is mainly by Marchman et al. He has investigated this phenomenon in the Stability Wind Tunnel at VPI and that concluded [5] the arrangement for mounting the models inside the tunnel was not responsible for the discrepancy of result and it was primarily due to the effect of the gap.

While previous studies have established the existence of a gap effect, there never has been any attempt made before to measure the change in pressure distribution with gap sizes. The present study is the first effort to investigate how the pressure distribution changes with the gap size. This documentation of change in pressure distribution corroborates the observation made on force data and also limited study previously done in the field of force measurements. It's very important to carry out more studies on pressure distribution patterns on a wide range of airfoil and Reynolds numbers. Tests have to be conducted in these two fields to come up with a standard test condition.

The main objective of this study is to document the effect of wing/endplate gap in low Reynolds number semi-span tests for cambered airfoils and to analyze the origin of such effects so that a standard test condition can be prescribed, if possible. Another objective of this study is to investigate whether this effect is dependent on airfoil camber. One of the most important objectives is to record the pressure distribution at various angle of attacks for different gap sizes and to understand how the pressure distribution changes with wing/endplate gap altering the lift generated by the wing.

1.4 Tests Conducted

Wind tunnel tests were conducted in VPI Stability Tunnel to investigate this disagreement of data and to make a qualitative as well as quantitative analysis of the

effect of gap sizes on wind tunnel measurements including the effect of sealed gap. A large rectangular end plate was used as the wall to simulate the effect of gap on the wings of three different cross sections. Both lift coffecients (C_L) and pressure distributions (C_p) were measured on NACA 1412, NACA 2412 and NACA 4412 wing sections. Lift coefficient measurements were made to investigate the behavior of lift curve slope and its shift and change in stalling angle. Lift coefficient (C_L) data was taken over a range of angle of attack (α) from -5^0 until stall with 1^0 interval for all three airfoils using three different gap sizes and at two different Reynolds numbers of 100,000 and 200,000. The three wing/plate gaps used were 0.000", 0.006" and 0.024" which were 0.00%, 0.05% and 0.020% of the span of the model. However in some cases measurement data was taken for gaps 0.080" and 0.099" which were 0.67% and 0.825% of the span and some measurements were made at Reynolds numbers 300,000, 400,000 and 500,000.

The pressure measurements were made on the same airfoil cross sections and at Reynolds numbers of 100,000 and 200,000 between angles 0^0 to 20^0 with an interval of 5^0. Pressure distributions were measured on both top and bottom surfaces along the chord near the tip of wing. Span-wise distributions were also measured at the wing quarter chord for both the surfaces. Pressure measurement was carried out in order to achieve a better insight into the flow pattern due to the presence of the gap. The data obtained from both force and pressure measurements are in very good agreement regarding the effect of gap size on the wind tunnel experiments.

Chapter 2

Apparatus and Instrumentation

This chapter describes the facility used for the measurements, which include the wind tunnel, instrumentation and data acquisition techniques, models used, the model support and uncertainty analysis. The Virginia Tech Stability Wind Tunnel was used for both force and pressure measurements.

2.1 The Wind Tunnel

The VPI Stability Wind Tunnel is a closed circuit, single return, subsonic wind tunnel with a large closed rectangular test section. The test section dimensions are 6ft x 6ft x 25ft with a nozzle contraction ratio of 10:1. The large size of the test section minimizes the blockage effect, induced incidence and buoyancy effects due to the presence of the model. The buoyancy correction for a similar test set up was calculated by Marchman et al [5] and was found to be negligible. The schematic diagram of the tunnel top view is shown in figure 2.1. One of the test section side walls is made of transparent Plexiglas so that the operator can monitor the model visually from the control room. The flow is driven by a 14-ft diameter propeller. The tunnel can produce a steady flow from 20 ft/s to 240 ft/s in the test section. The large cross section of the wind tunnel makes the flow nearly parallel in the middle of the section. The flow angle is around 2^0 near the walls due

to the development of the boundary layer. The turbulence level is measured to be less than 0.1% [13]. The reported turbulence level was obtained after filtering frequencies bellow 0.1Hz.

The control room is located adjacent to the test section. The whole facility, which includes all controls, model support and instrumentation, surrounds the test section and is airtight. It is accessible only through two air lock doors and only one of them is opened at a time to enter the facility during tests. This ensures a steady static pressure during the test and also allows easy access of instrumentation and model without disturbing the pressure.

2.2 Models and Test Set Up

Six wing models were made for this experiment, three each for force and pressure distribution measurements. These model cross section were NACA 1412, NACA 2412, and NACA 4412 as shown in figure 2.2. All models were of the same aspect ratio of 2 and external dimension of 6" in chord and 12" in span as shown in figure 2.3. Each had a circular metal bar attached to it at the quarter chord section that held the model with the strut during the experiment. The model construction and test set up for force and pressure measurements are discussed in detail in the next section.

2.3 Force Measurement Models

2.3.1 Model Construction

The model for force measurements was made of a foam core with thin plywood skin on the outside. Hard cardboard was cut out for each airfoil cross section of 6" chord length and used as templates for the wing. Two templates were made for each wing. These templates were attached on two ends of a 2" thick and 12" long piece of foam. The foam was then cut out with a thin long electrically heated steel wire along the template on both sides as shown in figure 2.4. The templates were then removed and a thin plywood skin wrapping the foam core was glued to the foam using Dura-Cote epoxy resin to achieve the desired strength. For the skin to get the exact shape of the airfoil and to remove the possibility of any air bubble trapped between the skin and the foam it was kept under vacuum for 24 hours after the glue was applied. A circular hole was then drilled to the mid-span on the foam core at quarter chord. A circular metal spar was inserted through the hole and was attached to the model with the help of epoxy resin. This spar was used to attach the wing to the tunnel force balance strut. The model was then given a coat of primer and finally two coats of spray paint to achieve better surface smoothness. The model surface smoothness was about 0.001".

2.3.2 Model Support

The model support system for force tests is shown in figure 2.5. A strut (SR-1) was mounted at the center of the test section, which is at a distance of 3 ft from the side walls. The entire strut was shrouded by a streamlined metal cover to prevent the wind force on the balance and their influence on the actual force to be measured on the model. For the force measurement a flat plate was mounted horizontally at the top of the shroud and the model was attached to the balance through a hole in the plate. This plate served as the end plate for the semi-span tests and it had a dimension of 3’x3’x3/8". The flat plate with the hole was mounted to the strut with four corner screws and four tie wires were also attached to the tunnel floor. This allowed precise alignment of the flat plate and also prevented any vibration during the experiment. The gap between the model and the flat plate was adjusted by moving the model from the top by the desired length into the sleeve of the strut through the hole on the plate. The exact gap was introduced by holding the model steady and inserting feeler gauges of desired width and then tightening the screw on the strut to hold the model at that position.

2.3.3 The Balance

The balance used for the force measurement experiment was the three-component SR-1 strut equipped to measure normal, axial and side forces, using strain gauge bridge amplifiers. This strut has a maximum load rating of 200lb normal and 100lb for axial and

side load. Excitation voltage used for the strain gauges was 5 V. The schematic diagram of the balance and the arrangement of strain gauge bridges are shown in fig. 2.6. For the test set up used in this experiment the side and axial force were designed to give the lift and the drag on the model respectively. The balance was mounted on the strut turntable of the tunnel, which can rotate along a vertical axis. This was originally designed to perform yawing motion. But the with the test set up used in the present research this arrangement was found most suitable for changing the angle of attack on the model as the model was aligned vertically. The strut was rotated with a solenoid-controlled motor and gives a resolution of 0.01^0. Measurements were taken from an angle of attack of -6^0 through 25^0 with an interval of 1^0.

2.3.4 Sealing of Gap

Tests were to be run with the wing/end plate gap ranging from zero (sealed) to 0.024". In the zero gap case sealing the gap was crucial for the force measurement. This posed the greatest difficulty at lowest Reynolds number. The best way to seal it with out transferring any force to the plate is to use oil to fill up the gap. But it was rejected because it was found that the oil was being blown away by the flow at higher Reynolds number irrespective of its surface tension. So a previously tested technique was used. A strip of self adhesive low density foam rubber weather stripping was cut to the airfoil cross section and attached to the model at the root. The height of the foam layer was kept at the minimum so that it didn't change the aspect ratio of the wing. To reduce friction

between the plate and the model the foam was soaked with machine oil. This also enhanced the sealing. This method was previously proved to be non-contaminating [6] i.e. forces were not transferred through the sealing. With all the precaution taken still there was transfer of force between end plate and the model for airfoil NACA 1412 at Reynolds number 100,000 is indicated as will be seen in the later examination of the test data.

2.4 Data Acquisition

The data acquisition system used in the force measurements consisted of a Measurements Group 2310 signal conditioning amplifier which provided balance excitation and signal amplification for the strain gage output and National Instruments AT-MTO-16XE-50 data acquisition card installed in a Pentium 133 computer. The centerpiece of the system is a SCXI-1001 Mainframe from National Instruments. This result in a total of 32 isolated differential analog input channels with an analog to digital conversion resolution of 16 Bits. The schematic diagram for the data acquisition system is shown in fig. 2.7. Force data measurement included reading from strain gauge balance as well as the readings of static and dynamic pressure and temperature from which the lift coefficient and the Reynolds number could be found. The angle of attack of the test wing was also recorded.

The signal conditioner has an accuracy of ±0.04%R ±1 digit at 26^0 to 35^0 C. The ADC used was a 16 single ended, 8 differential channels input successive approximation type

instrument. It has a 16-bit resolution with a sampling rate of 100kS/sec and is compatible with Windows operating system. The ADC has a relative error of maximum ±1 LSB. The software, written using LabView 4.0 under the Windows 95 environment, developed by Mr. Troy Jones, was capable of storing the data in a file for later review as well as generating plots of lift and drag on the model vs. the angle of attack, during the experiment.

The pressure transducer used for measuring tunnel dynamic pressure was a SETRA model 239 sensor with bi-directional differential range of 0" to 15" of water. The full-scale output is 0 to ±10 VDC. The accuracy is ±0.14% of FS at constant temperature and non-linearity is of ±0.1% of full range output. The operating temperature range is 0^0 to 175^0 F.

Validyne Engineering Corporation manufactured the digital barometer used to measure the static pressure. It was a Model DB-99 with an operating temperature range of 40^0 to 110^0 F. This instrument can measure the barometric pressure over the range of 25.00 to 31.00 inch of Hg. It has a resolution of ±0.01 in. Hg and drift of ±0.02in. Hg/3 months. The temperature error is ±0.01 in. Hg in the operating range.

The temperature sensor was thermistor type 44004 which has a range of -80^0 to 150^0 C. It uses a dual slope ADC with 15 bit input resolution and has a accuracy of $\pm 0.2^0$ C at 25^0 C. It has a 30 minute warm up time. The thermistor was mounted through the tunnel wall on a wooden platform to insulate it from the heat transfer from the wall.

For each recorded data point 100 samples were taken for each quantity to be measured and the average was stored. This reduced the uncertainty of the data to a great extent. A detail of uncertainty analysis is shown in section 2.7. A tare data set of force readings was taken prior to each test run to eliminate any zero shifts on the balance. For each set the computer reduced the forces recorded automatically to C_L and C_D for corresponding angle of attack and dynamic pressure and stored in a file.

2.5 Pressure Measurement Models

2.5.1 Model Construction

The procedure for construction of the models for pressure distribution measurement was different from that used for force measurements. The models made for measuring the pressure distribution had 46 pressure holes of 0.0625" diameter. There were 22 holes near the tip of the wing with 11 holes each on upper and lower surface. The rest of the 24 holes were distributed with equal spacing along the span of the wing at quarter chord length as shown in the fig 2.3. The location of these holes is presented in table 2.1. Twelve of these holes were on upper surface and remaining twelve holes were on lower surface of the wing. It was found to be very difficult to route the PVC tubing for all these 46 pressure ports inside a 12" long wing. So it was decided to make two separate 6" long wings similar to that made for force distribution using the same template. Then the foam core was melted out under the skin. To maintain the cross section shape only a part of the

core at the quarter chord was left, which looked like an “I” section as shown in figure 2.8. This provided the reinforcement similar to a spar in a real aircraft wing and also helped to retain the shape. Holes were then drilled on the skin for each of the 46 pressure ports. A 6' long PVC tube of 1/16" diameter was inserted through each hole. The tubes, which ran inside the wing, were then glued to the skin using epoxy resin and the protrusion of the tubes outside the skin was removed carefully so that the outside surface was smooth. Then the two small pieces were glued together side by side to develop the complete wing as illustrated in fig 2.9. Similar coats of primer and paint were given on the skin and care was taken so that the paint didn’t clog the pressure ports. The surface irregularities around the pressure ports were undetectable with naked eye after painting and the surface smoothness near these ports was within 0.001".

2.5.2 Model Support

The set up for the pressure measurements was also slightly different from that of the force measurements. Running the pressure tubes out through the “base” of the wing through the gap would have blocked much of the gap and would have made the measurement meaningless. Therefore the tubes were made to run out of the other end of the wing leaving a pure gap between the wing and the plate. The whole arrangement is shown in figure 2.10. A rectangular metal frame made of mild steel angle held the Plexiglas end plate parallel to the side wall of the tunnel at 18" from the wall. The metal frame joints were welded to give structural stability. The metal frame was bolted firmly

to the both tunnel wall and floor to minimize vibration when the tunnel would run. A 3’ x 3’ x 3/8" rectangular Plexiglas plate with rounded leading edge was attached to the frame with four flat head corner screws. The screws were sunk with the Plexiglas surface so that it did not induce any disturbance to the flow

A strut at the center of the test section, which is 3’ from the side wall, held the model with its axis parallel to the floor of the tunnel. The angle of attack was defined as the angle the chord of the wing with the tunnel axis. This angle is zero when the chord is parallel to the tunnel axis. The angle of attack could be changed by rotating the wing along the horizontal axis perpendicular to the tunnel side wall. The gap size was adjusted by moving the wing side ways. Pressure tubes connected to each of the holes ran through the wing to the wing root and entered the shroud enclosing the strut for the model support and then were connected to a scanivalve pressure measurement system. This reduced the disturbances due to the presence of the tubes. Same procedure as that used in the force measurement tests was employed to seal the gap during the pressure measurement tests although the transfer of forces to the plate was not an important criterion here since we were not trying to measure the force on the model in this case.

2.5.3 Scanivalve System

The scanning valve pressure measurement system, CTLR2P/S2-S6 by Scanivalve Corp., was used to take the pressure measurement readings. It has a 48 port scanning device that

is controlled by a solenoid motor run by a 286 IBM PC. Dr. Devenport and Dr. Simpson at Virginia Tech developed this system. Each port is connected to a pressure transducer in a predetermined programmable sequence and the computer reads the output of the pressure transducer, calculates the value of pressure coefficients (C_P) and stores it in a file with the specific port number. It uses two pressure transducers, Setra 239; one for measuring pressure for each port and the other one as a reference transducer for the tunnel dynamic pressure. A data acquisition board (DT 2801) was used for analog to digital conversion.

2.6 Difficulties Involved in Testing

The greatest difficulty was to measure the forces on the model with the gaps sealed since it is extremely difficult to seal the gap as well as not allow the forces to be transferred to the wall through the sealant. This problem has already been discussed.

There were a few other difficulties involved in the measurements. Galbraith [11] observed the boundary layer on the end wall could affect the flow near the junction of the plate and the wing section, which makes it difficult to measure the effect of the gap. The effect of endplate boundary layer separating in front of test airfoil can cause a decrease in lift near the wall and the trailing vortices generated by the end plate can alter the lift distribution on the model altogether.

Another drawback of this experiment is that the turbulence generated due the presence of the end plate may have affected the flow through the gap, although the over all turbulence level in the test facility is reported to be as low as 0.1% [10]. The effect of turbulence level on low Reynolds number measurements is yet to be fully understood. However it is known to have significant effect on the stall hysteresis loop. The data was taken with a small chord (6") model in a large test section to minimize the need for blockage, induced incidences and buoyancy correction. Marchman et al. [1] calculated the effect of buoyancy and found it to be negligible.

There was a possibility that the flow would be separated on the end plate. To reduce the chance of flow separation the leading edge of the Plexiglas plate was rounded off to give a smooth shape. This level was also qualitatively monitored by attaching tufts to the leading edge of the plate (fig 1.10) and it was found to that the flow always remained nicely attached to the plate.

There are other difficulties associated with the measurement of such small effects and aligning the end plate in parallel with the cross section of the model. This was eliminated by using a highly accurate data acquisition system with very low uncertainty that is discussed in more details in the next section.

2.7 Uncertainty Analysis

2.7.1 Force Measurements

For force measurements we have to consider uncertainty involved with each instrument used.

(i) Tunnel dynamic pressure transducer (0 to 15 inches of water)

Non-linearity : ± 0.1 % FS

FS error : ± 0.14 % FS

Therefore, $\delta\left[\frac{1}{2}\rho v^2\right]$ is equal to $\sqrt{0.1^2 + 0.14^2} \approx \pm 0.17\%$

(ii) Static Pressure transducer

Non-linearity : ± 0.01 % FS

Temperature error : ± 0.04% FS

FS error : ± 0.04% FS

Therefore, $\delta[p]$ is equal to $\sqrt{0.01^2 + 0.04^2 + 0.04^2} \approx \pm 0.057\%$ of the absolute value.

(iii) Temperature transducer

Non-linearity : ± 0.1 % FS

FS error : ± 0.8 % FS

Therefore, $\delta[T]$ is equal to $\sqrt{0.1^2 + 0.8^2} \approx \pm 0.806\%$ of the absolute value.

(iv) Signal conditioning amplifier

Non-linearity : ± 0.0015 % FS

FS error : ± 0.04%

Therefore, $\delta[A]$ is equal to $\sqrt{0.0015^2 + 0.04^2} \approx \pm 0.0400\%$

(v) Analogue to digital converter

Digitizing error : ± 0.0016 % FS

(vi) Strain gauge bridge

Total error : ± 0.014% FS

Now we have in the present research $C_L = \dfrac{S.F}{\frac{1}{2}\rho v^2 S}$

(i) So error in measuring C_L was $\pm\sqrt{0.17^2 + 0.04^2 + 0.0016^2 + 0.014^2} \approx \pm 0.18\%$.

(ii) The value of Reynolds number is given by Re = $\dfrac{\rho u l}{\mu}$

Error in measuring Reynolds number was due the error in measuring density ρ, obtained from temperature and static pressure measurement and tunnel velocity (u), which was obtained from dynamic pressure.

Error in u : $\pm\sqrt{0.057^2 + \frac{1}{2}\times 0.17^2 + 0.806^2} \approx \pm 0.8168\%$

Error in ρ : $\pm\sqrt{0.057^2 + 0.8^2} \approx \pm 0.806\%$

Total error in Re : $\pm\sqrt{0.806^2 + 0.8169^2} \approx \pm 1.15\%$

(iii) Error in measuring angle of attack (α) can also be estimated from the information available regarding flow angularity of the tunnel, orientation of the endplate and finite thickness of the trailing edge.

The average up wash and side wash angles of the flow in the area of the test section where the experiment was conducted, are 0.25^0 and 0.5^0 respectively[13].

The endplate centerline was made parallel to the tunnel axis by measuring a distance of 3’ from the side wall (half of the tunnel cross section) at the leading and trailing edge of the plate. The least count of the measuring instrument was ± 0.03125". So the total error in measuring the distance was ± 0.12%

Total error in measuring the angle was = ±0.15%

The trailing edge thickness of the model was 0.0625" and the distance from the pivot to the trailing edge was 4.5". So the Error induced for the finite width of the trailing edge was = ±1.4%

So the total error in measuring (α) is at $\alpha=10^0$ is $\pm\sqrt{0.12^2+1.4^2+2.5^2+5^2} \approx \pm 5.75\%$

2.7.2 Pressure Measurements

The uncertainty analysis for the scanivalve measurement was done by Simpson [14] et. all. The uncertainty in the measurement of C_p is calculated by the method outlined by Kline and McClintock (1953). As mentioned earlier, C_p is defined as

$$C_p = \frac{P - P_{ref}}{P_{oref} - P_{ref}}$$

The measurement of C_p with the two transducers (called the measurement transducer and the reference transducer) were calculated using the reduced expression for C_p which is

$$C_p = \frac{P - P_{ref}}{P_{o\,ref} - P_{ref}} = \frac{(\Delta P)_{meas}}{(\Delta P)_{ref}}$$

It may be noted that $(\Delta P)_{meas}$ was measured using the measurement transducer which had a range of -2.5 to +2.5 inches of water and $(\Delta P)_{ref}$ was measured using the reference transducer (range of 0 to 15 inches of water). The uncertainty in the measurement of C_p would be due to the uncertainty in the measurement of these two quantities. For the purpose of calculation the range of pressure sensed is taken to be 2.5 inches of water.

Let $\delta[(\Delta P)_{meas}]$ be the uncertainty in $(\Delta P)_{meas}$ and $\delta\lfloor(\Delta P)_{ref}\rfloor$ be the uncertainty in $(\Delta P)_{ref}$, then the uncertainty in C_p, which is δC_p, is given by

$$\frac{\delta C_p}{C_p} = \sqrt{\left(\frac{\delta(\Delta P)_{meas}}{(\Delta P)_{meas}}\right)^2 + \left(\frac{\delta(\Delta P)_{ref}}{(\Delta P)_{ref}}\right)^2}$$

Uncertainties in the individual transducers

(i) Measurement transducer (-2.5 to +2.5 inches of water)

Non-linearity : ± 0.1 % FS (full scale)

Zero error : ± 0.4 % FS

FS error : ± 0.4 % FS

Therefore, $\delta[(\Delta P)_{meas}]$ is equal to $\pm\sqrt{0.001^2 + 0.004^2 + 0.004^2} \approx \pm\ 0.0058$ FS

That is, $\frac{\delta(\Delta P)_{meas}}{(\Delta P)_{meas}}$ is $\approx \pm 0.0058$

(ii) Reference transducer (0 to 15 inches of water)

Non-linearity : ± 0.1 % FS

Zero error : ± 0.4 % FS

FS error : ± 0.4 % FS

Therefore, $\delta[(\Delta P)_{meas}]$ is equal to $\pm\sqrt{0.001^2 + 0.004^2 + 0.004^2} \approx \pm\ 0.0058$ FS

For our range of pressures , $\frac{\delta(\Delta P)_{ref}}{(\Delta P)_{ref}}$ works out to be $\pm\ 0.0058 \times 15/5 \approx \pm 0.0174$

Hence, the net uncertainty in C_p is $\pm\sqrt{0.0058^2 + 0.0174^2} \approx \pm\ 0.018$ which is ± 0.018

Chapter 3

Results and Discussion

Symmetrical airfoils were previously tested to determine the effect of the wing/endplate gap in semi-span testing [10]. In the present research, tests were conducted on a series of three different airfoils, all of same thickness but increasing camber. The NACA 1412, NACA 2412 and NACA 4412 were tested do determine the influence of gap on lift coefficient, zero lift angle of attack, stall behavior and also to determine the influence of camber on the low Reynolds number gap effect. These airfoils were chosen because they are commonly used in variety of applications and also would give us a better insight into the dependence of gap effect on the camber of an airfoil.

3.1 Airfoil NACA 1412

3.1.1 Lift Coefficient Measurements

Figures 3.1 and 3.2 compare the lift coefficient (C_L) vs. angle of attack (α) curves for different gap sizes and Reynolds number for the smallest camber airfoil used in the experiment. The angle of attack was taken as the angle between the chord of the airfoil and the tunnel axis. With flow angularity being small we can take α as the wind axis angle. Fig 3.1 shows the NACA 1412 at Reynolds number 100,000 for the gap size

0.000", 0.060", 0.024" and 0.099". Fig 3.2 shows the same plots at Reynolds number 200,000. In both cases there is a significant shift in the curve towards the left reducing the zero lift angle of attack when the gap is sealed. They also show that the gap effect is significant even with the smallest gap and it does not change much with the gap size. The shift of the curves with increasing gap sizes at Reynolds number 200,000 almost coincides with those at 100,000. In both cases there are significant effects as soon as there is a gap and this effect reduces faster at lower Reynolds number.

It is quite clear that a significant gap effect is present even with the minimum gap which is 0.05% of the span. This is contrary to the observation made by Pope. These figures also show conclusively that the sealed gap case has a higher $(C_L)_{\text{max.}}$ There is an 8% increase in maximum value of lift coefficient ($C_{L\,\text{max}}$) at Reynolds number 200,000, as shown in fig 3.2. It can be concluded here that the change in C_L is not due to transfer of forces between the plate and the wing when the gap was sealed. Because except for airfoil NACA 1412 at Reynolds number 100,000 for all other cases examined in this study the data was highly repeatable within the experimental error and in each case it shows similar change of C_L.

However the stall angle is higher in the presence of a wider gap. At Reynolds number 100,000 the stall angle is 11^0 and at 200,000 the stall angle is 13^0 for the sealed gap case. For the intermediate gap, which is 0.05% of span, stalling is delayed by 1^0 at 100,000.

For a higher gap of 0.2% of span of the model the stalling is delayed by 2^0 at Reynolds number 200, 000 and by 1^0 at 100,000. An even higher gap size of 0.8% of span was tested at 200,000. This doesn't show any significant difference in the measurement from that of 0.2 % gap as indicated in figure 3.2. But there is a shift of about 0.5^0 in zero lift angle of attack towards left for the sealed gap case.

Figure 3.1 shows the difficulty in sealing the gap without transferring the force to the end plate at very low Reynolds numbers. When the plot was compared to other lift coefficient measurements for the same airfoil at 200,000 in figure 3.2 and other airfoils in figures 3.11,3.12, 3,33 and 3.34 (shown later in this chapter) it seems that only 4 data points on this plot may be accurate. The rest of the data shows an upward shift that may have been caused by the transfer of force through the sealant and introduced a biased error in the recorded data.

3.1.2 Pressure Measurements

Figures 3.3 to 3.10 show the pressure distribution on the airfoil NACA 1412 in both chord wise and span wise direction at Reynolds number 200,000 at increasing angle of attack. Pressure ports were located near base of the airfoil at an interval of 0.5" along the chord at both upper and lower surface and also along the span at quarter chord with same interval (fig 2.3). The chord wise distribution was measured at mid-span and the span

wise distribution was measured at the quarter chord for this airfoil. Figures 3.3 to 3.6 compare the chord wise distribution for both upper and lower surfaces, for all three gap sizes at 0^0 to 15^0 angle of attack with 5^0 interval.

Figure 3.6 shows the airfoil has stalled at 15^0 for the sealed gap case as expected from the force measurement data in figure 3.2. It has partially stalled at this angle for the other two gap sizes also, but stalling is more prominent in the sealed gap case. It also shows the effect is more visible near the leading edge than the trailing edge. Since the curvature for this category of airfoil is more near the leading edge. The pressure difference is higher between the lower and upper surface near the leading edge than the trailing edge. That is why the effect is more dominant near the leading edge. Because of this pressure difference the air flows through the gap and helps the flow on the upper surface to remain attached at higher angle of attack as shown in fig 1.10. When the gap was sealed the air could not move through the tip clearance and makes the airfoil to go into stall faster than other cases.

Figures 3.3, 3.4 and 3.5 show the pressure distribution before stalling. The difference of C_p between the upper and lower surface is higher for the sealed gap indicating a higher lift at the same angle of attack. This supports the previous observation made from force measurement data. But once the airfoil goes into stall the airfoil loses lift faster in a sealed gap case. We can observe this phenomenon in the force measurement data also as

shown in fig 3.2. Figures 3.3, 3.4 and 3.5 also indicate that the change in C_p is dominant on upper surface than in lower. The flow on the upper surface accelerates more rapidly because of the camber of the airfoil. This lowers the local static pressure. In presence of the gap there is a secondary flow to the upper surface through the gap altering the pressure distribution on the upper surface.

Figures 3.7 to 3.10 show the span wise pressure distribution. The data is plotted from the mid-span to the edge near the wall. Figure 3.10 shows difference of C_p between the upper an lower surface start falling rapidly towards the edge indicating a more complete stall in the sealed gap case. Before the airfoil stalls the difference of C_p between the upper and lower surface is almost constant for the sealed gap indicating a two dimensional test condition. When a gap was introduced, the pressure difference started falling as one moved from mid-span to the edge of the model. Figure 3.8 shows that this effect is not restricted to a small portion near the gap. The gap affects the pressure over the entire inboard portion of the wing giving a wing tip behavior instead of 2-D behavior near the wall. This also confirm the existence of a higher $(C_L)_{\max}$ for the sealed gap case as observed in the force data of fig 3.1.

The pressure measurement data results are in good agreement with the observations made in the force measurements. In that the lift is higher in the sealed gap case before stalling. This also explain the shift in the C_L vs. α curves towards the left as gap size decreases, lowering the zero lift angle of attack. Significant loss of lift occurs due to the presence of

a gap. However the gaps tend to delay stalling to higher angle of attack because of the flow through the gap resulting a 3-D wing tip like effect. So any low Reynolds number 3-D airfoil data obtained from semi-span testing with a wing /end plate gap needs to be corrected for the gap size. It is quite conclusive that the gap, however small it is, significantly affects the measurements.

End plate mounted semi span models can therefore give different test results from full three-dimensional wing tests [6]. There are few standard correction techniques for the semi span tests although according to Pope and Harper [8] it introduces other errors during subtracting the drag acting on the plate. Marchman [6] noted that, even a very small leak through the gap may result in loss of lift at low Reynolds numbers and must be evaluated. Data obtained in the present research for both pressure distribution and force measurement supports his observation.

3.2 Airfoil NACA 2412

3.2.1 Lift Coefficient Measurements

Figures 3.11 and 3.12 show the C_L vs. α data for an NACA 2412 airfoil at Reynolds number 100,000 and 200,000 for the same gap sizes used for the NACA 1412 airfoil. Data is plotted from angle of attack α=-5^0 to 16^0 with a 1^0 interval. Again both the figures show that the closed gap C_L is higher than that for the open gap cases although the

difference is not great. Figure 3.12 compares the three gaps at Reynolds number 200,000. In the presence of gaps the airfoil stall is again delayed and this supports the observation made on the previous airfoil. It's quite obvious that there is a sizable effect of gaps on C_L and this effect is always present no matter what size the gap is.

Figure 3.11 shows the gap effect is more prominent at higher angle of attack. It also shows there is about 10% increase of $(C_L)_{max}$ in the in case of sealed gap, a significant amount. Fig 3.12 shows that the airfoil stalls at 15^0, whereas for the open gap case it doesn't stall until beyond 17^0. It's also quite obvious from this figure that as long as a gap exists the gap size does alter stall angle for this airfoil.

For both the gaps it stalls at the same angle of attack. The gap size affects the value of C_L at a particular angle of attack. It can be concluded that the as soon as a gap is introduced the C_L is reduced by an amount which is not negligible, as it is assumed in many experiments. But this effect is only a function of the existence of the gap not the size for this airfoil. There no a significant difference of C_L when the gap size increases from 0.2% of span to 0.8% of span. This shows the effect of gap on C_L is not linear in nature. It can also be concluded that whatever size of gap is introduced, it delays the stall for the model by 1^0 to 2^0 depending upon the Reynolds number.

At higher Reynolds number a gap tends to delay stall more than at lower numbers. This is an important point to note since stall behavior is one of the important aspects of choosing one airfoil over another and the data for this needs to be quite accurate. In case the data is

generated by semi-span model testing technique one needs to be very careful regarding stall data and accurate data can be best achieved by sealing the gap. This observation is further supported by the pressure distribution data.

3.2.2 Pressure Measurements

Figures 3.13 to 3.32 show all the pressure distribution data for the NACA 2412 airfoil tests. Each plot compares the C_P on both upper and lower surface of the airfoil for sealed gap and for two other gaps of 0.05% of span and 0.2% of span. Figure 3.13 to 3.17 shows the chord wise distribution of C_P at quarter of an inch from the base of the airfoil at a Reynolds number 200,000. These plots are from angle of attack 0^0 to 20^0 with a 5^0 interval. Figure 3.13 to 3.15 compares the behavior of the airfoil before stall and figure 3.16 and 3.17 compares the effect as the model stalls.

From figure 3.14 and 3.15 it is evident that the effect on pressure distribution is greater near the leading edge of the airfoil similar to what was seen on the airfoil NACA 1412. This effect gradually diminishes towards the trailing edge and finally disappears at the trailing edge. This shows that flow through the gap slowly reduces as one moves from leading to trailing edge. This is quite obvious because the difference of pressure between the upper and lower surface is small near the trailing edge as one can normally expect to satisfy Kutta condition. But there is always a significant overall effect produced due to the large difference in C_P near the leading edge.

At angle of attack 5^0 the difference of C_P between upper and lower surfaces changes by almost 15% near the leading edge in case of a gap of 0.2% span as compared to sealed gap. This difference is about 18% at an angle of attack of 10^0 as indicated in figure 3.15. However this change reduces to zero at the trailing edge and integration over the whole chord length reveals that there is an almost 9.5% change of C_L along this chord line. The force measurement data shows that at this angle of attack the over all change in C_L is about 6%. Span wise pressure distribution plots show that the effect of the gap is greater near the base and reduces along the span. It is obvious that the overall effect should be somewhat less than 9.5%. This shows how the gap effect becomes important at higher angle of attacks.

Figure 3.16 shows that the airfoil has gone into stall for the sealed gap case but still has attached flow for the two other gap sizes. It also shows nearly 40% reduction in C_P near the leading edge on the upper surface after stalling. But there is no change in the value of C_P on the lower surface. This indicates the change in flow pattern due to stall is limited to the upper surface; i.e. the flow separation takes place only on upper surface. At 20^0 the airfoil goes into full stall as the C_P falls for all three cases and once it stalls for all cases, the gap effect is negligible. When the airfoil stalls the flow generally separates on the upper surface, recovering a part of the static pressure and the pressure difference between the upper and lower surface reduces. Hence there is no significant leakage effect through the gap and that is why the effect of the gap is not visible at this angle of attack.

Figure 3.18 to 3.20 shows the span wise distribution of C_P at quarter chord and figure 3.21 and 3.22 shows the same after it stalls. From figure 3.18 and 3.19 it can be concluded that the effect of the gap is evident over the entire airfoil span and not just at the base although the lift increases as one moves from the edge to the mid section of the model. This is evident from the fact that the difference of pressure increases along the span. There is a sudden dip in the C_P at a distance of 7" from the edge but appears to be a bad data point. As one can see in figure 3.21 the difference of C_P has fallen by a large amount, almost by 10% in the sealed gap case, when the angle of attack changes from 10^0 to 15^0. But this value has increased by about 10% for the 0.2% gap for the same change in angle of attack. This is because the airfoil has stalled for the sealed gap case at 15^0 but still shows good lift for the open gap. The span wise distribution (fig. 3.21) further shows that the change in C_P due to gap is negligible once the airfoil goes into stall. Three data points near the opposite end of the gap are a little erratic in figure 3.21. There were 46 pressure tubes coming out at this end which ran to the scani valve pressure measurement system. The flow may have been affected due the presence of these tubes near this end.

Figures 3.22 to 3.31 show the plots in same sequence at a Reynolds number of 100,000. The plots are almost identical except in that the difference of C_P between the upper and lower surfaces is slightly higher at 200,000. Comparing figure 3.14 with 3.24 and figure 3.15 with 3.25 similar observations can be made to those of Reynolds number 200,000.

Upon integration this result in a change of around 6% in the value of C_L. The change in C_L obtained from the force data is in good agreement with this result.

There is a marginal shift of the C_L vs. α curve towards the left with increasing Reynolds number. This is documented in the force data too. There is a minor shift in the zero lift angle of attack towards the left with increasing Reynolds number. The change on C_P due to the gap near the leading edge in this case is about 14% at 5^0 angle of attack. This change is almost 17% at 10^0 where as near the trailing edge these values are in the order of 3%. The instrumentation used for this experiment was accurate within 1.8%, which is very near to the change measured in the value of C_P. So it can be concluded that the difference in C_P is negligible near the trailing edge as observed earlier. But there is an over all effect due to a 2% gap about 8% and 9.5% respectively for 5^0 and 10^0 when integrated over the chord line. This difference is around 9.5% for a 0.05% gap also. So clearly the effect is not linear with the gap. In fact the effect for 0.2% and 0.8% gap is almost the same as observed in force measurement data.

Figure 3.26 shows that the airfoil stalls at a lower angle of attack when the gap was sealed. This is very significant since even a very small gap of 0.05% of span can delay stall. So to investigate the stall hysterisis behavior of the airfoil using a semi span model one must consider the effect of the gap size. A convenient gap size has to be maintained throughout the experiment and the gap should be precisely measured and well documented. After the airfoil stalls for all gap sizes (fig. 3.27) the gap effect on the upper

surface C_P become negligible, however, the lower surface C_P are still affected by the gap size.

C_P distribution on lower surface remains almost unchanged before and after stall. The lower surface also shows less dependency on the gap at higher angle of attack. This is primarily because of the reason that the flow separates on upper surface only. Figures 3.28 to 3.32 show the span wise distribution for this case. It can be observed that the effect of the gap is spread over the whole airfoil surface to some extent and not restricted only to the base of the model. The over all gap effect reduces with angle of attack for the low camber airfoil.

3.3 Airfoil NACA 4412

3.3.1 Lift Coefficient measurements

C_L vs. α curves for the NACA 4412 test models were plotted in figures 3.33 and 3.34 at Reynolds number 100,000 and 200,000. Three Gap sizes were used at Reynolds number 100,000 and four were used at Reynolds number 200,000 in addition to a sealed gap. The sizes were 0.05%, 0.2% and 0.825% of the span as used for all the previous airfoils in this research. Both the plots show significant change in C_L due to the existence of the gap. The values of C_L again are higher at any given angle of attack when the gap was sealed. The curves shift towards the right with increasing gap size, changing the zero lift angle of

attack. The dependency on Reynolds number is small as with other airfoil sections. The curves tend to shift to left by a marginal amount with increasing Reynolds number. The Zero lift angle of attack is about -2^0 at 200,000 where as it is about -1.5^0 for the sealed gap case. At the gap size of 0.2% this angle is -1.5^0 at 200,000 and -1^0 at 100,000.

Data was taken for an additional gap size of 0.825% at 200,000. The zero lift angle of attack for this size is found to be 0^0. For the closed gap case the airfoil shows a lift curve slope of 0.072/degree in the linear range. Now if we calculate the slope of the same curve using lifting line theory[17] (pg. 256, equation 5.70) for the same wing section with an aspect ratio of 4, we get a value of exactly 0.0721/deg. This clearly establishes the fact that the semi-span models give accurate results when the model/endplate gap is sealed. Beyond 10^0 it start showing the non linear effect. There is a minor change in slope of the lift curve slope with the gap size, which is more prominent at Re=100,000, but drawing conclusions about this is quite difficult because the measured change is with in the range of experimental error.

It can be shown [(15)] that with increased sampling the uncertainty can be lowered below the least count of the instrument.100 samples were taken for each point to statistically reduce the uncertainty. Qualitative conclusions can be drawn with this increased number of samples and repeatability of data. The data regarding the slope of the curve was found to be highly repeatable. It was found that there is a gentle drop in the slope of the lift curve with increasing gap size and the difference of $C_{L,}$ measured at higher angle of

attack, is increased. This feature is same in all the three airfoil tested and more prominent at a Reynolds number of 100,000.

The stall behavior for this airfoil is similar to the previous two. It stalls at almost same angle for the sealed gap and gaps of 0.05% and 0.2% of span. But stalling is delayed for the 0.8% gap. This airfoil is more cambered than the other two airfoils used in this experiment. Due to the higher camber the pressure difference is larger in this case between the upper and lower surface. It appears to need a wider gap for the higher volume of flow required from the lower surface to delay the stall. It can be inferred that only higher gap sizes have a significant effect on the stalling angle for a high camber airfoil. However at lower cambers even small gap sizes have large effects. The stall angle changes almost by 1.5 to 2 degrees from the NACA 1412 and NACA 2412 airfoils at Reynolds number of 200,000. Change in $(C_L)_{\max}$ for the higher camber airfoil is not significant. So it can be inferred that the gap effect on the airfoil is not independent of the camber. It needs a very careful analysis to determine all the possible parameters for this effect. The pressure measurement data further explain the dependency on this parameter.

3.3.2 Pressure measurements

Pressure measurement data for NACA 4412 airfoil are shown in Figures 3.35 to 3.54. Figures 3.35 to 3.39 and figures 3.35 to 3.49 compare the effect of gap size on the pressure distribution on the airfoil surface in a chord wise direction near the end plate at

Reynolds number 200,000 and 100,000 respectively. Data was plotted for the same three gap sizes as before and for sealed gap. Figures 3.40 to 3.44 and 3.50 to 3.54 depict the same for a span wise pressure distribution. All these data sets are useful in establishing the effect of gaps in semi-span model wind tunnel testing at low Reynolds number.

The observations made from these plots are very similar to those made for the other two airfoils. Figure 3.35 to figure 3.38 show that the effect is pronounced at the wing leading edge. A $\delta(-C_P)$ 1.080 is seen for the sealed gap while it is only 0.104 for the 0.2% gap at 0^0 angle of attack. The difference is an order of magnitude. For the intermediate gap of 0.05% the value of

$\delta(-C_P)$ is 0.248 at 0.5" from the leading edge. The difference at trailing edge is 0.340 for the sealed gap, 0.265 for the 0.05% gap and 0.191 for the 0.2% gap. On the upper surface the difference of C_P between the sealed gap and 0.05% gap is 0.297 and that value between sealed gap and 0.2% gap is 0.685. These same values at trailing edge are 0.001 and 0.050.

At $\alpha=5^0$ the $\delta(-C_P)$ at the leading edge is 2.491 for the sealed gap and 1.628 for the maximum gap used. The difference of C_P on the upper surface between the sealed gap and two other open gaps are 0.625 and 0.725. This difference increases with gap size but not at the same rate. These values at the trailing edge are 0.029 and 0.005. These trailing edge differences are so small that they are with in the range of experimental error and we

can actually conclude that the difference at trailing edge is negligible for all practical purposes.

All the airfoils tested have shown the same effect on the upper surface at all Reynolds number and for all angle of attacks before stalling. The effect on the lower surface has always been much less than upper surface. Even at 10^0 the difference in C_P between the sealed gap and the 0.05% gap is 0.021 and 0.006 at 0.2% gap near the trailing edge on the lower surface. This difference changes by only a small amount at the leading edge. These values near the leading edge are 0.009 and 0.008. But all the figures point to the fact that this difference on the lower surface remains almost constant from leading edge to trailing edge, unlike the pressure on the upper surface. This effect is not altered by change in angle of attack. Comparing figure 3.35, 3.36 and 3.37 makes this quite clear. The lower surface pressure distribution maintains its pattern even after stalling as indicated in figure 3.38.

The behavior of this airfoil at Re=100,000 is similar to that at 100,000. Although the values of C_P measured at this number are different, the pattern of the distribution remains the same. $\delta(-C_P)$s near the leading edge are 1.006, 0.634 and 0.389 in the increasing order of gap size. The difference of C_P between the sealed gap and the two open gaps are 0.250 and 0.373 on the upper surface. On the lower surface it is 0.124 and 0.243. These differences near the trailing edge are 0.013 and 0.024 on upper surface and 0.009 and

0.017 on the lower surface. So the change on C_P near the trailing edge is also negligible in this case.

This effect, however, increases with angle of attack and at 10^0 it shows increased effect near the trailing edge too. This effect is in the order of 7 to 8%.Unlike the Re=200,000 case at 15^0 the airfoil is stalled (fig 3.48) for all gap sizes at Re=100,000. At Re=200,000 the airfoil resists stalling to some extent for the 0.2% gap as indicated in fig 3.38. At 100,000 although the airfoil produces marginally higher lift for this gap, it has clearly stalled. This is also supported by the fact that stalling is delayed with a increase in Reynolds number. At 20^0 there is no difference in C_P due to the gap effect due to heavy stall.

The span wise distribution of C_P gives a very good picture of how the effect of the gap varies along the span. Figures 3.41 and 3.42 show that the effect due to the gap gradually diminishes near the mid-span. At 5^0 angle of attack the difference of C_P between the sealed gap case and the highest gap near the edge is 13% and this difference is 6% at the center. At 10^0 angle of attack these values are in the order of 27% near the edge and 3% near mid-span. Integrating the pressure distribution shows there is a 14% drop in C_L due to a gap of 0.2%. At 10^0 angle of attack the drop in C_L calculated from the pressure distribution is about 13% near the edge. The span wise distribution in figure 3.42 clearly shows the change in C_L reduces from the edge to the center. It's difficult to calculate the drop in over-all lift from the span wise pressure distribution data. But one can ascertain

that the over-all drop in lift will be less than 13 % as the effect reduces along span. This drop in C_L recorded in the force tests data is about 8%, which is in very good agreement with pressure measurement data.

Fig 3.43 and 3.44 shows the span wise distribution after stalling. It's quite evident that after stall there is no difference in pressure due to the presence and size of the gap. But size of the gap is still an important determining factor for stalling angle for a higher camber airfoil. Figure 3.33 shows the airfoil has stalled for sealed gap and 0.05% gap where as it is still resisting stall for a higher gap of 0.2%. After stall the effect is spread uniformly over the whole upper surface and not just restricted to the edge.

3.4 Review of experimental Data

C_P is calculated by the vortex panel method at Reynolds number 200,000 for angle of attack 5^0 and 10^0 for wing section NACA 2412 and the plots are shown in figure 3.55 and 3.56. it shows a little upward shift of the experimental data. Similar plots for wing section NACA 4412 is shown in figure 3.57 and 3.58. In both figures one data point (at 0.4 C) shows a drift from rest of the points. This may have been due to local disturbances. For all cases the lower surface shows very good agreement with the numerical values. However the values of C_P near the leading edge on upper surface is slightly different than the numerical values. Considering the fact that the numerical values are calculated using a full 2-D model and ignoring the viscous effects it can be concluded that there is good

agreement with the experimental data. At gaps 0.000", 0.006" and 0.024" the estimated C_L (upon integration of C_P) at Reynolds number 200,000 are 0.52, 0.48 and 0.45 where as the directly measured values of C_L are 0.66, 0.64, and 0.59 at 5^0 angle of attack for wing section NACA 4412. At 10^0 angle of attack these value are 0.92, 0.93 and 0.82 and the direct measured values are 0.98, 0.97 and 0.91. The Value of C_L calculated from the pressure distribution is only a rough estimate (since pressure distribution is available at only one span wise direction) to check how the pressure measurement data agrees with the force measurement data and it can be concluded that the estimated C_L agrees reasonably well to the measured C_L. The value obtained for the lift curve slope for airfoil NACA 4412 from the experimental data was 0.072/deg. This value is the same when calculated for a wing of aspect ratio 4, twice the aspect ratio of the semi-span models tested using lifting line theory [(17)].

Additional plots were made to verify the trend of variation of C_L with gap size in figure 3.59 and 3.60. We can clearly see the nonlinear effect of the gap size on C_L from both direct measurements and the estimated values from surface pressure distribution. The effect of the gap on C_L is prominent for the gap sizes between 0% to 0.1% of the span. Beyond 0.1% of the span the effect flattens out and no significant effect is observed till it reaches stall. However it would be difficult to predict the degree of non-linearity with the set of data recorded in the present study all though one might be tempted to infer that the nature of the curve follows an exponential decay.

Chapter 4

Conclusions

Experiments were conducted in the Virginia Tech stability wind tunnel to investigate the effect of an end plate/wing gap at low Reynolds number wind tunnel tests for semi-span models. Both force and pressure measurement data were taken for airfoil sections NACA 1412, NACA 2412 and NACA 4412 of wing aspect ratio of 2 for two gap sizes of 0.05% and 0.2% of span and also for a sealed gap at Reynolds number 100,000 and 200,000. The lift force was measured on these airfoils over an angle of attack range from -5^0 to the stalling of the airfoil in 1^0 increments. Pressure distributions were measured on both top and bottom surfaces along the chord and the span. From these results the following can be concluded.

- Semi-span model testing of wings at low Reynolds numbers has an inherent deficiency. To obtain the most accurate results by semi-span testing techniques the gap between the tunnel wall or end plate and the model should be sealed completely. Because if we take the sealed gap case for the models tested (Aspect Ratio 2) and measure the lift curve slope that matches exactly with the theoretical value obtained for an wing of aspect ratio of 4. We need to remember that for semi-span testing the data obtained should match that of a double aspect ratio wing in a full span test or theoretical values. But sealing the gap may result in transfer of forces from the model to the wall or vice versa, degrading the

reliability of the obtained data. Hence full span tests are always preferable over semi-span tests if the data is corrected for the presence of the strut that holds the model inside the wind tunnel.

- At low Reynolds numbers the effect of a wing/end plate gap is not negligible even at very small clearance. Significant effects creep in as soon a gap is introduced no matter how small it is.

- A drop in lift is one of the most significant effects of the gap. Changes in zero lift angle of attack and stalling angle are other prominent effects.

- The drop of lift is highly non-linear with the gap size. This effect tends to become insensitive to the size of the gap with increasing gap size.

- The stalling of the airfoil is delayed with the introduction of the gap. Increasing gap size tends to resist stall even more.

- For a low camber airfoil the delay in stall is visible at a very low gap size. However for a higher camber airfoil stall is delayed only at higher gap sizes.

- Reynolds number doesn't have a significant effect on the pattern of the gap effect, but the stall angle changes to some extent with the Reynolds number.

- The effect of the gap on surface pressure is greater near the edge and is reduced as one moves away form the edge. But it is not restricted to the edge. This makes the model behave more like a smaller aspect ratio, 3-D wing than a semi-span model.

- The influence of gap on pressure distribution is always more prominent near the leading edge than the trailing edge and also more significant on upper surface than on lower surface.

- The gap-induced change in pressure distribution on the upper surface is almost negligible when the airfoil goes into stall. However the lower surface maintains a significant difference even after stall.

- The gap-induced change of pressure distribution due to stall is restricted mostly to upper surface.

- The loss of lift that occurs with introduction of a gap seems to be mostly due to the flow through the gap from lower surface to the upper surface.

- For semi-span testing techniques one needs to be particularly careful to maintain a uniform gap through out the experiment. Other wise it could be difficult to correct the data for gap effect since it is highly non-linear in nature.

- To determine the stalling angle accurately the gap should be sealed, because the change in stalling angle due to the gap size is also dependent on the camber of the airfoil and it would be difficult to correct the data if any gap is used during the experiment.

Present study reveals the complex nature of the effect of a small gap between the wing base and the wind tunnel wall or end plate. Further study is needed to investigate this phenomenon in more detail and to determine the standards for semi-span testing

with wing/end plate gaps based on tunnel test section dimension, model span and aspect ratio and flow Reynolds number.

Chapter 5

References

1. J.F. Marchman, “Aerodynamic testing at low Reynolds numbers”, Journal of Aircraft, Vol. 24, No. 2, pages 107-114, February 1987.
2. W.G. Bastedo, Jr. and T. J. Mueller, “performance of Finite Wings at low Reynolds Numbers”, Proceedings of the conference on Low Reynolds Numbers Airfoil Aerodynamics, UNDAS-CP-77B123, Univ. of Notre Dame, Pages 195-205, June 1985.
3. J.F. Marchman, A.A. Abtahi and V. Sumantran, “Aspect Ratio Effects on Aerodynamics of a Wortmann Airfoil at Low Reynolds Number”, Proceedings of the conference on Low Reynolds Numbers Airfoil Aerodynamics, UNDAS-CP-77B123, Univ. of Notre Dame, Pages 183-193, June 1985.
4. P.M. Render, “Airfoil Measurements at Low Reynolds Numbers,” COA Report No. 8508, Cranfield, England, May 1985.
5. J.F. Marchman and V. Sumantran, “A Comparison of Finite Wing Low Reynolds number Airfoil Data”, Department of Aerospace and Ocean Engineering, VPI & SU, July 1985.
6. J.F. Marchman and S. Kuppa, “Semi-Span Model/End-Plate Gap effects on Low Re Aerodynamic Test Results”, Department of Aerospace and Ocean Engineering, VPI & SU, July 1986.

7. Z. Sun, V. Sumantran and J. F. Marchman, “Acoustic and turbulence Influence on Low Reynolds Number Wing Pressure distribution”, Proceedings of the Conference on Low Reynolds Number Airfoil Dynamics, UNDAS-CP-77B123, Univ. of Notre Dame, Pages 323-334, June 1985.
8. A. Pope and J.J. Harper, *Low Speed Wind Tunnel Testing*, Wiley, New York 1966.
9. Subrahmanyam Kuppa and J.F. Marchman, “End Plate Gap effect on a Half wing model at Low Reynolds numbers”, AIAA paper No.87-2350, August 1987.
10. J.F. Marchman, C.L Gunther and J.F Gundlach, “Semi Span Testing at Low Reynolds number”, AIAA 36th Aerospace Science Meeting and Exhibits, January 12-15, 1998, Reno, NV.
11. R.A. McD. Galbraith, “The Aerodynamic Characteristics of a GU25-5(11)8 Aerofoil for Low Reynolds Number” *Experiments in Fluids*, vol. 3 pp. 253-256, 1895.
12. A. A. Abtahi and J.F Marchman, “Aerodynamics of an Aspect Ratio 8 Wing at Low Reynolds Number”, *AIAA*, Vol. 22 No.7, pp. 628-634, July 1985.
13. K Choi and R.L Simpson, Some mean velocity, turbulence and unsteady characteristics of VPI & SU Stability Wind Tunnel, Report VPI-AOE-161, VPI & SU, Blacksburg, 1989.
14. M. Semih Olcmen, Roger L. Simpson, Jacob George and Cindy Whitfield, “Experimental Study of high Reynolds number (Re=230000) two and three dimensional boundary layers, Technical Report VPI-AOE-260, VPI & SU, Blacksburg, Aug, 1998.

15. Ernest O. Doeblin, *Measurement Systems, Application and Design*, 4th edition, McGraw-Hill, 1990.
16. Ira H. Abbott and Albert E. Von Doenhoff , *Theory of wing sections, including a summary of airfoil data*, Dover Publication, N.Y., 1959
17. John D. Anderson Jr., *Fundamentals of Aerodynamics*, McGraw-Hill Book Company, Singapore, 1986.

	VPI [3]	Notre Dame [2]	Cranfield [4]
Tunnel size and type	Closed Circuit 6'x 6'	Open Circuit 2'x 2'	Unknown 8'x 6'
Turbulence* at 10 m/sec 30 m/sec	 0.018% 0.045%	 0.03% 0.08%	 0.1% 0.1%
Model chord	5.0"	6.0"	13.5"
Aspect Ratios	4,6,8,10	3,4,5.6, 2-D**	8.9, 2-D**
Model Mounting	Full span strut to wing center	Semi-span end plate with gap	Semi-span end plate attached to the wing
Corrections	Calculated and found negligible	No correction mentioned	Blockage, Induced incidence mount plate drag

* As reported or published by the respective authors.

** Aspect ratio based on semi-span mount, 2-d uses two end plates.

Table 1.1 Summary of Test Conditions [5]

Upper Surface			Lower surface		
Port No.	X/C	Y/C	Port No.	X/C	Y/C
1	0.0833	0.0208	24	0.0833	0.0208
2	0.1667	0.0208	25	0.1667	0.0208
3	0.25	0.0208	26	0.25	0.0208
4	0.3333	0.0208	27	0.3333	0.0208
5	0.4167	0.0208	28	0.4167	0.0208
6	0.5	0.0208	29	0.5	0.0208
7	0.5833	0.0208	30	0.5833	0.0208
8	0.6667	0.0208	31	0.6667	0.0208
9	0.75	0.0208	32	0.75	0.0208
10	0.8333	0.0208	33	0.8333	0.0208
11	0.9167	0.0208	34	0.9167	0.0208
12	0.25	0.0417	35	0.25	0.0417
13	0.25	0.2083	36	0.25	0.2083
14	0.25	0.375	37	0.25	0.375
15	0.25	0.5417	38	0.25	0.5417
16	0.25	0.7083	39	0.25	0.7083
17	0.25	0.875	40	0.25	0.875
18	0.25	1.0417	41	0.25	1.0417
19	0.25	1.2083	42	0.25	1.2083
20	0.25	1.375	43	0.25	1.375
21	0.25	1.5417	44	0.25	1.5417
22	0.25	1.7083	45	0.25	1.7083
23	0.25	1.7917	46	0.25	1.7917

Table 2.1 Location of all pressure ports.

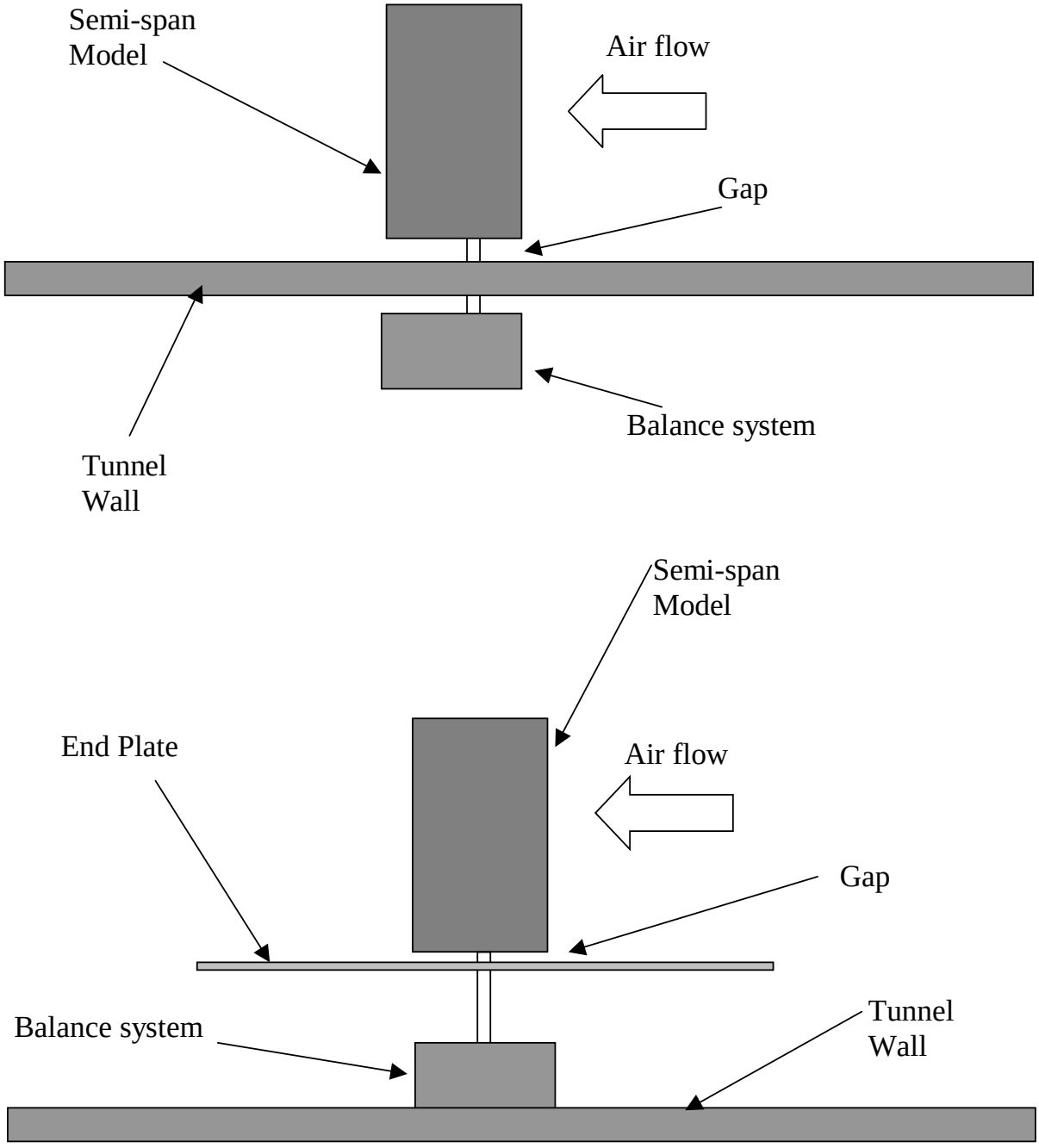

Fig 1.1 Two commonly used set ups for semi-span testing

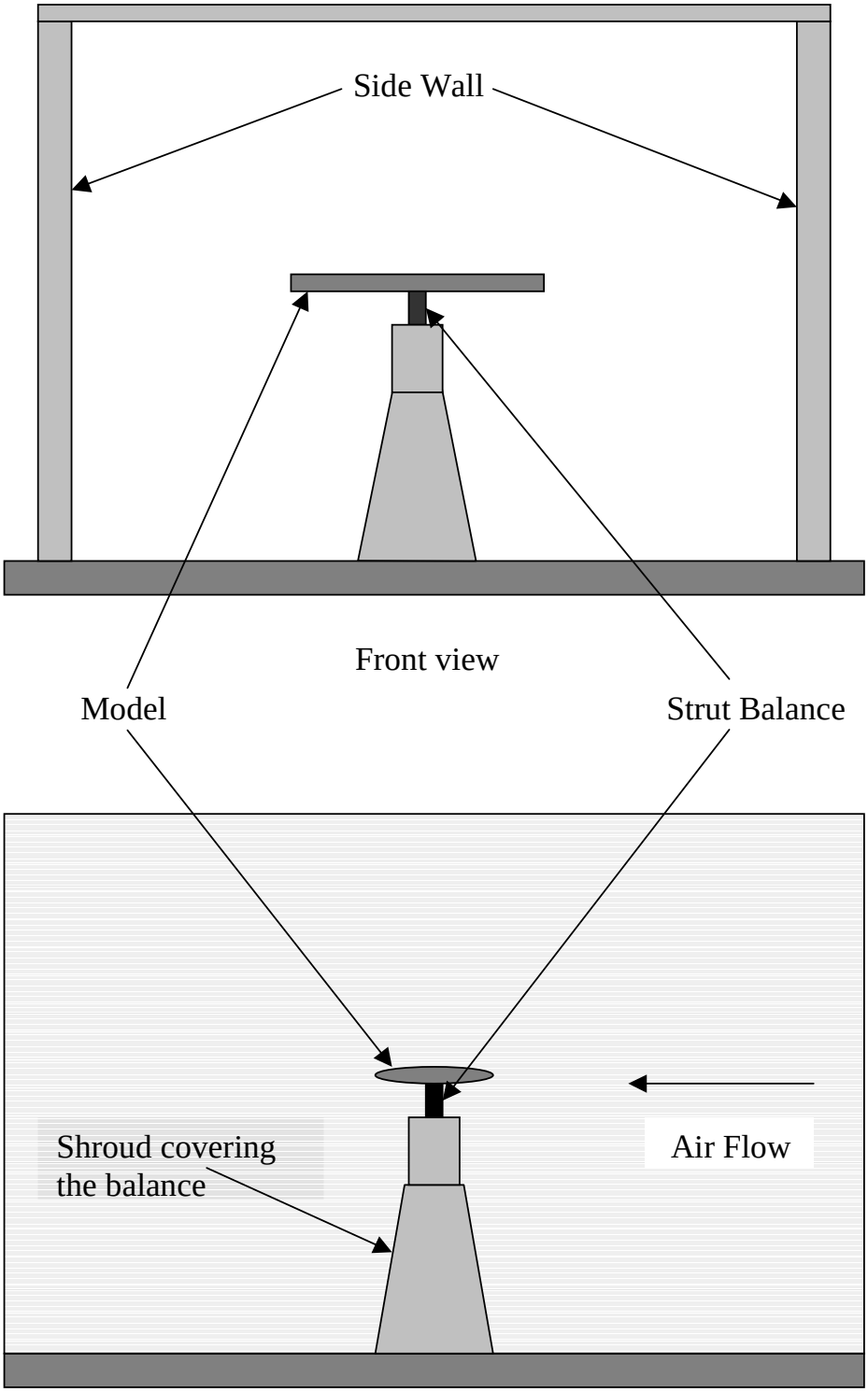

Fig 1.2 Full span testing arrangement

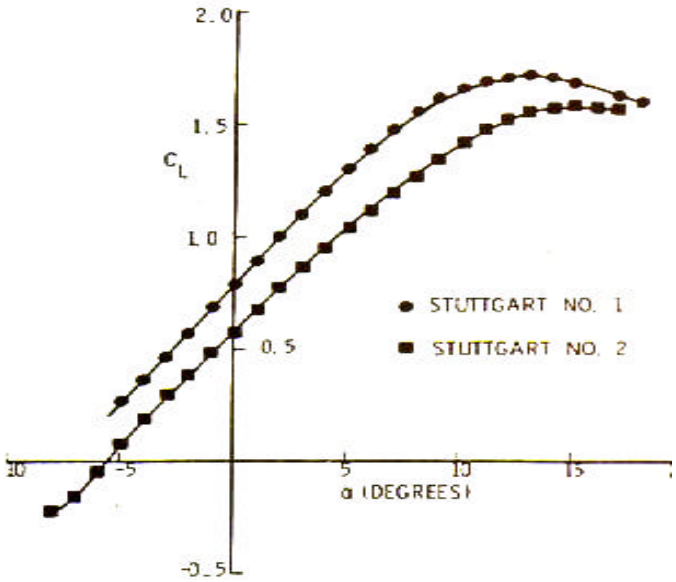

Fig 1.3 Comparison of Stuttgart data for FX63-137
(Figure taken from ref. 2)

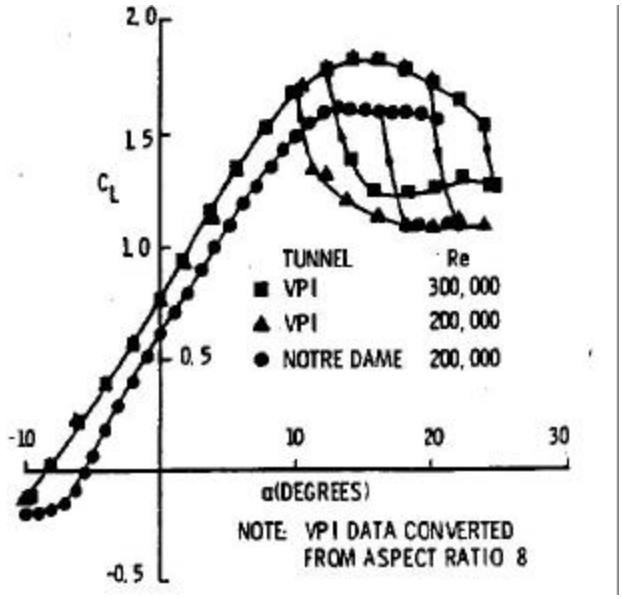

Fig 1.4 Comparison of low Reynolds number test data[2]
(Full 3-D models in both the cases, Figure taken from ref. 2)

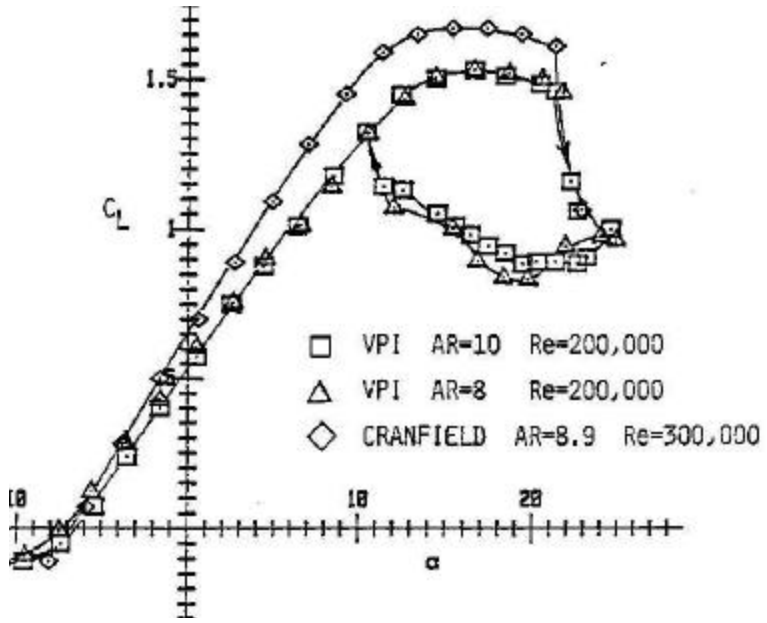

Fig 1.5 Comparison of VPI and Cranfield 3-D Data[2] for FX63-137 (Figure taken from Ref 2)

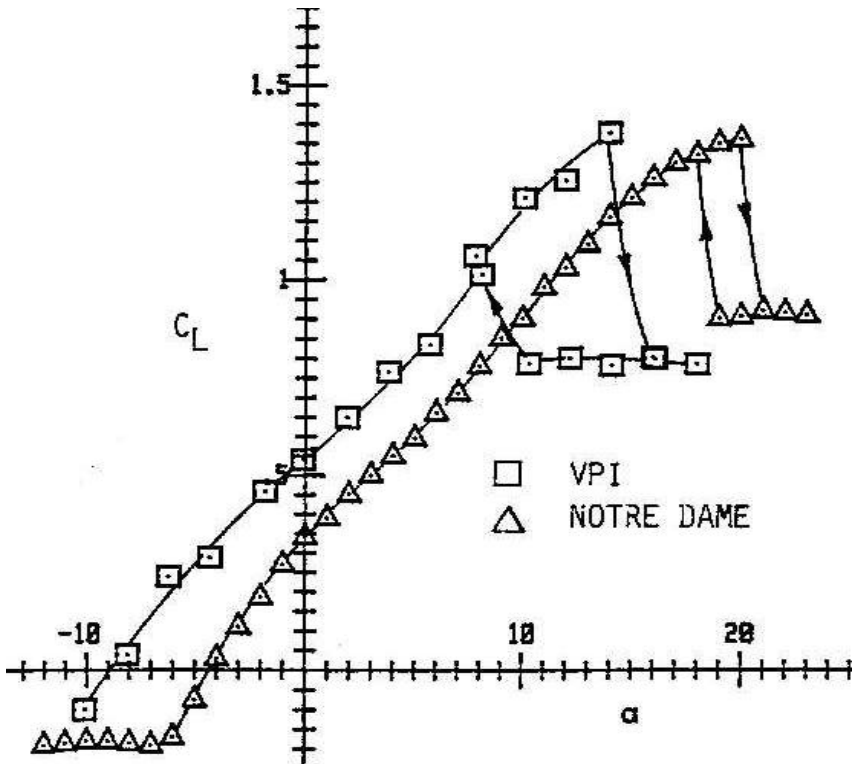

Fig 1.6 Comparison of data[2] for FX63-137, AR=4, Re=100,000 (Figure taken from Ref 2)

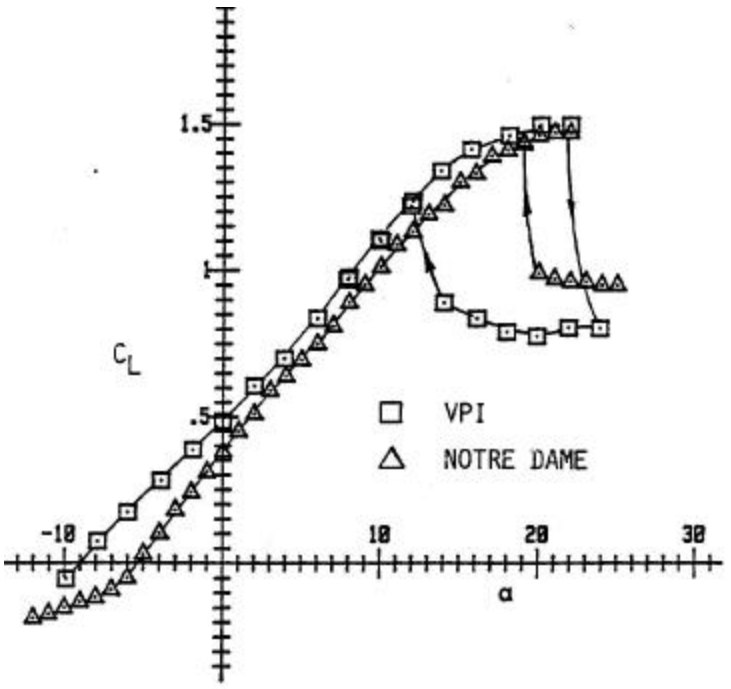

Fig 1.7 Comparison of data for FX63-137, AR=4, Re=200,000
(Figure used from ref. 2)

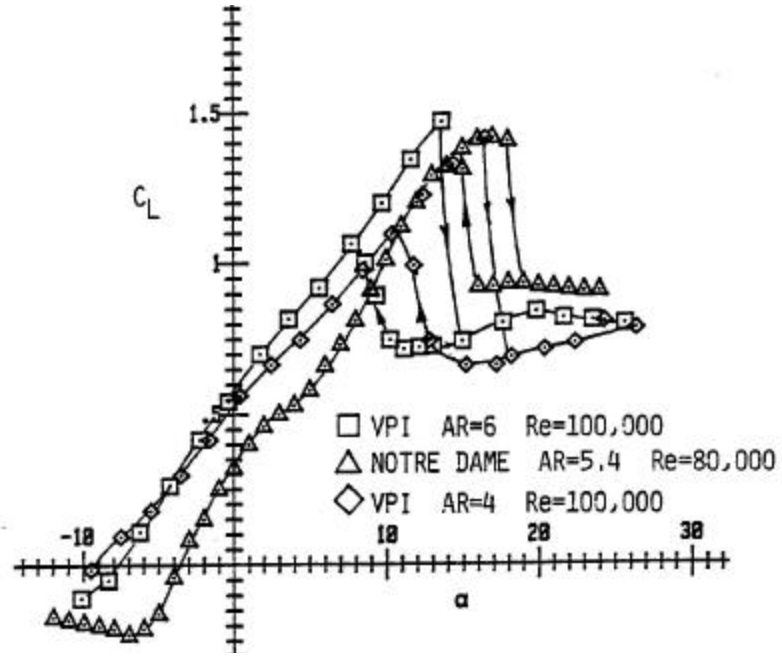

Fig 1.8 Comparison of VPI and Notre Dame data[2] for FX63-137
(Figure used from ref. 2)

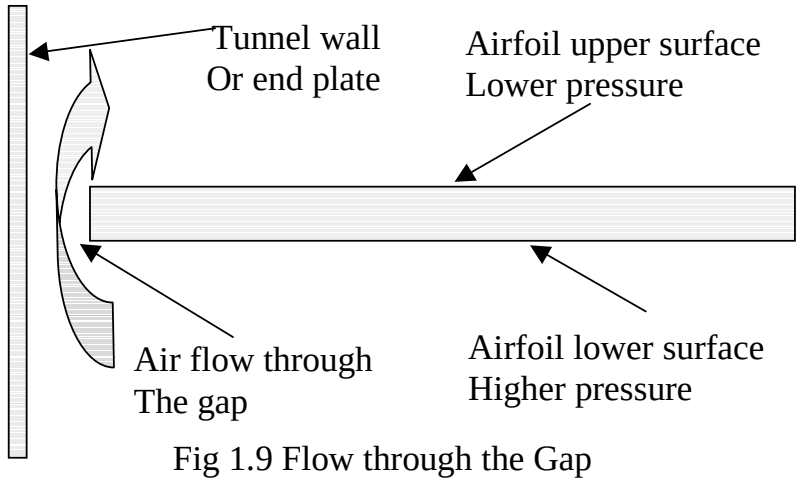

Fig 1.9 Flow through the Gap

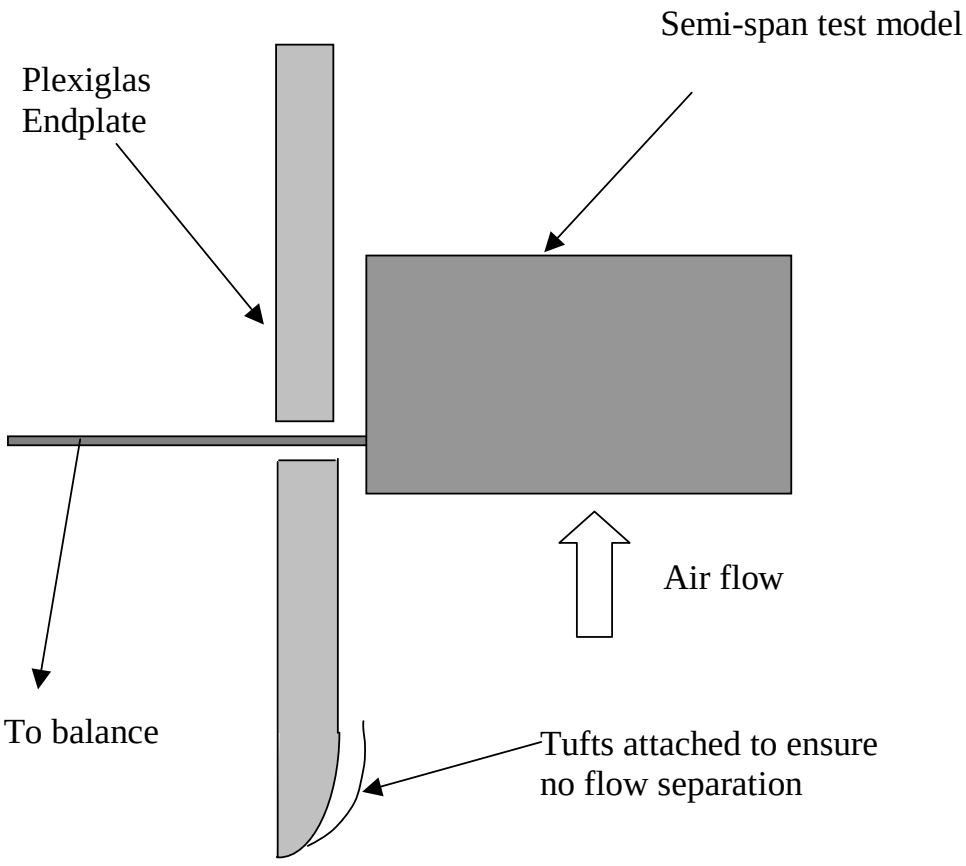

Fig 1.10 End plate/wing sectional view

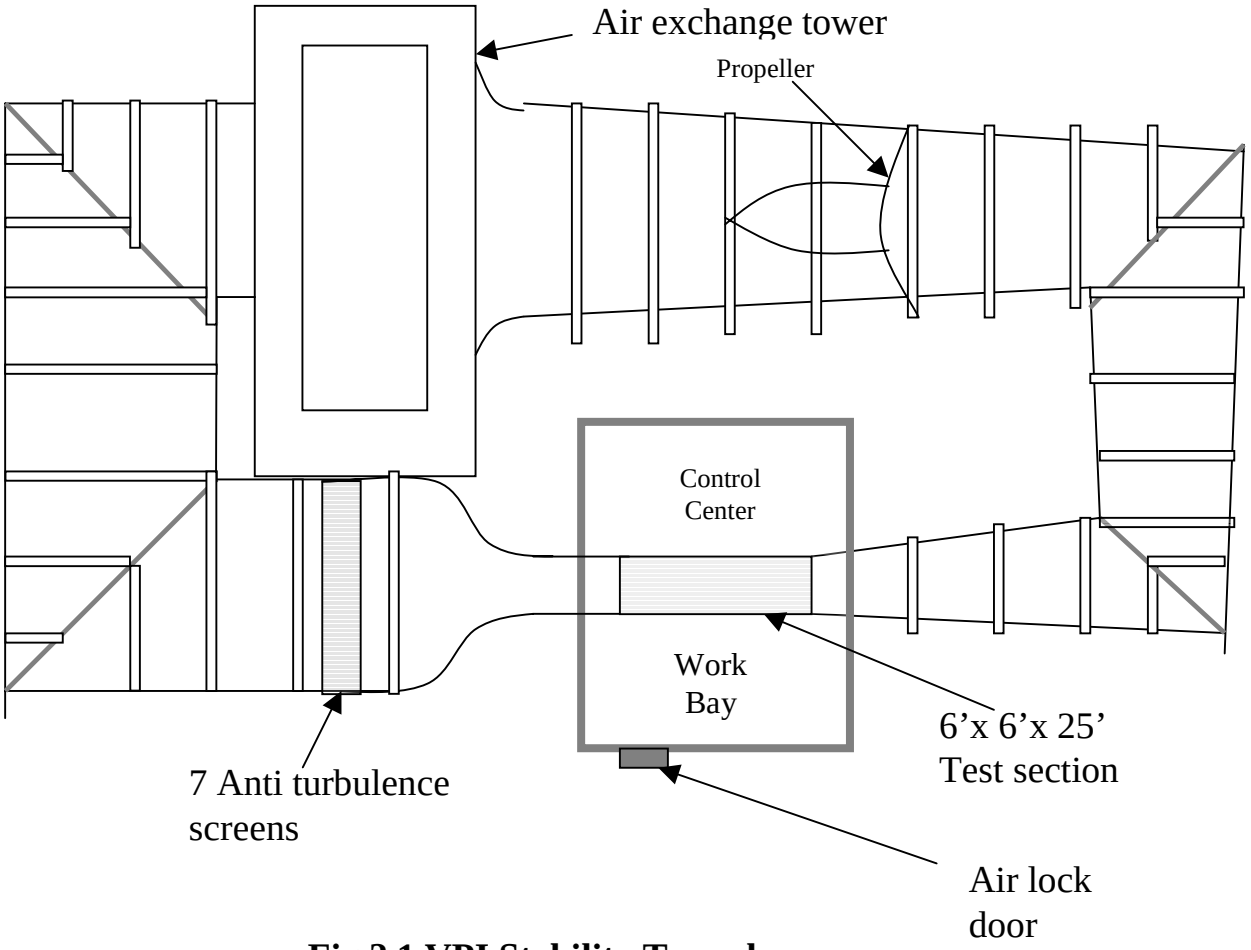

Fig 2.1 VPI Stability Tunnel

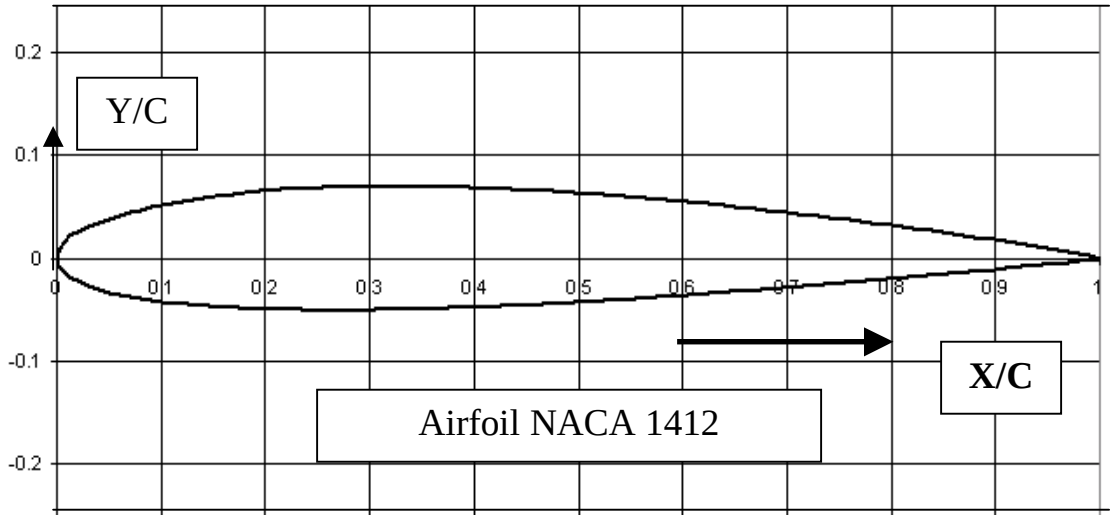

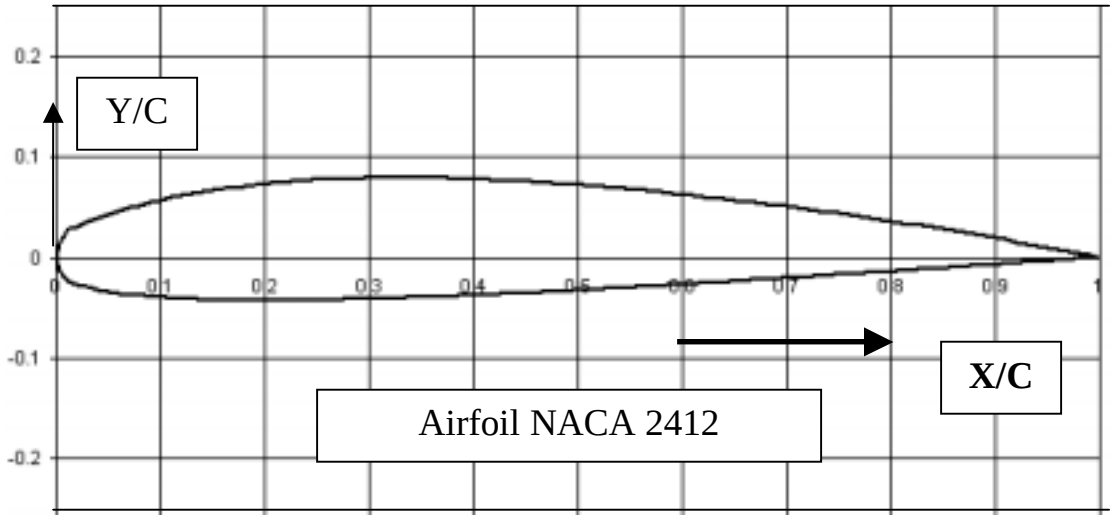

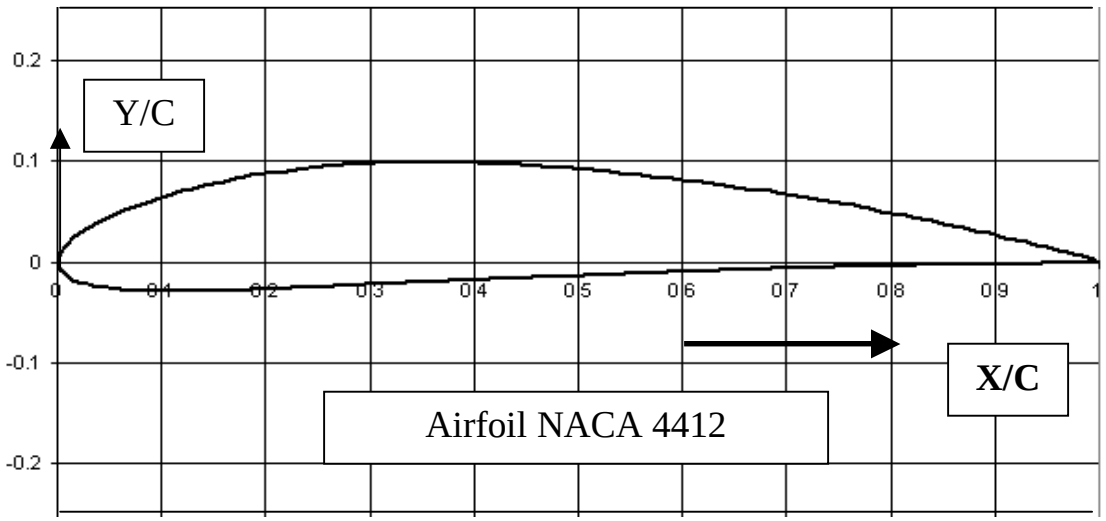

Fig 2.2 Airfoils Shapes Tested

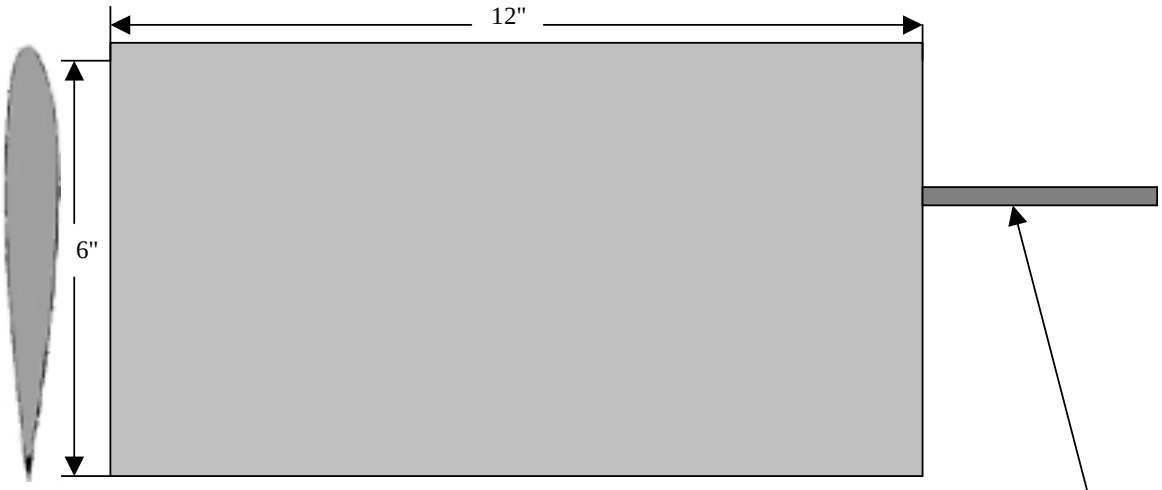

Force measurement models

Model Supporting spar

Location of
Pressure ports

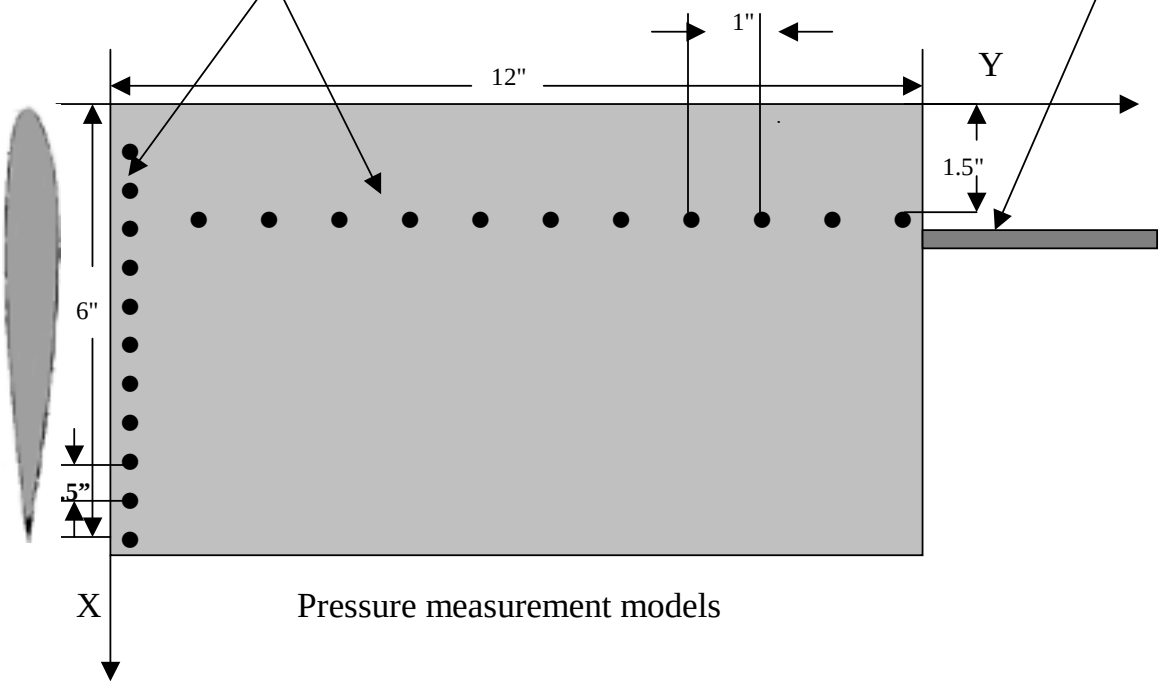

Pressure measurement models

Fig 2.3 Schematic diagram of the models and location of pressure ports

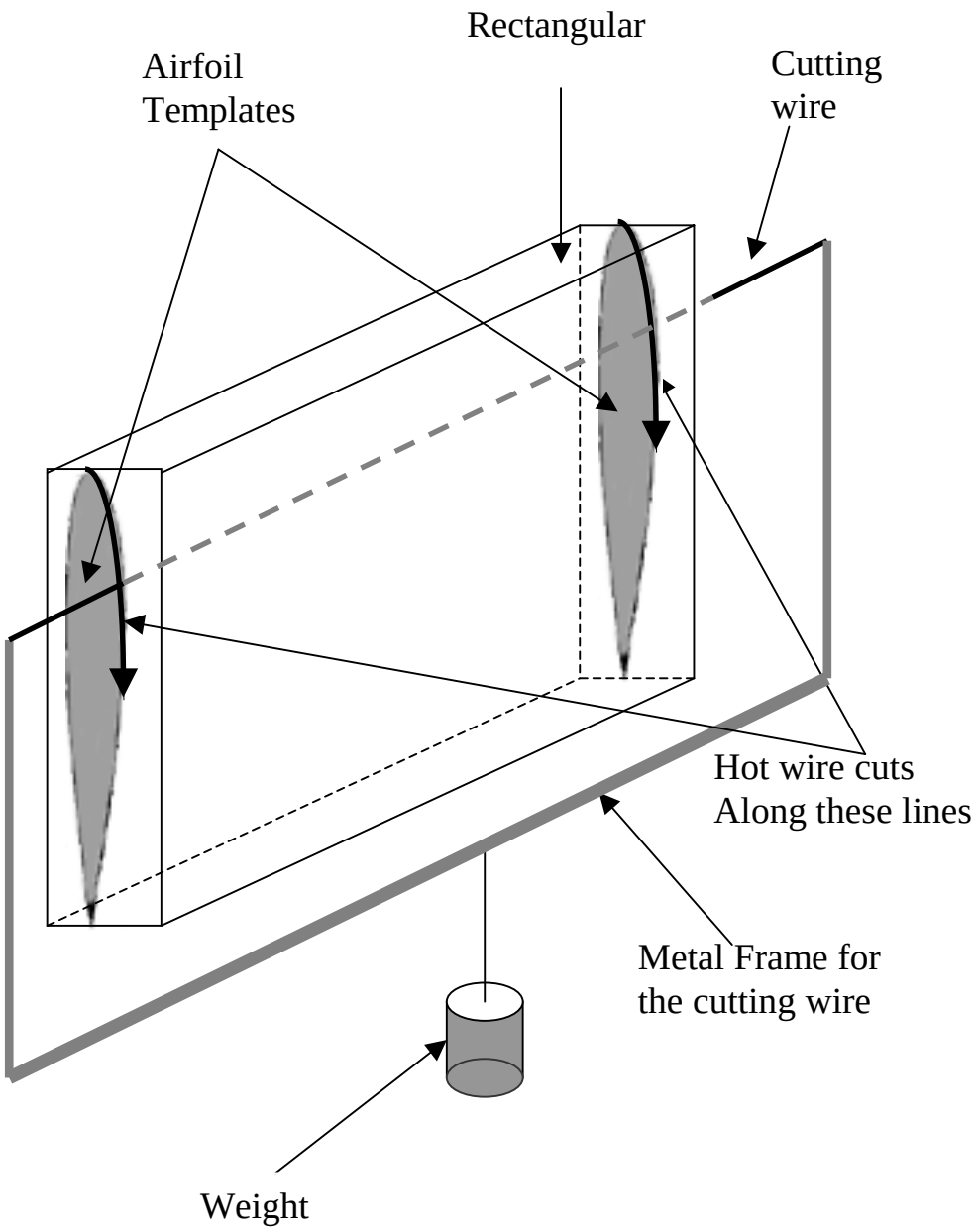

Figure 2.4 Hot wire cutting arrangement for the foam core.

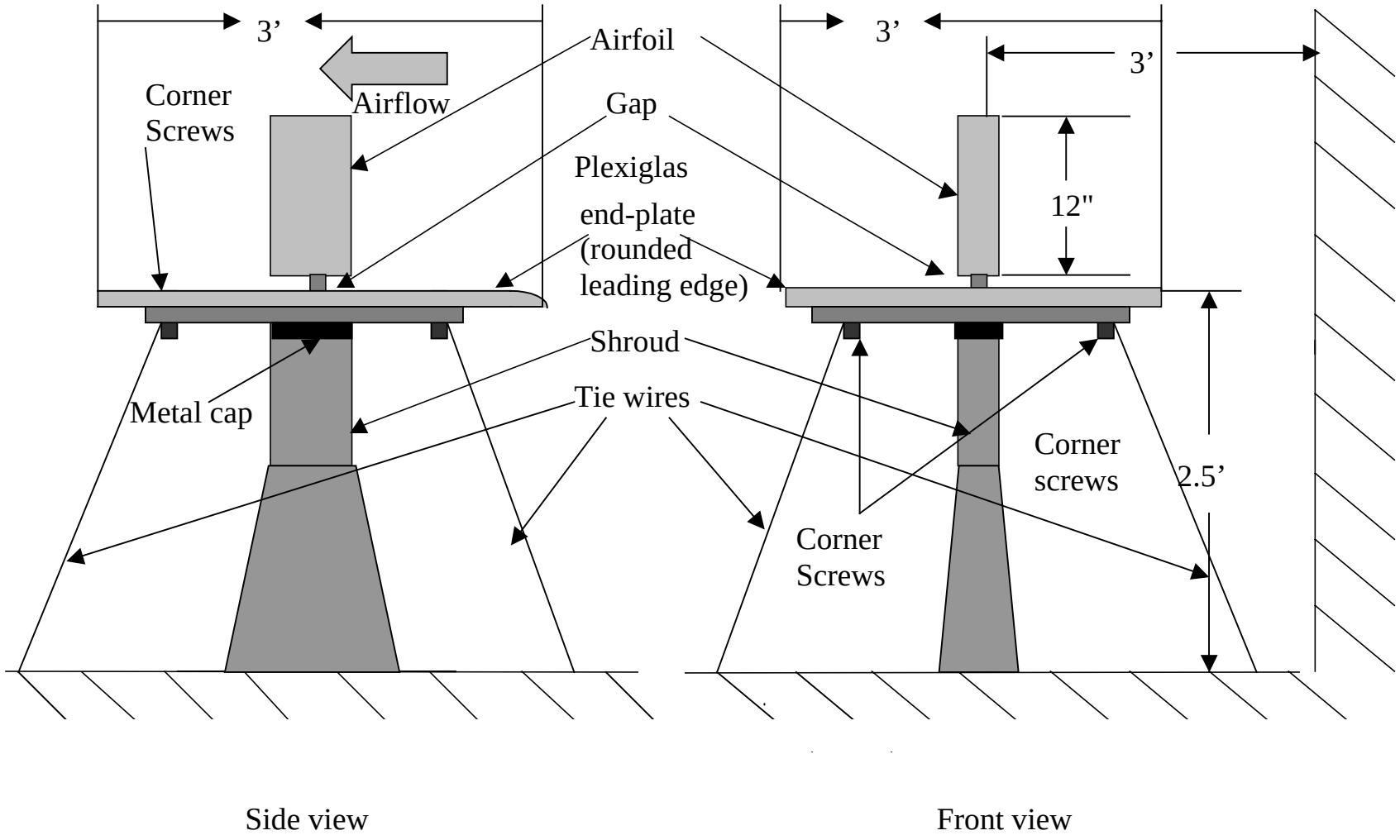

Fig 2.5 Model support for force measurements

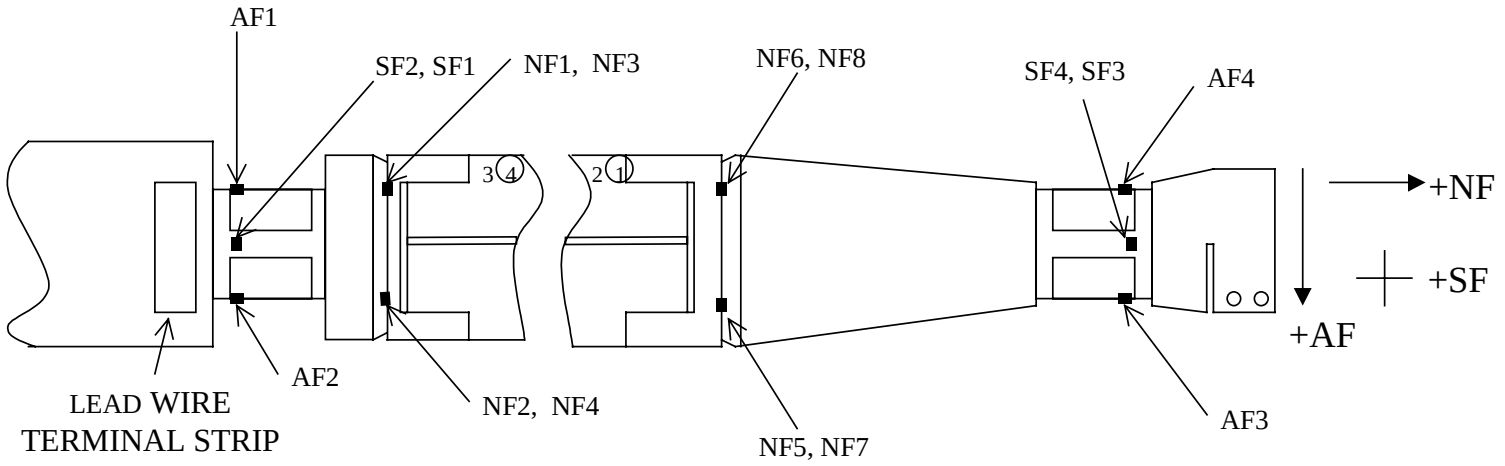

Location of strain gauges for Axial (AF), Side (SF) and Normal (NF) forces (above) bridge arrangements (bellow)

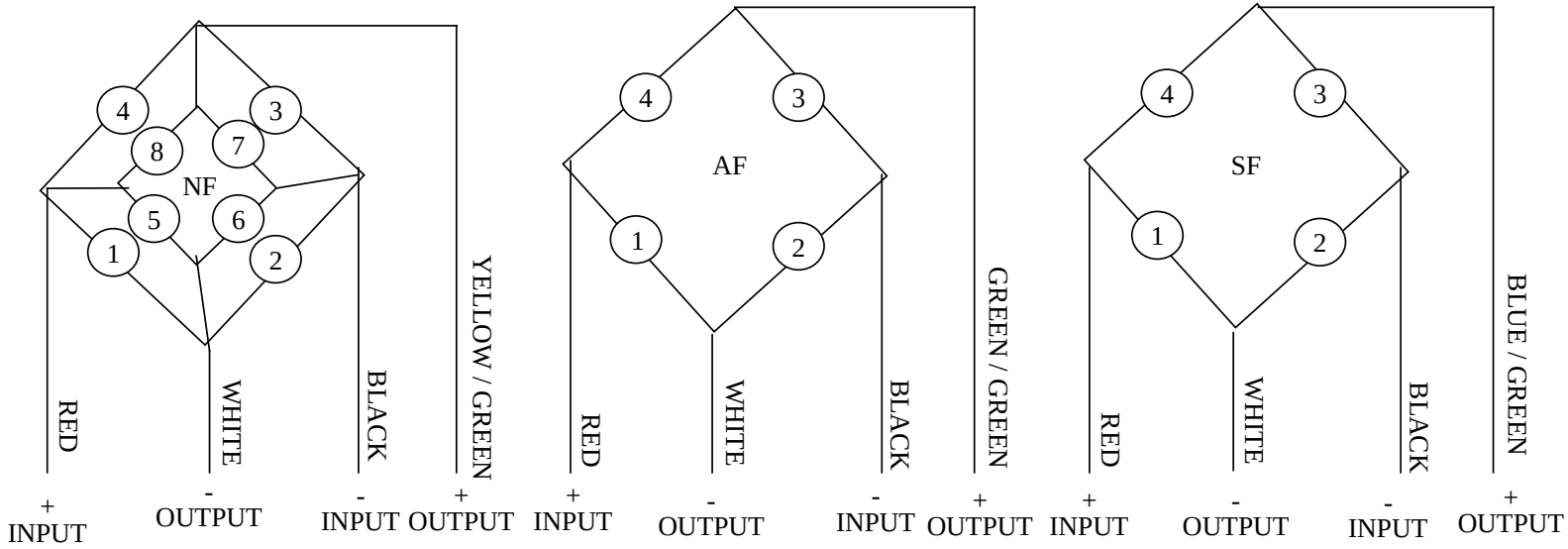

Fig 2.6 Schematic diagram of Strain Gauge Balance SR-1

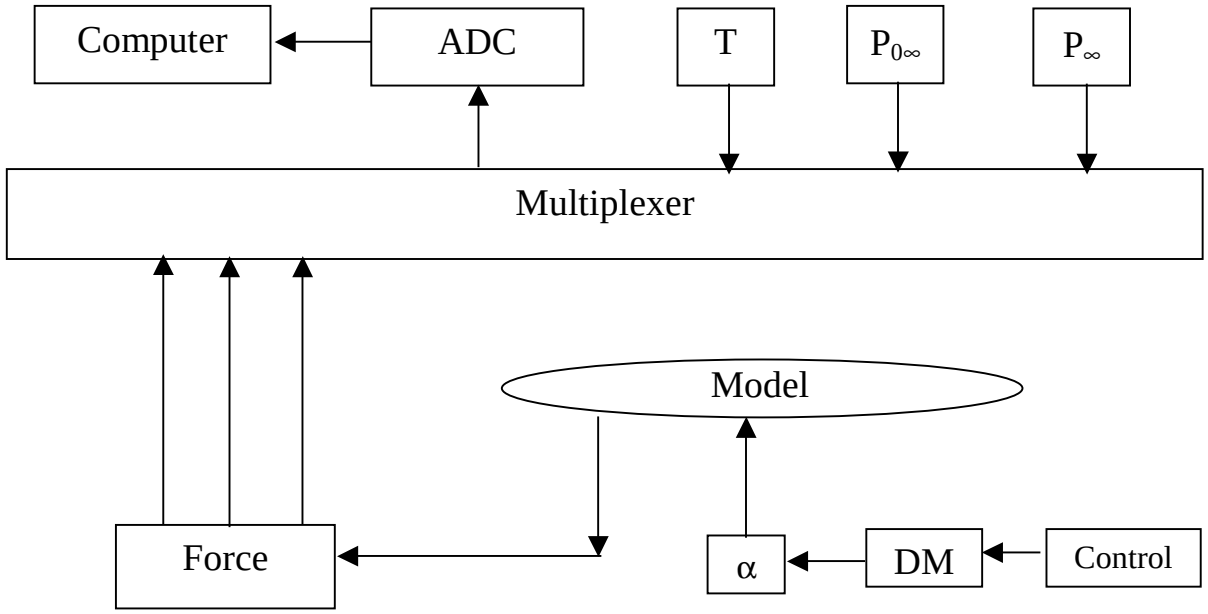

Fig 2.7 Block Diagram for data acquisition system

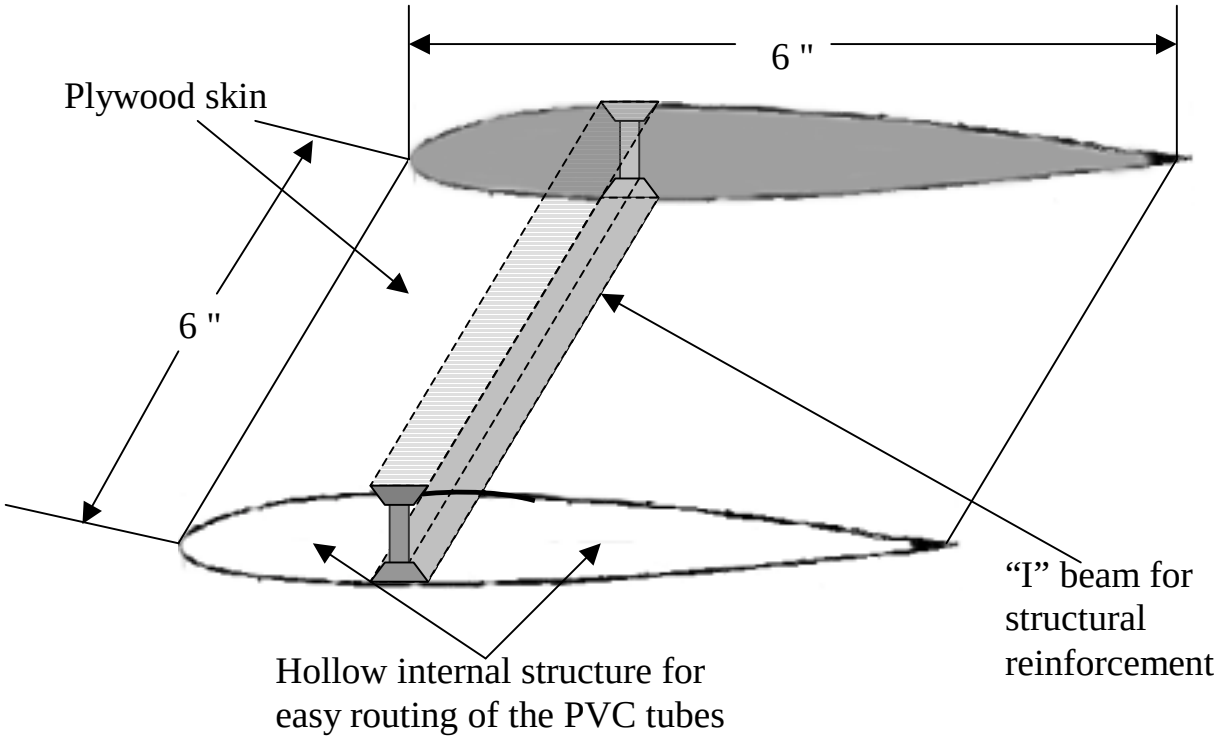

Fig 2.8 Schematic diagram of pressure measurement models

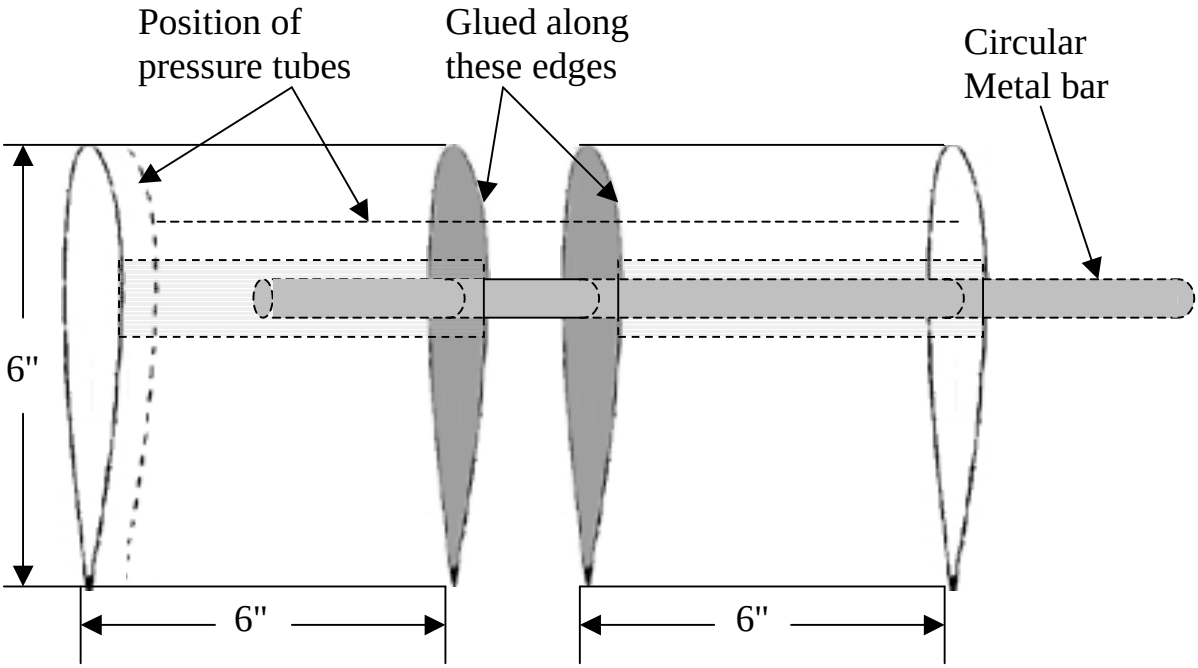

Fig 2.9 Construction of Pressure measurement models

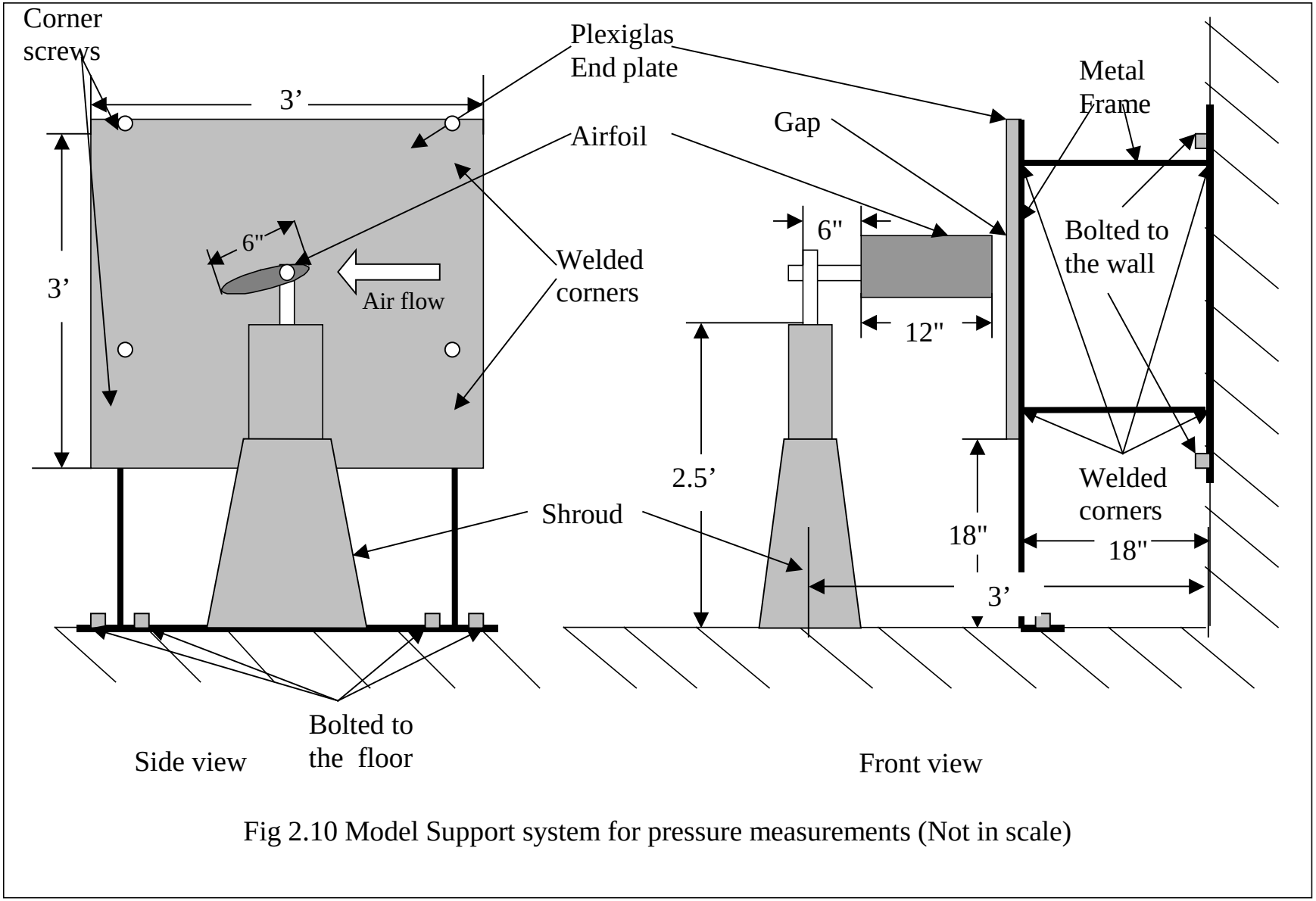

Fig 2.10 Model Support system for pressure measurements (Not in scale)

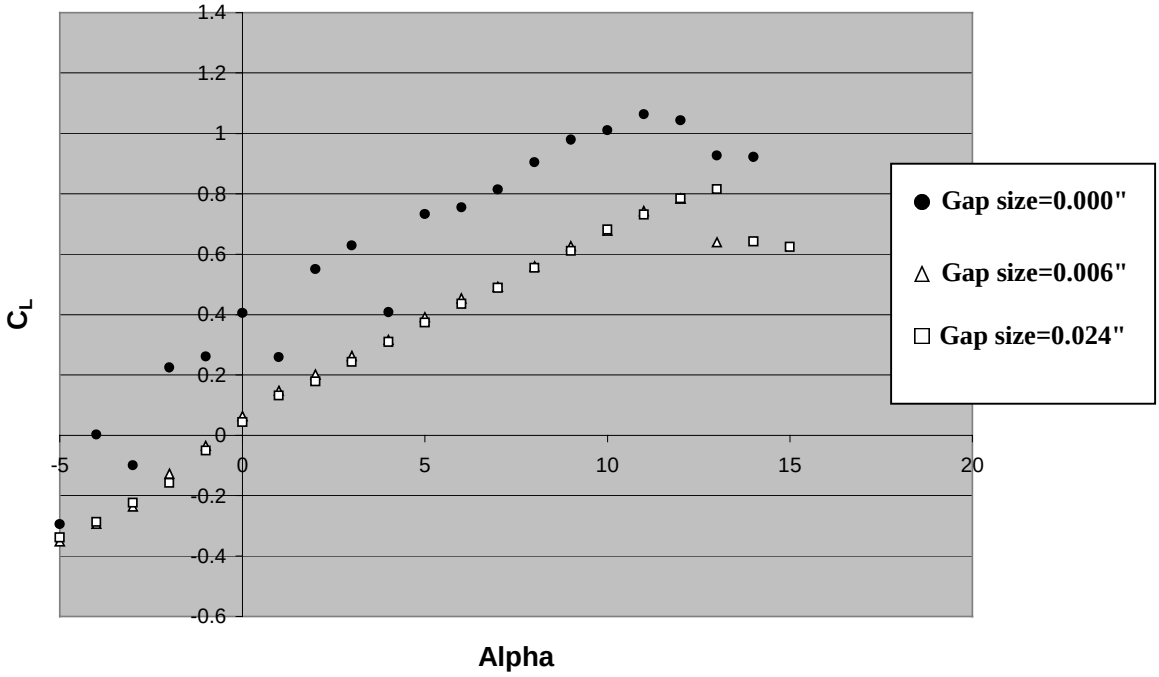

Fig 3.1 C_L vs. α for airfoil NACA 1412 at Reynolds No = 100,000

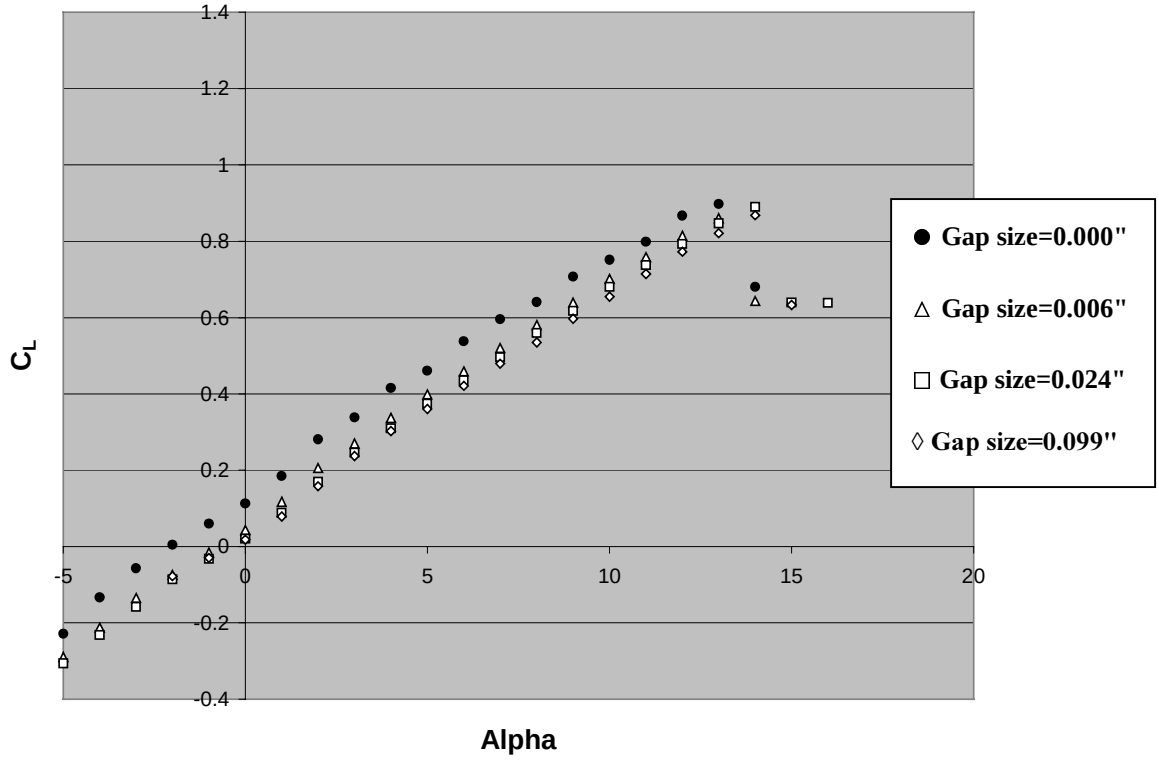

Fig 3.2 C_L vs. α for airfoil NACA 1412 at Reynolds No = 200,000

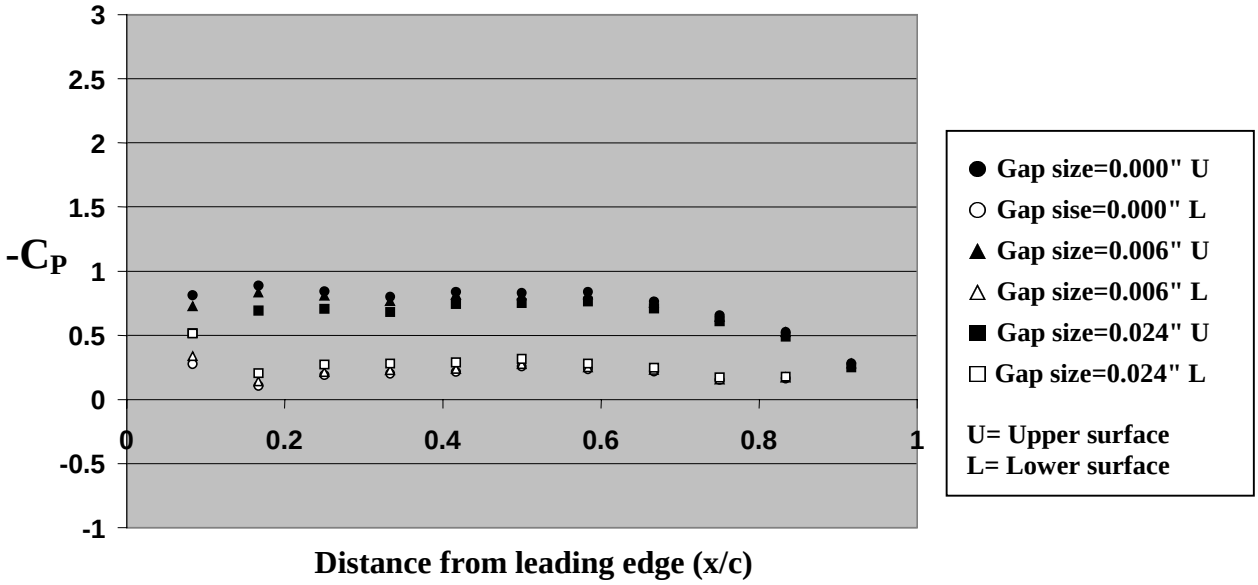

Fig 3.3 Chord wise pressure distribution (NACA 1412) at $\alpha=0^0$, Re=200,000

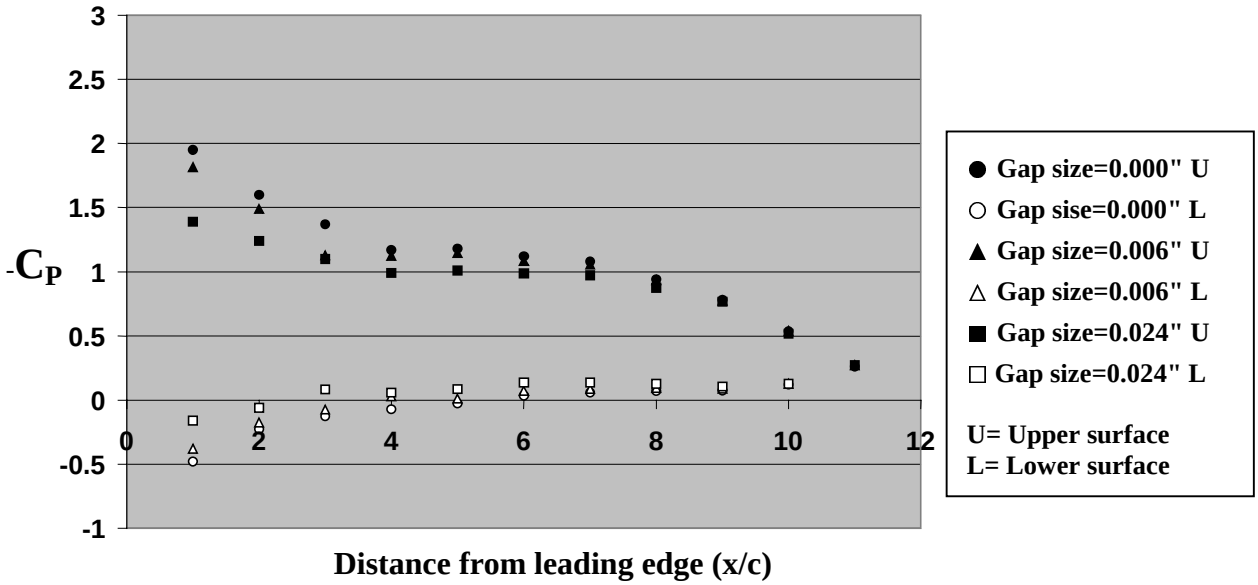

Fig 3.4 Chord wise pressure distribution (NACA 1412) at $\alpha=5^0$, Re=200,000

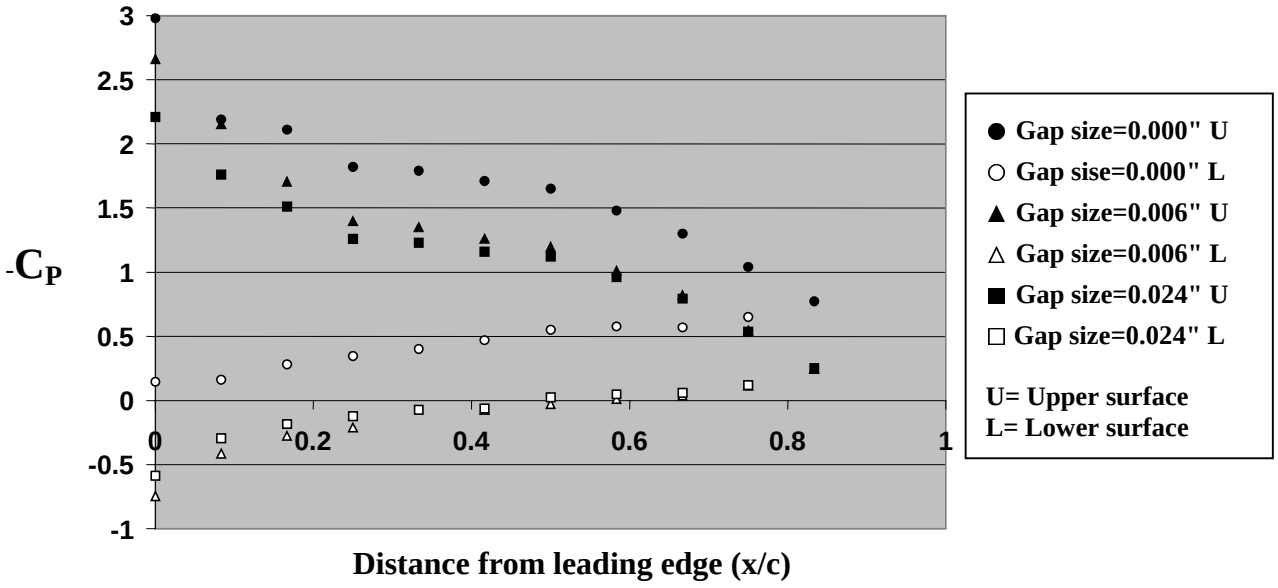

Fig 3.5 Chord wise pressure distribution (NACA 1412) at $\alpha=10^0$, Re=200,000

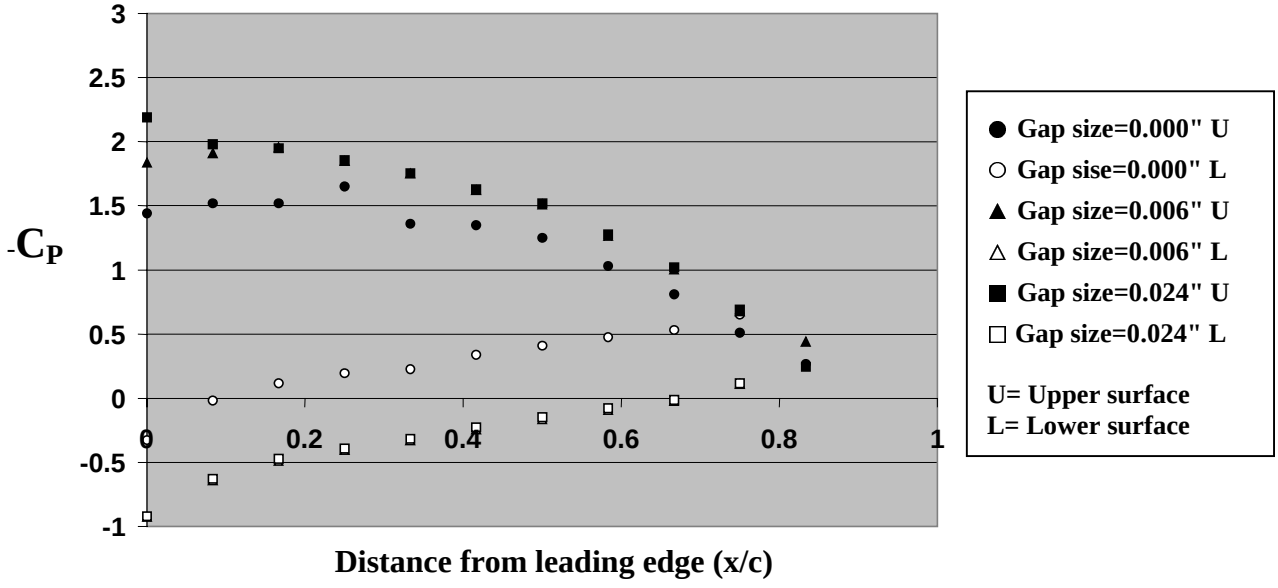

Fig 3.6 Chord wise pressure distribution (NACA 1412) at $\alpha=15^0$, Re=200,000

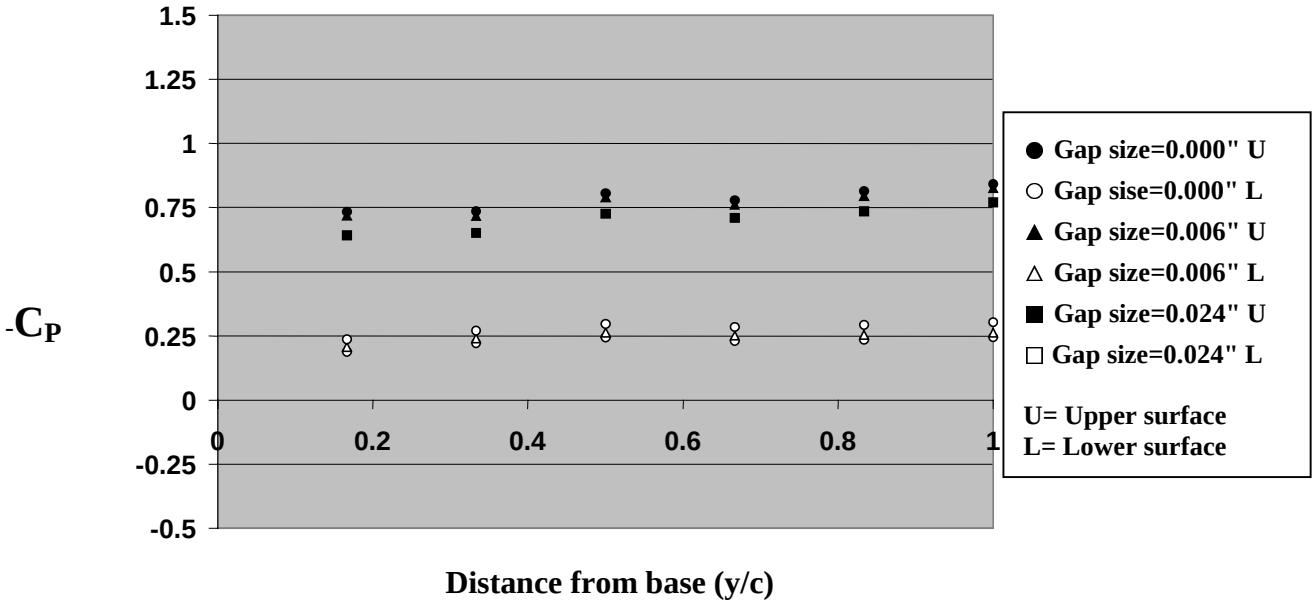

Fig 3.7 Span wise pressure distribution (NACA 1412) at $\alpha=0^0$, Re=200,000

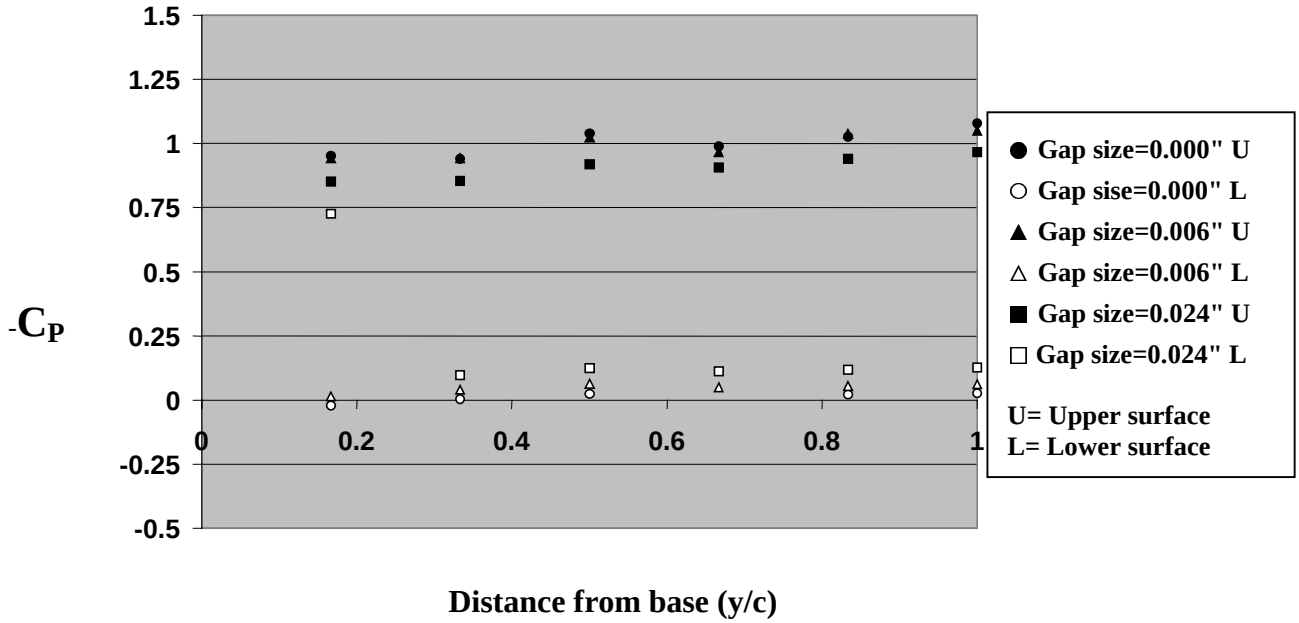

Fig 3.8 Span wise pressure distribution (NACA 1412) at $\alpha=5^0$, Re=200,000

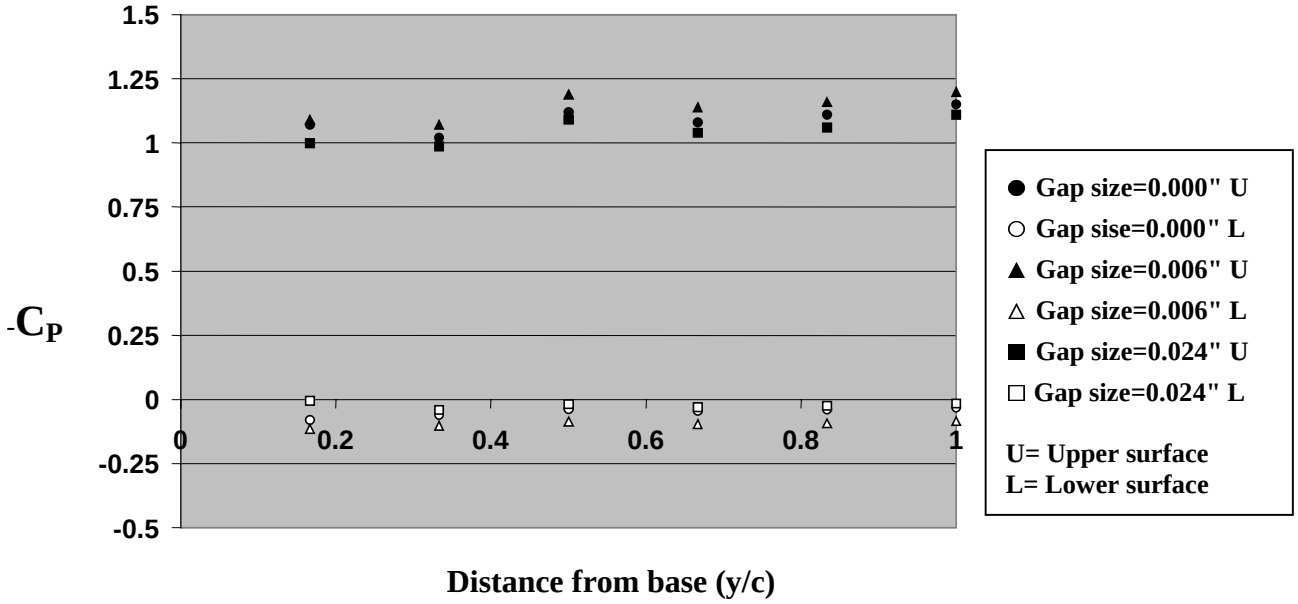

Fig 3.9 Span wise pressure distribution (NACA 1412) at $\alpha=10^0$, Re=200,000

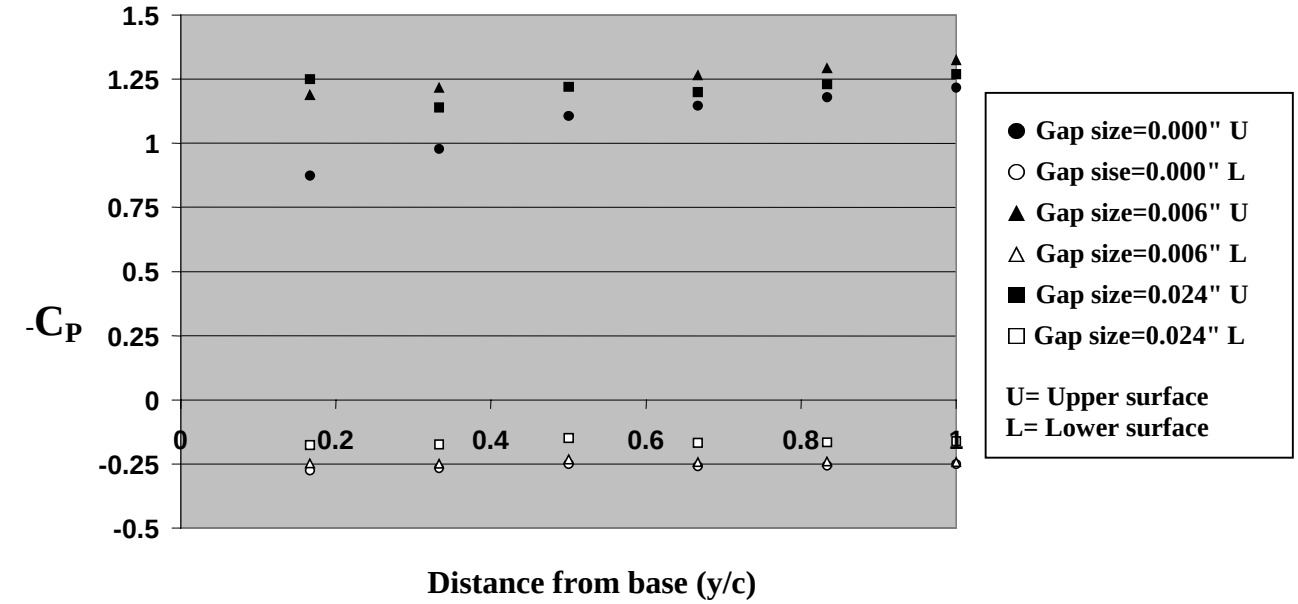

Fig 3.10 Span wise pressure distribution (NACA 1412) at $\alpha=15^0$, Re=200,000

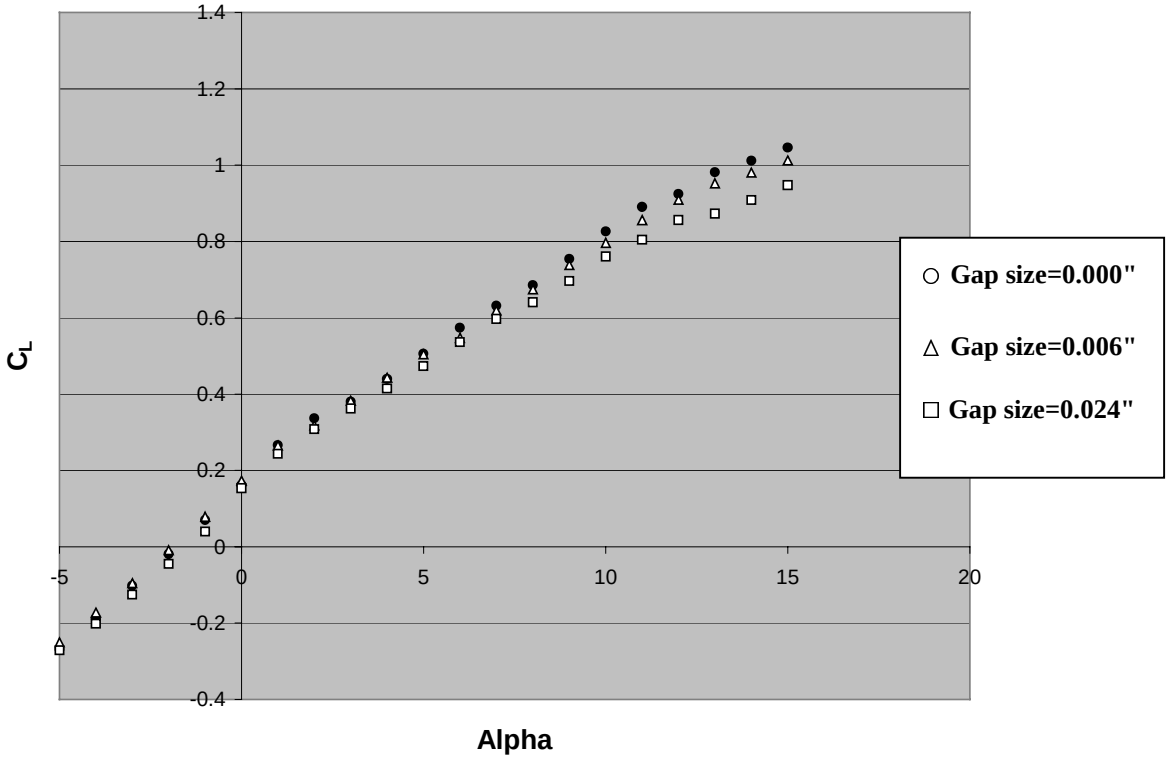

Fig 3.11 C_L vs. α for airfoil NACA 2412 at Reynolds No = 100,000

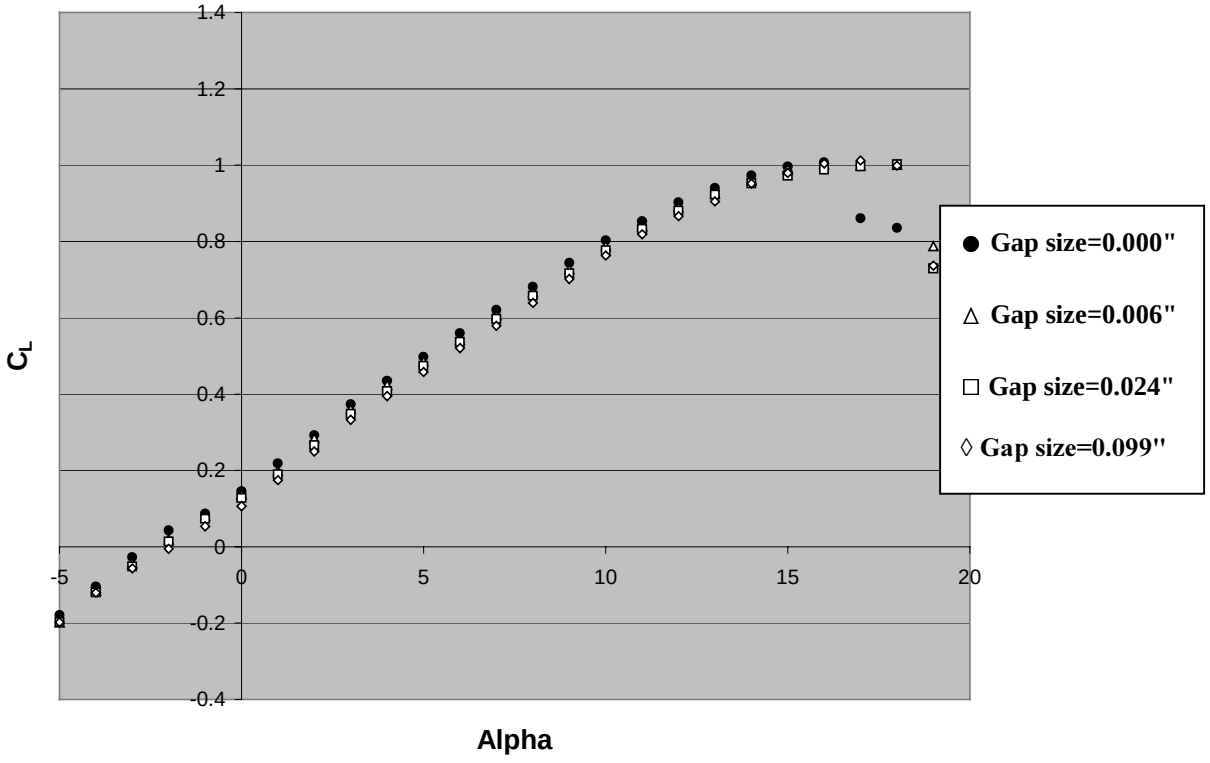

Fig 3.12 C_L vs. α for airfoil NACA 2412 at Reynolds No = 200,000

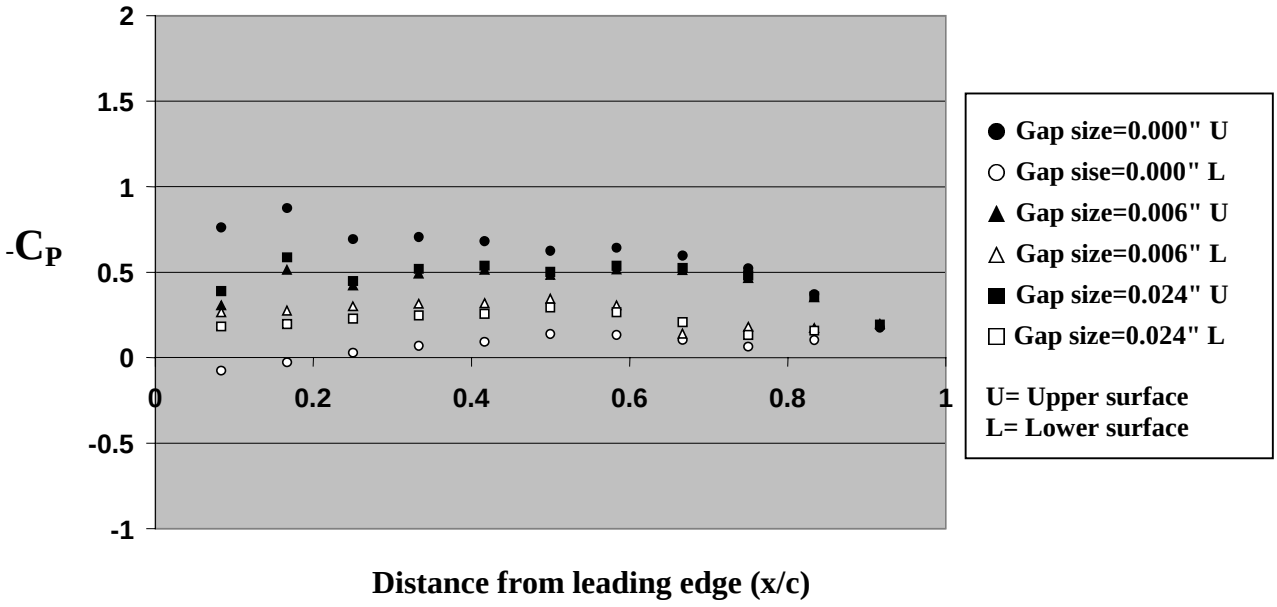

Fig 3. 13 Chord wise pressure distribution (NACA 2412) at $\alpha=0^0$, Re=200,000

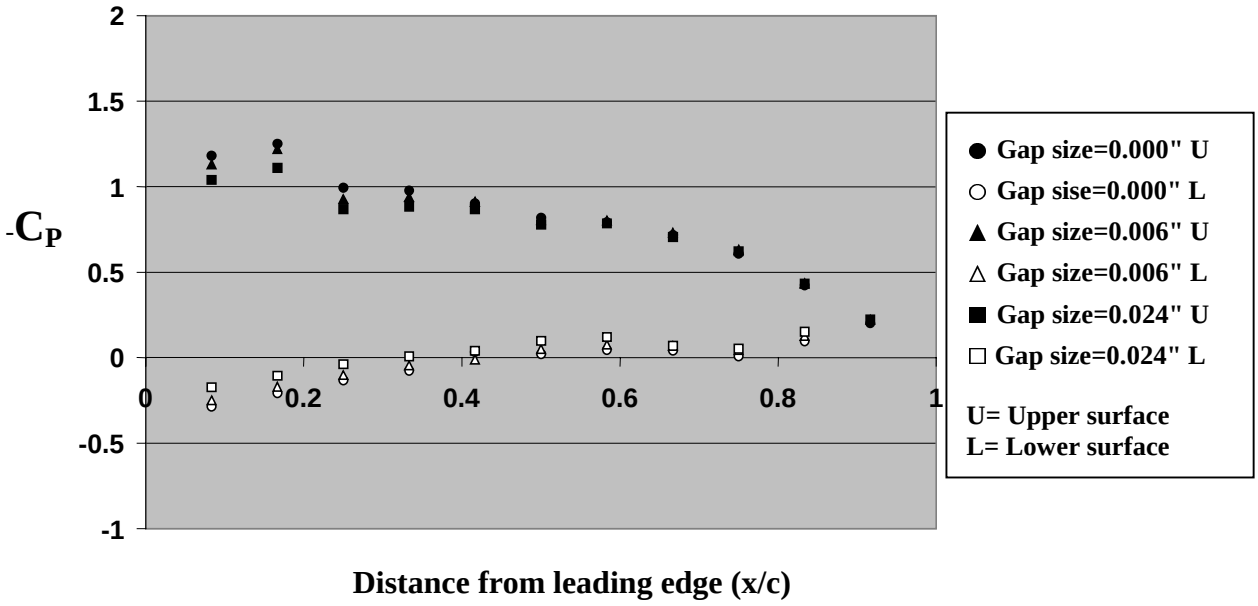

Fig 3.14 Chord wise pressure distribution (NACA 2412) at $\alpha=5^0$, Re=200,000

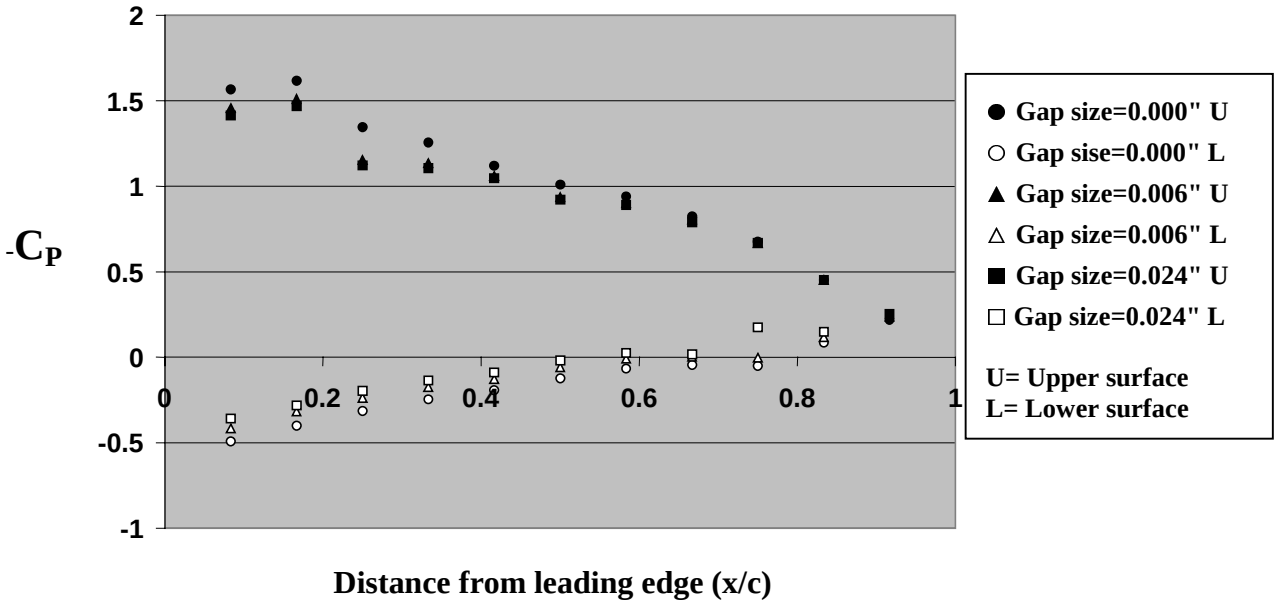

Fig 3.15 Chord wise pressure distribution (NACA 2412) at $\alpha=10^0$, Re=200,000

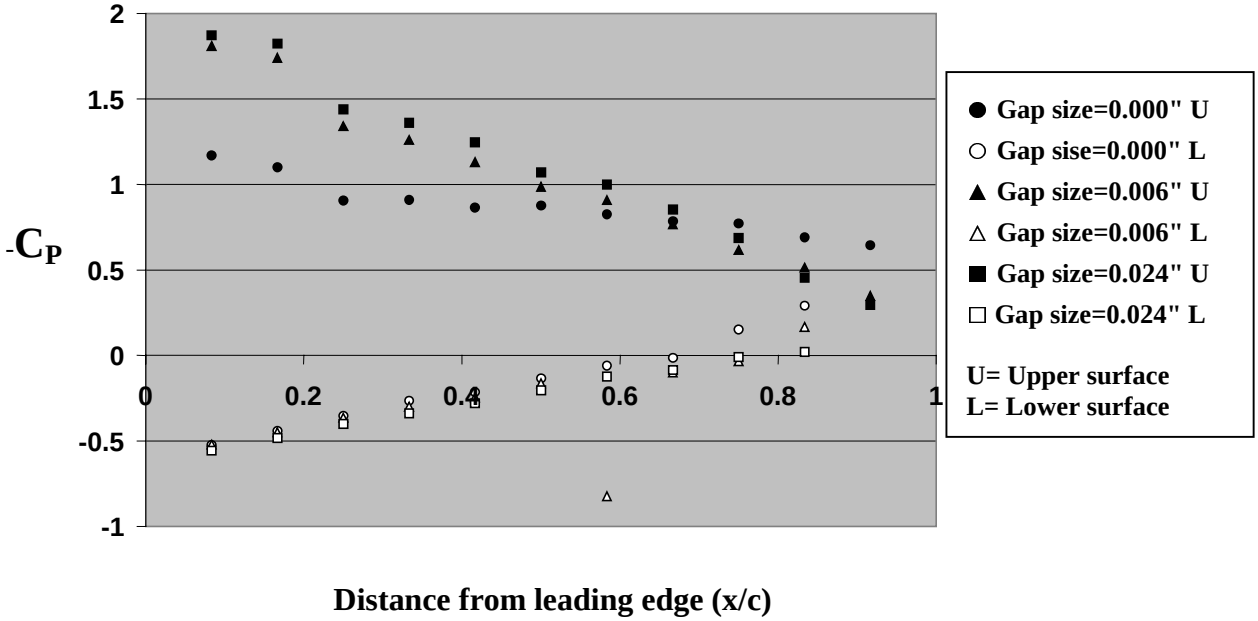

Fig 3.16 Chord wise pressure distribution (NACA 2412) at $\alpha=15^0$, Re=200,000

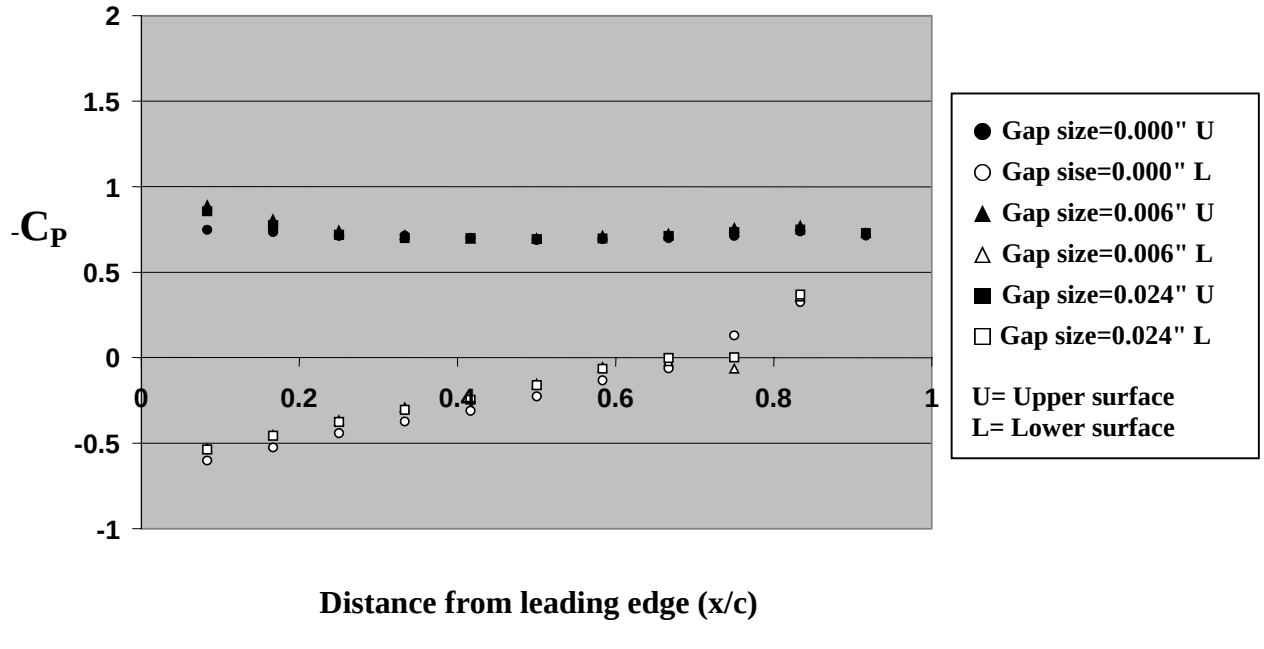

Fig 3.17 Chord wise pressure distribution (NACA 2412) at $\alpha=20^0$, Re=200,000

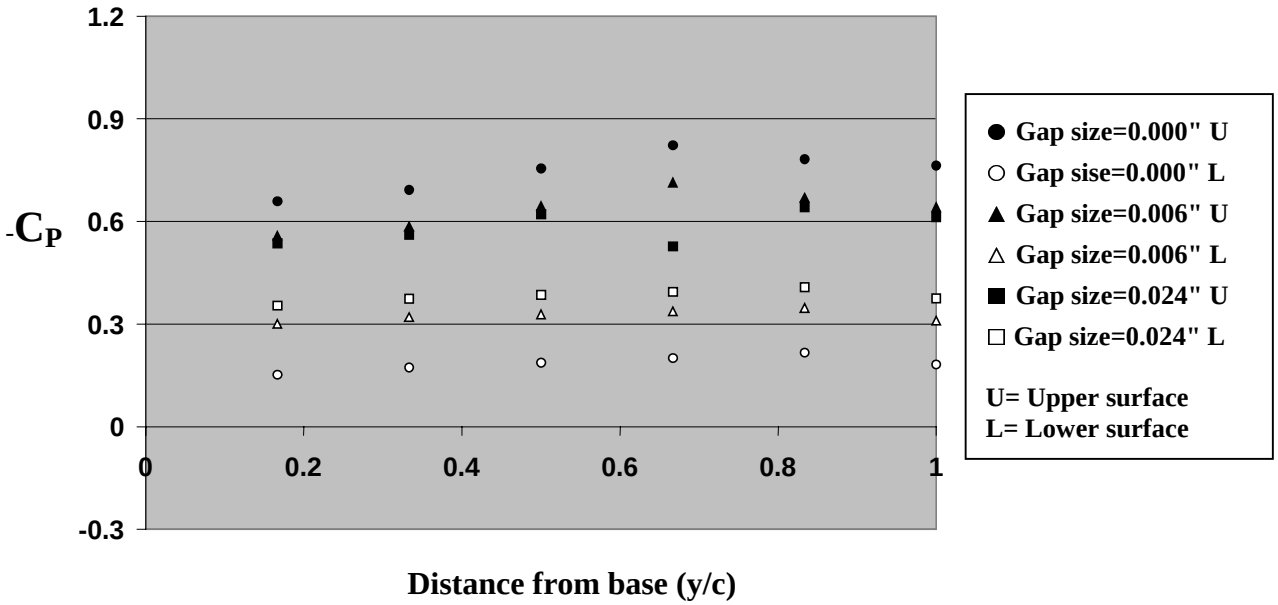

Fig 3.18 Span wise pressure distribution (NACA 2412) at $\alpha=0^0$, Re=200,000

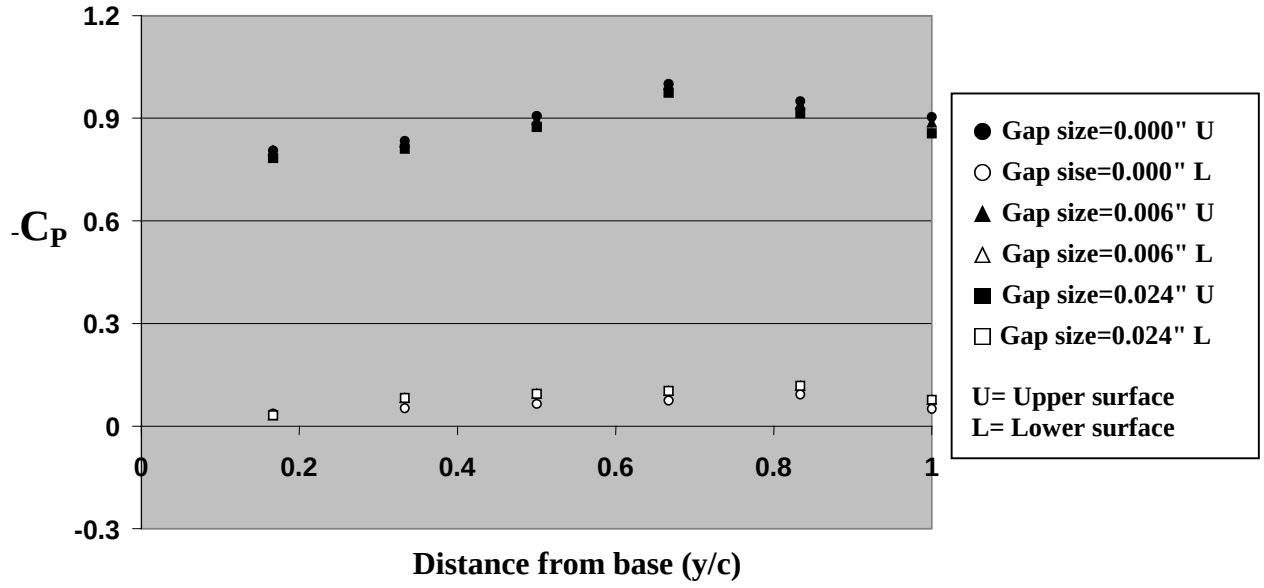

Fig 3.19 Span wise pressure distribution (NACA 2412) at $\alpha=5^0$, Re=200,000

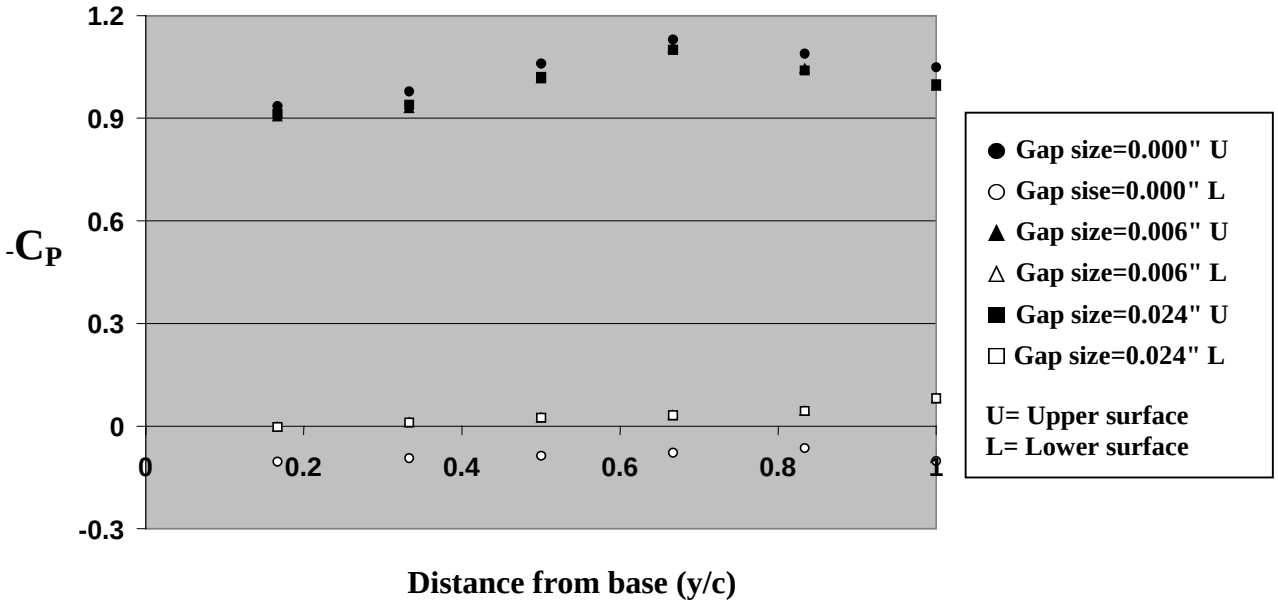

Fig 3.20 Span wise pressure distribution (NACA 2412) at $\alpha=10^0$, Re=200,000

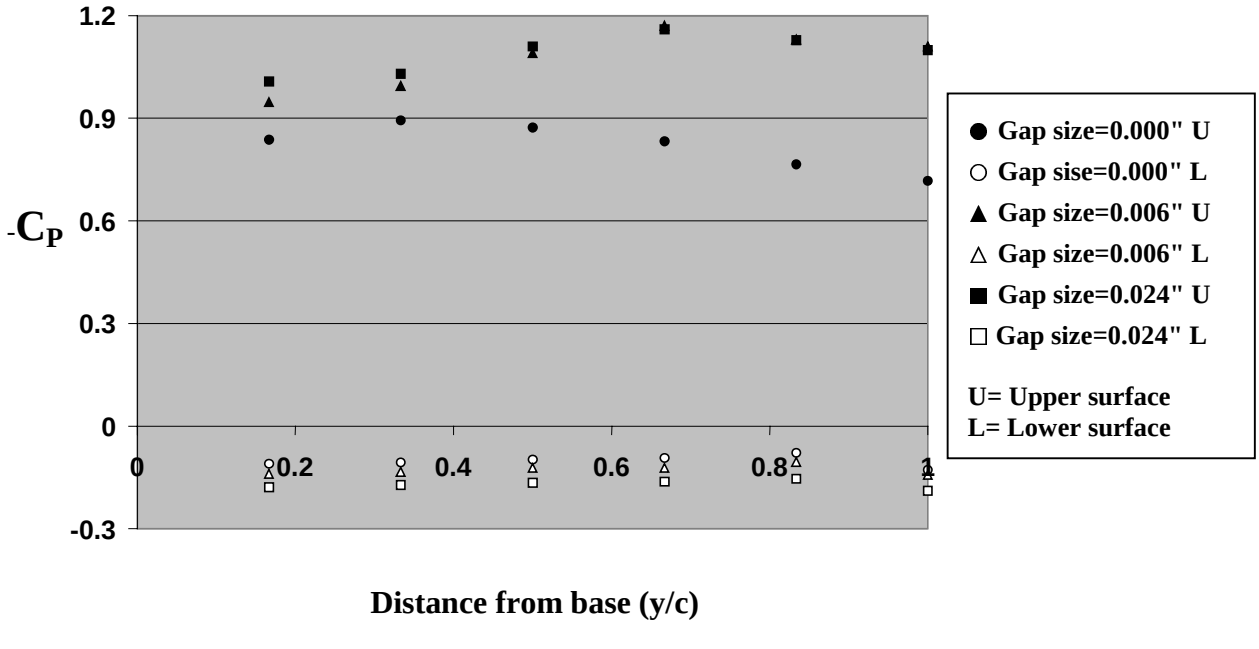

Fig 3.21 Span wise pressure distribution (NACA 2412) at $\alpha=15^0$, Re=200,000

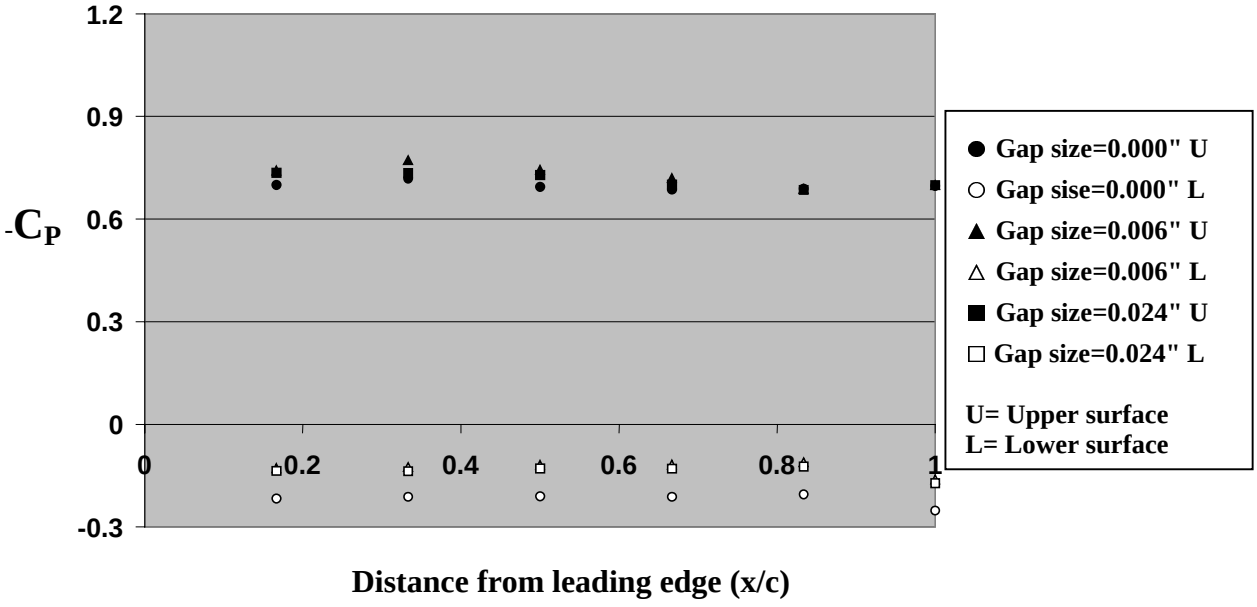

Fig 3.22 Span wise pressure distribution (NACA 2412) at $\alpha=20^0$, Re=200,000

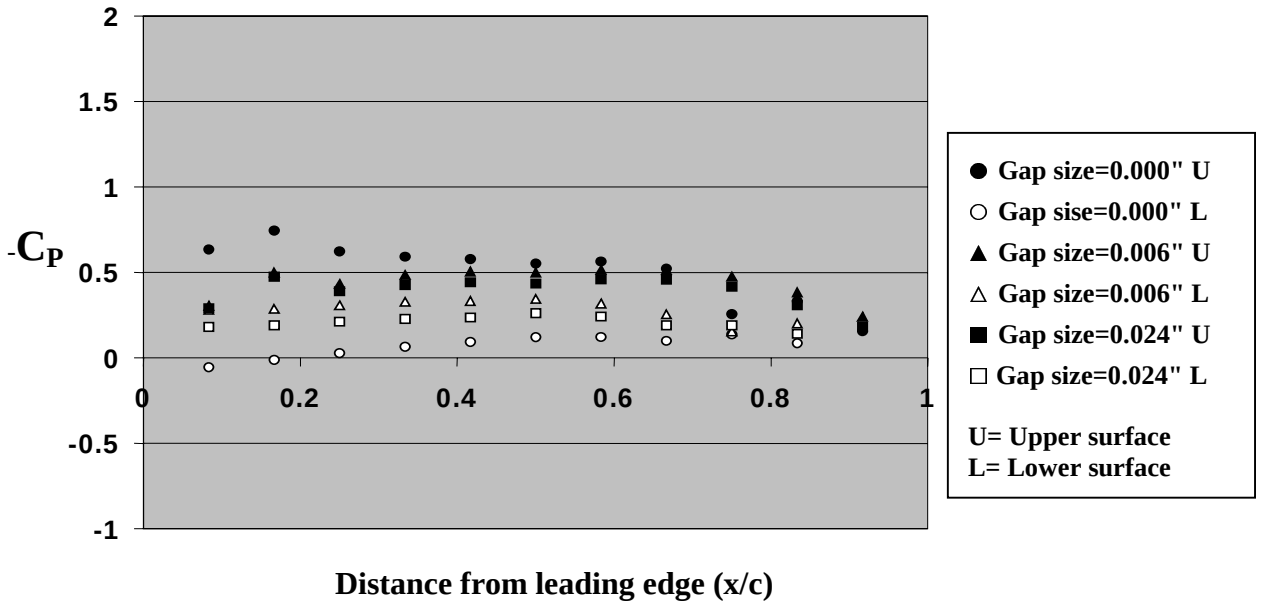

Fig 3.23 Chord wise pressure distribution (NACA 2412) at $\alpha=0^0$, Re=100,000

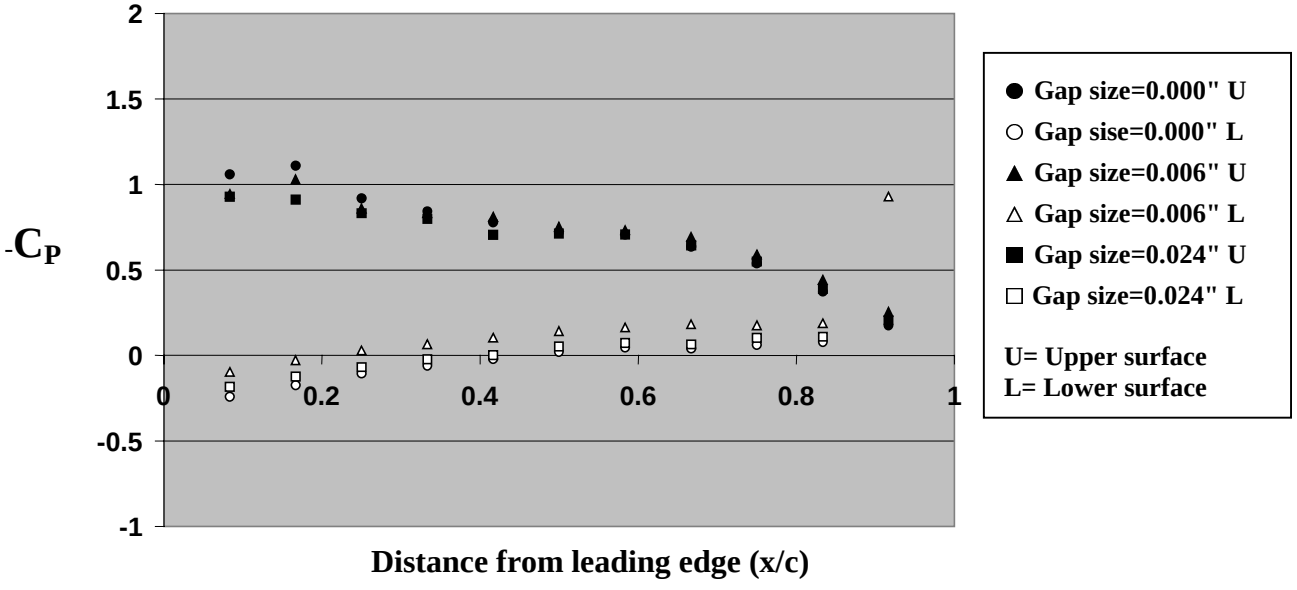

Fig 3.24 Chord wise pressure distribution (NACA 2412) at $\alpha=5^0$, Re=100,000

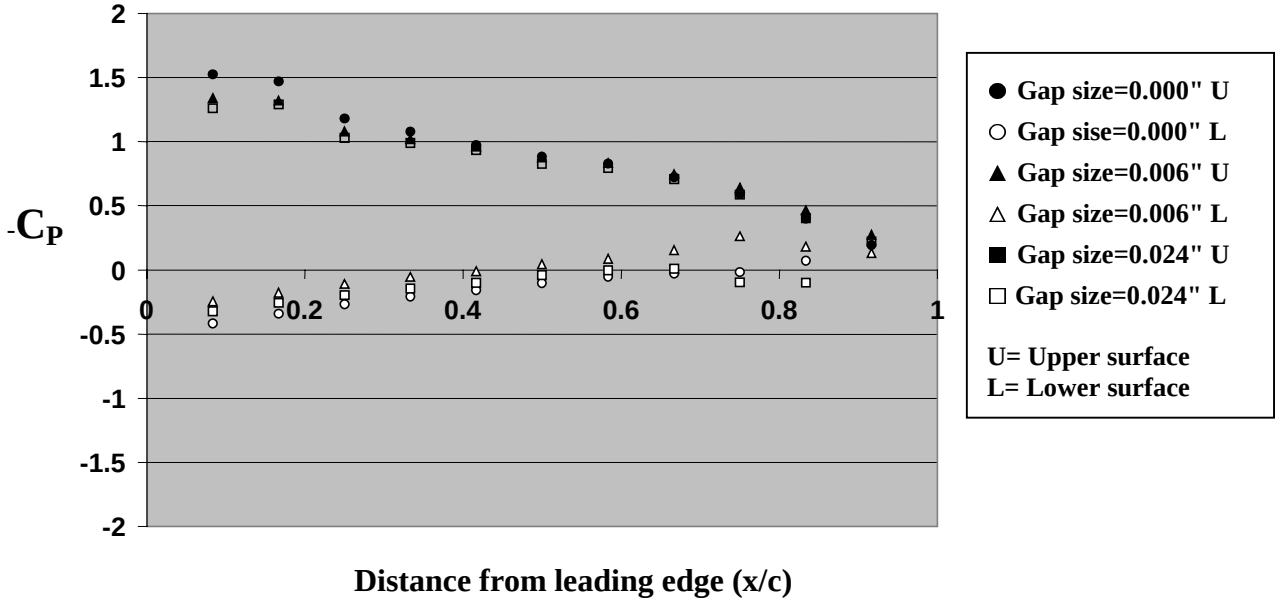

Fig 3.25 Chord wise pressure distribution (NACA 2412) at $\alpha=10^0$, Re=100,000

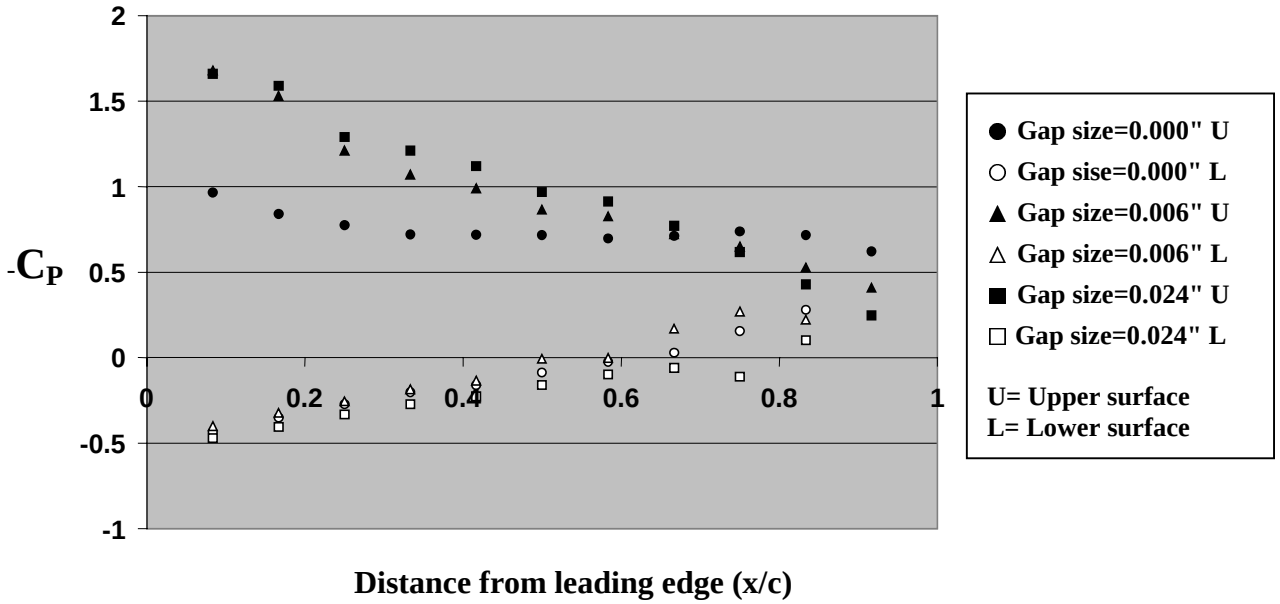

Fig 3.26 Chord wise pressure distribution (NACA 2412) at $\alpha=15^0$, Re=100,000

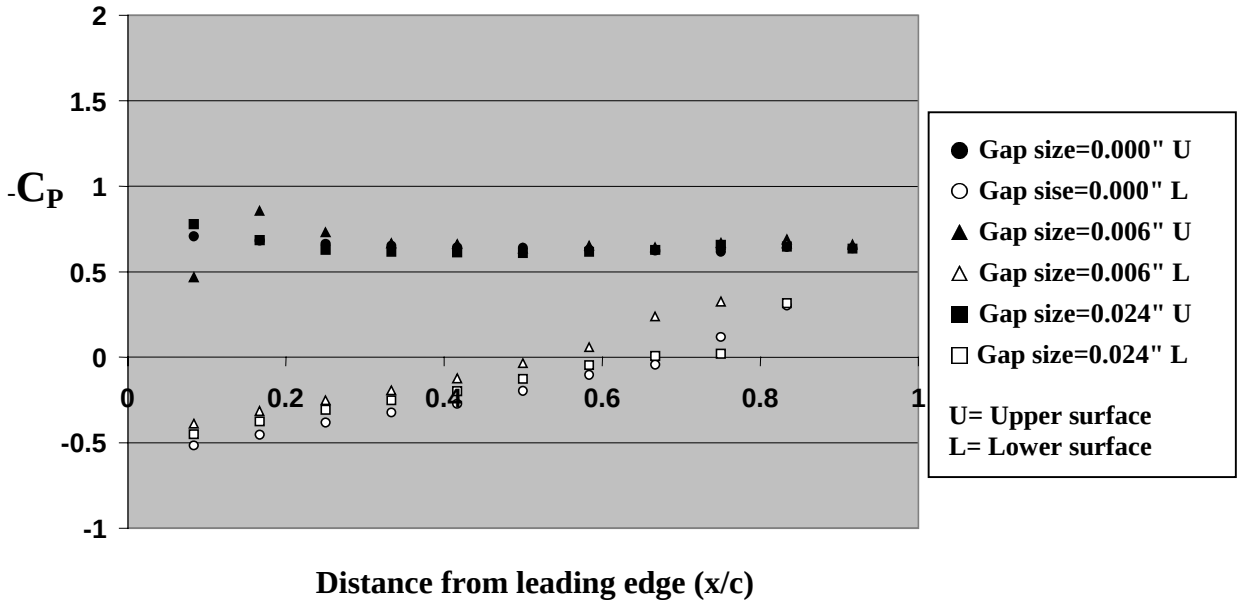

Fig 3.27 Chord wise pressure distribution (NACA 2412) at $\alpha=20^0$, Re=100,000

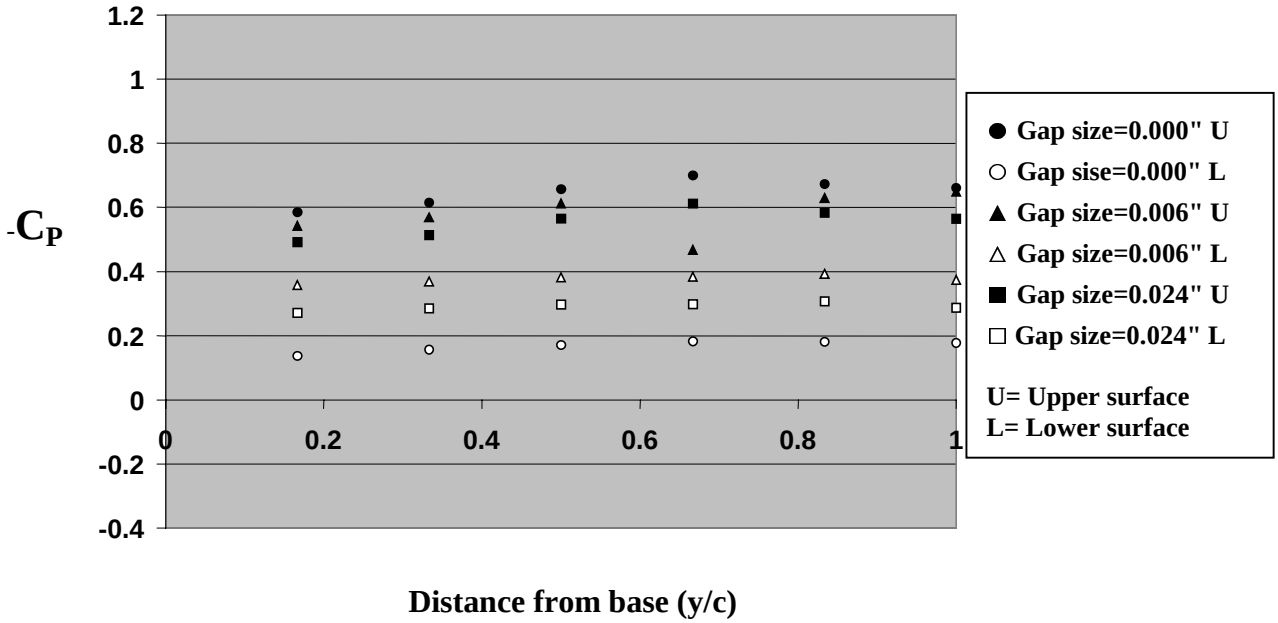

Fig 3.28 Span wise pressure distribution (NACA 2412) at $\alpha=0^0$, Re=100,000

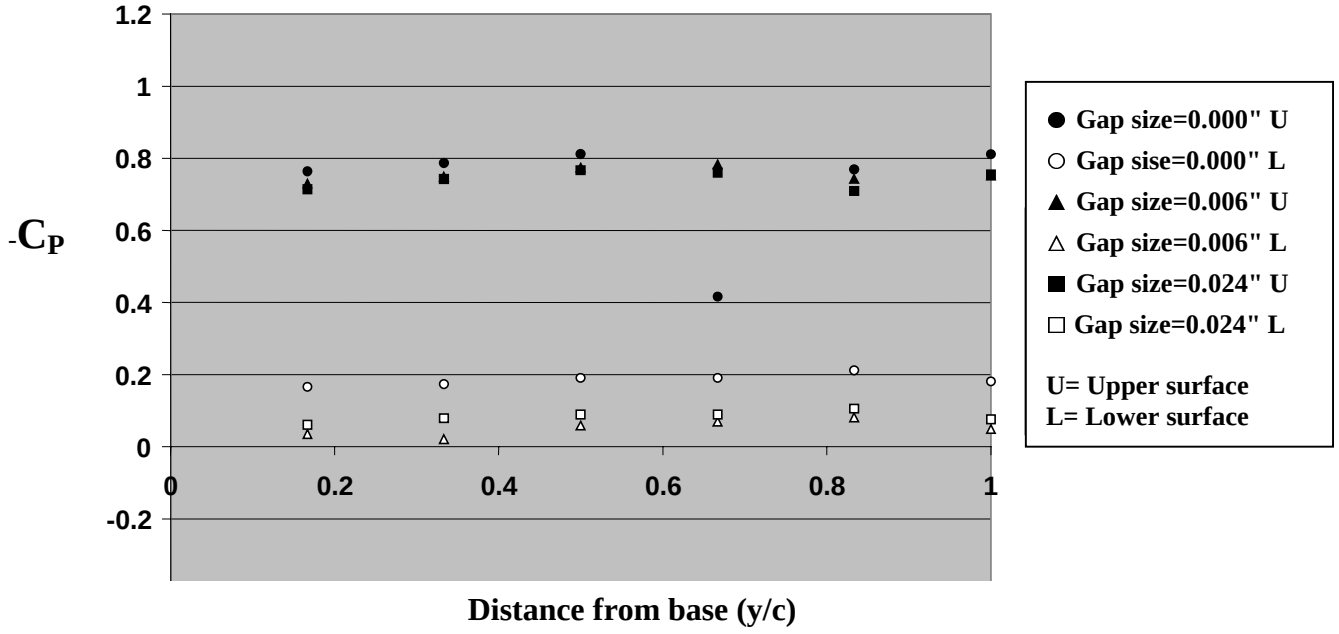

Fig 3.29 Span wise pressure distribution (NACA 2412) at $\alpha=5^0$, Re=100,000

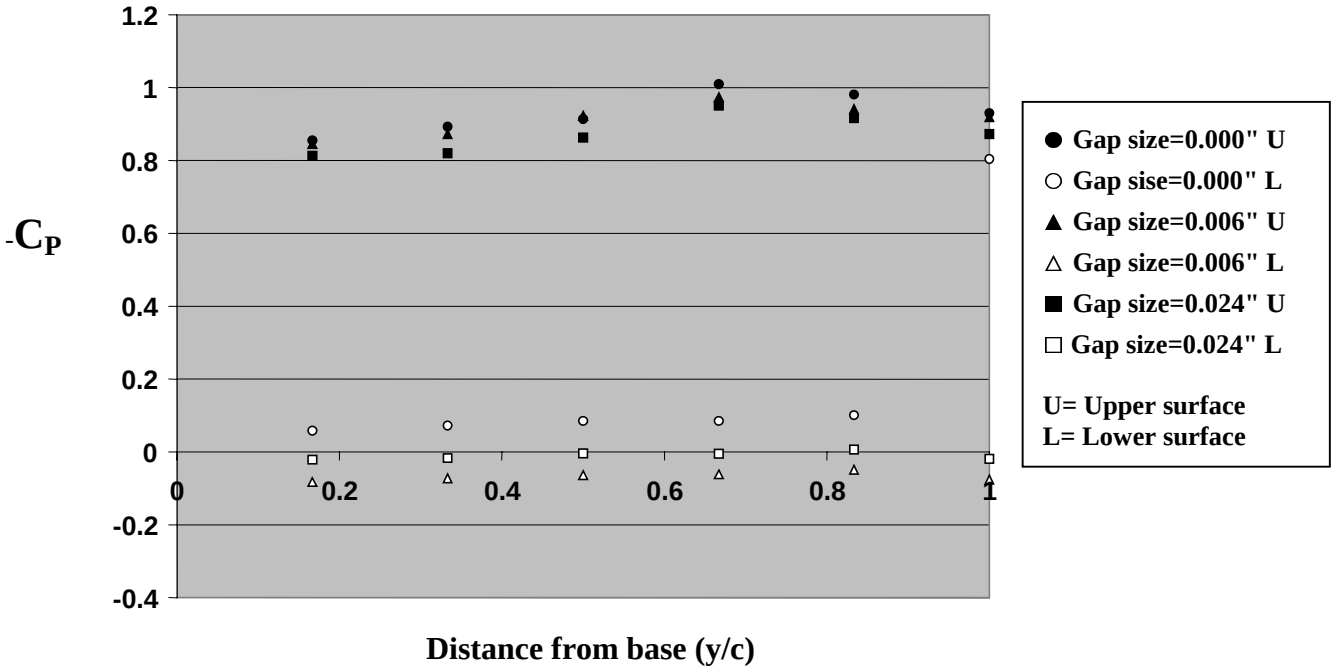

Fig 3.30 Span wise pressure distribution (NACA 2412) at $\alpha=10^0$, Re=100,000

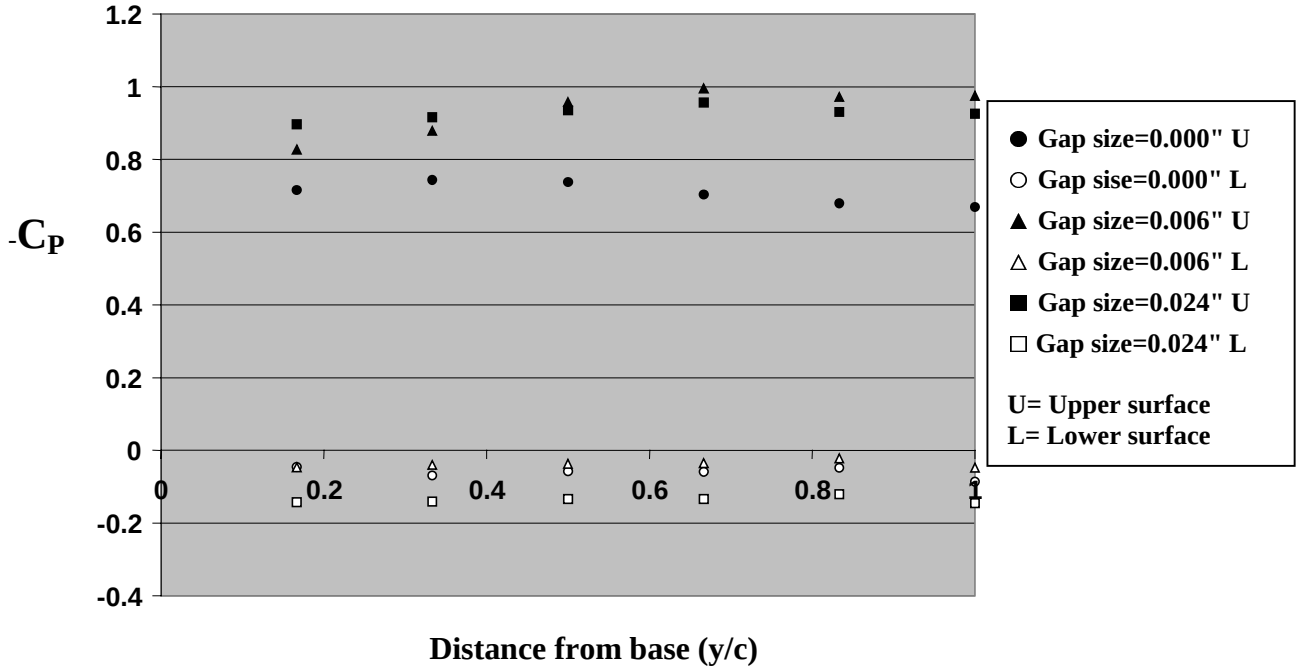

Fig 3.31 Span wise pressure distribution (NACA 2412) at $\alpha=15^0$, Re=100,000

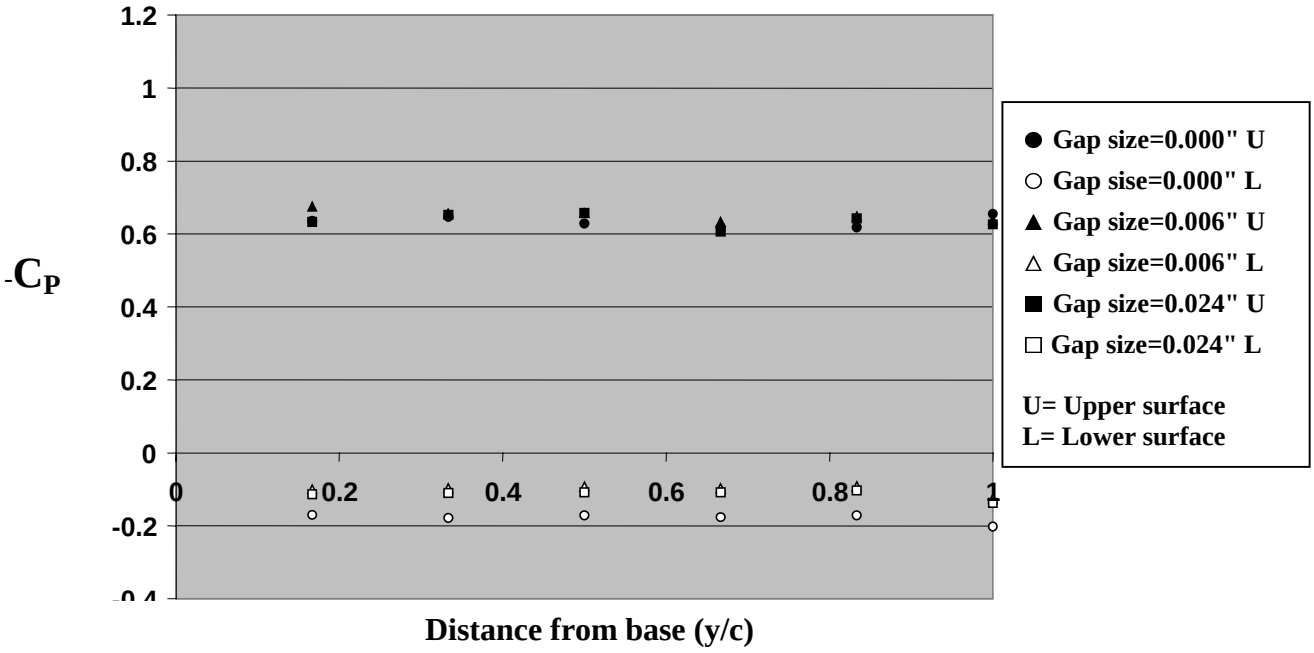

Fig 3.32 Span wise pressure distribution (NACA 2412) at $\alpha=20^0$, Re=100,000

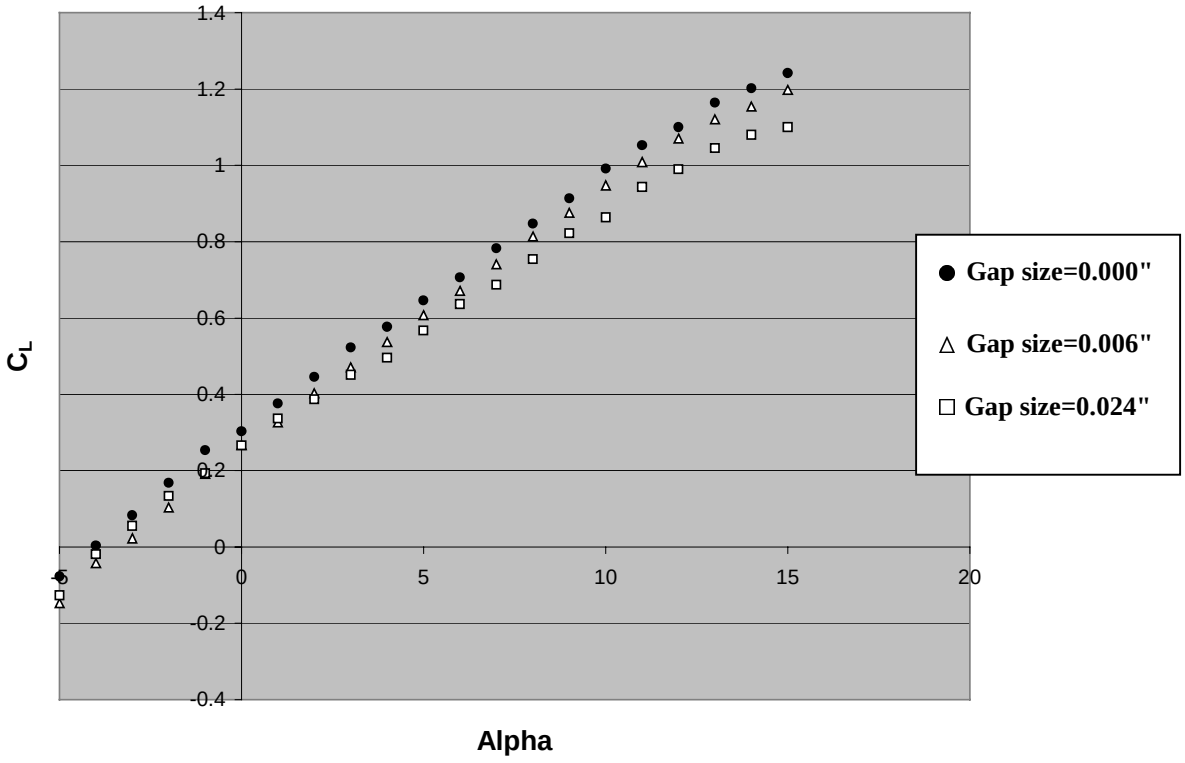

Fig 3.33 C_L vs. α for airfoil NACA 4412 at Reynolds no =100,000

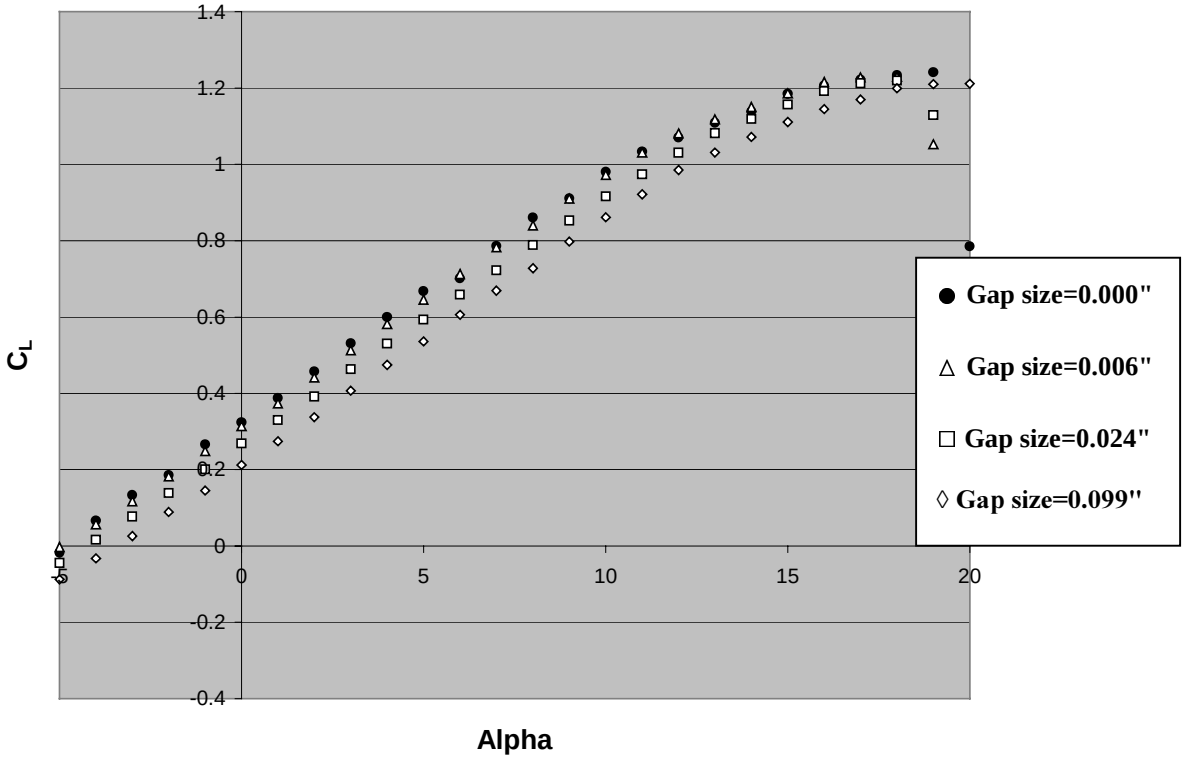

Fig 3.34 C_L vs. α for airfoil NACA 4412 at Reynolds no=200,000

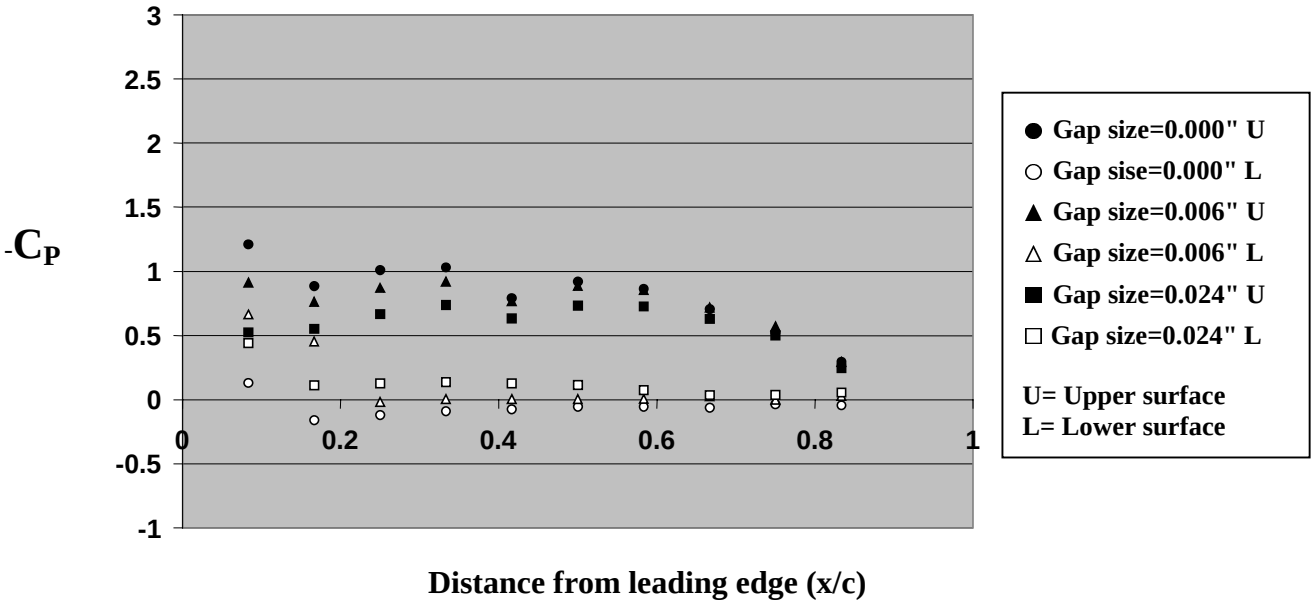

Fig 3. 35 Chord wise pressure distribution (NACA 4412) at $\alpha=0^0$, Re=200,000

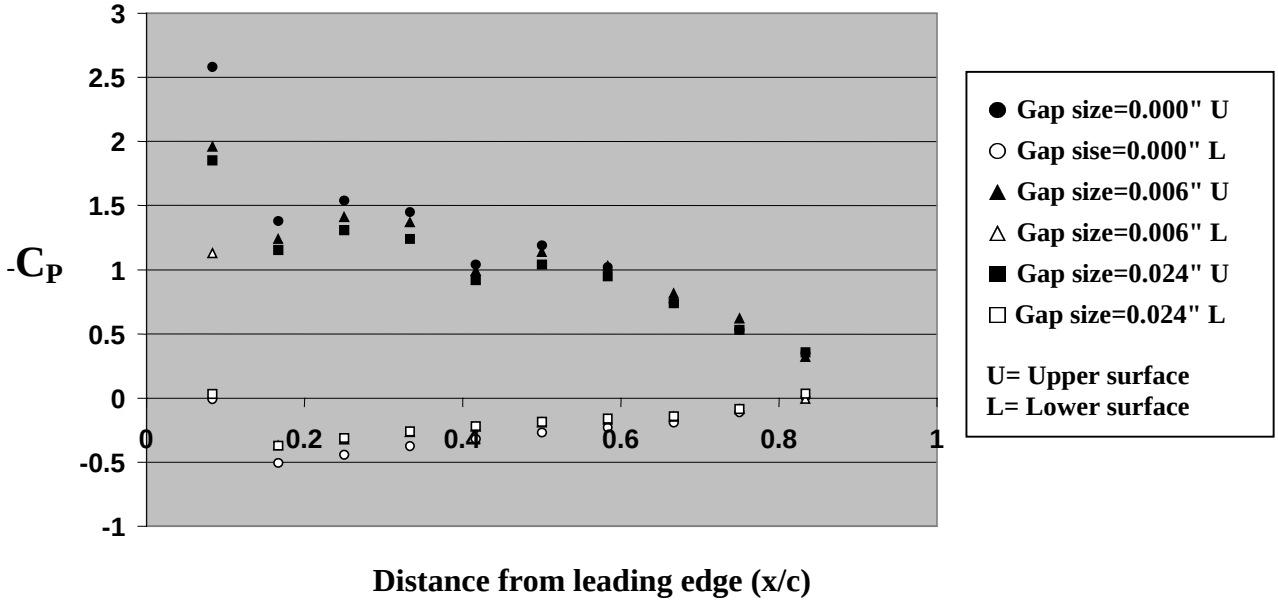

Fig 3. 36 Chord wise pressure distribution (NACA 4412) at $\alpha=5^0$, Re=200,000

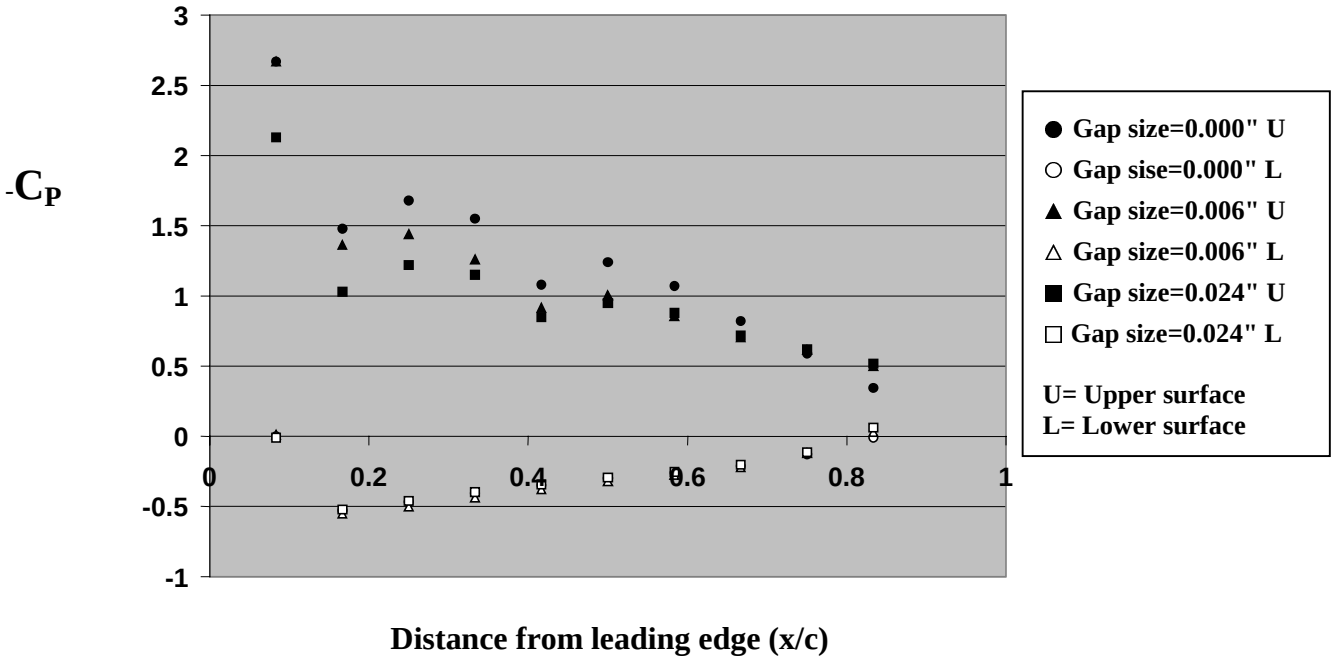

Fig 3. 37 Chord wise pressure distribution (NACA 4412) at $\alpha=10^0$, Re=200,000

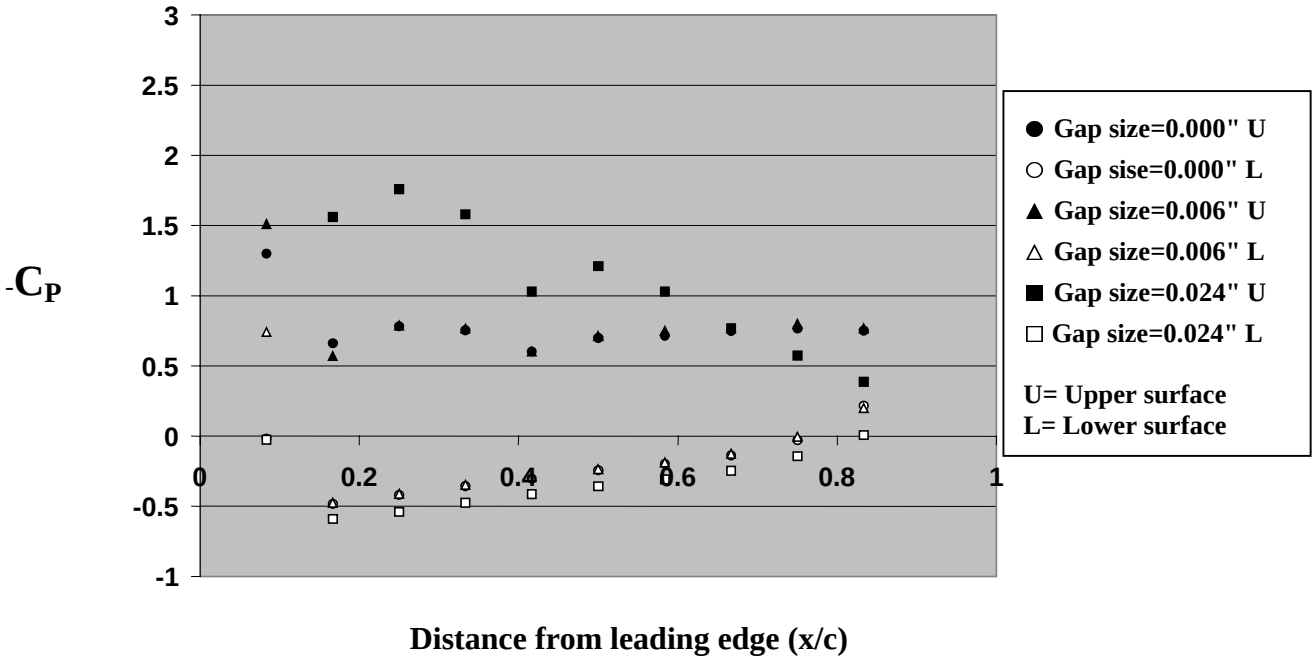

Fig 3. 38 Chord wise pressure distribution (NACA 4412) at $\alpha=15^0$, Re=200,000

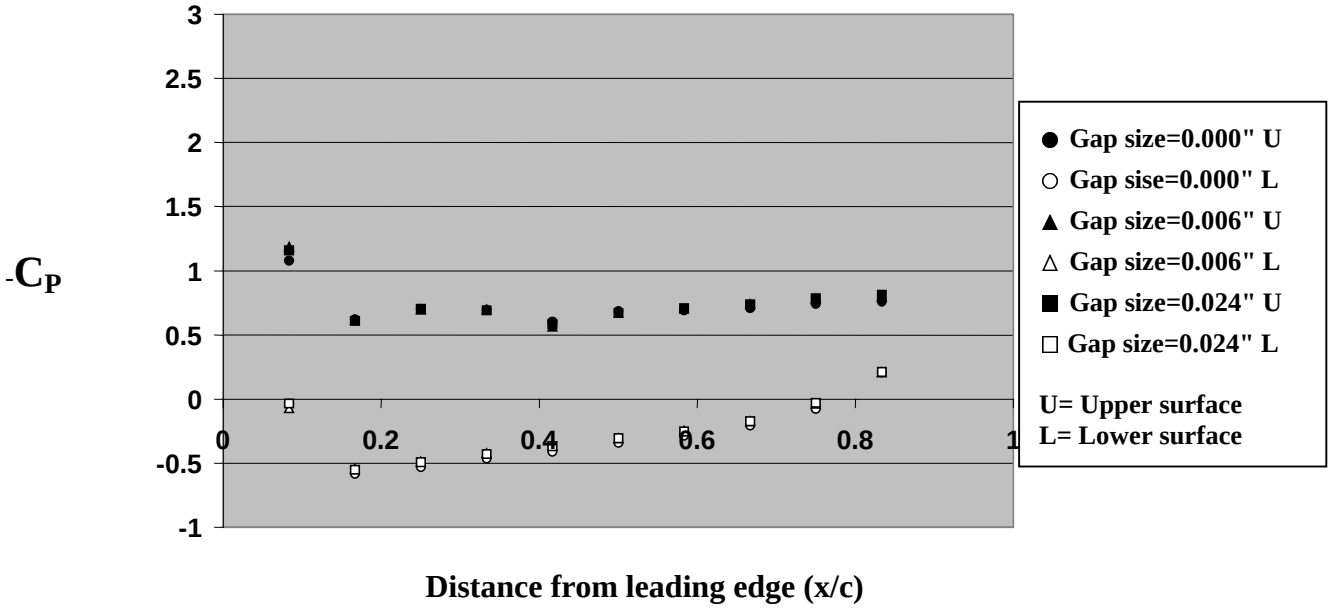

Fig 3. 39 Chord wise pressure distribution (NACA 4412) at $\alpha=20^0$, Re=200,000

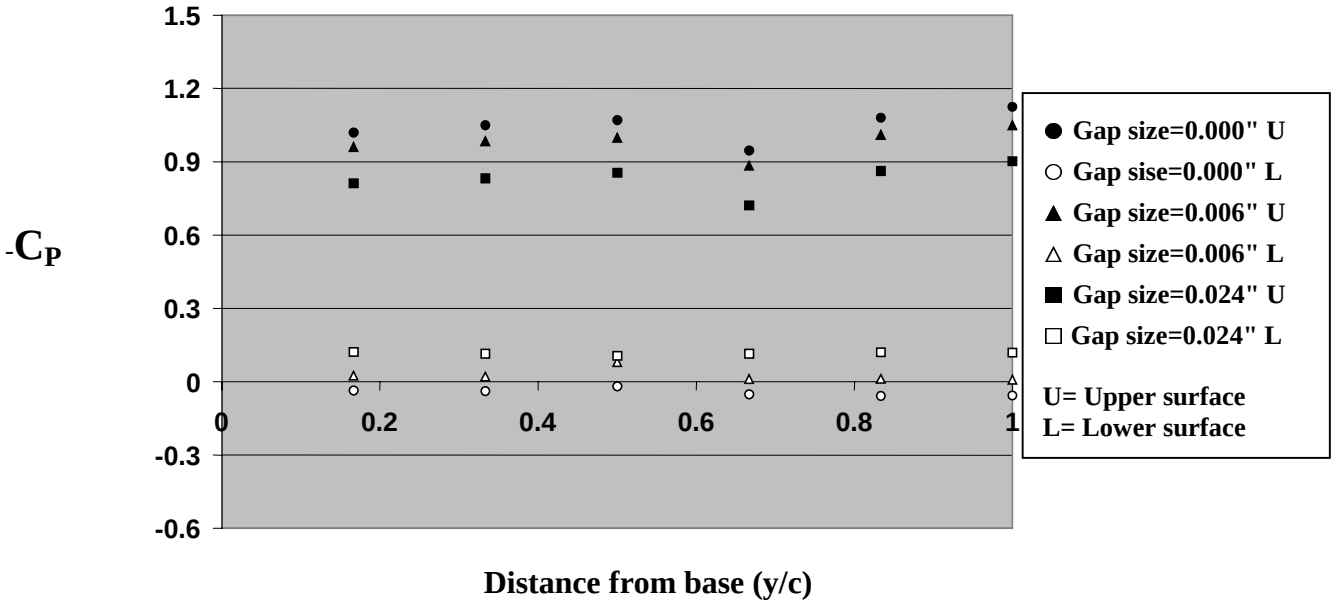

Fig 3. 40 Span wise pressure distribution (NACA 4412) at $\alpha=0^0$, Re=200,000

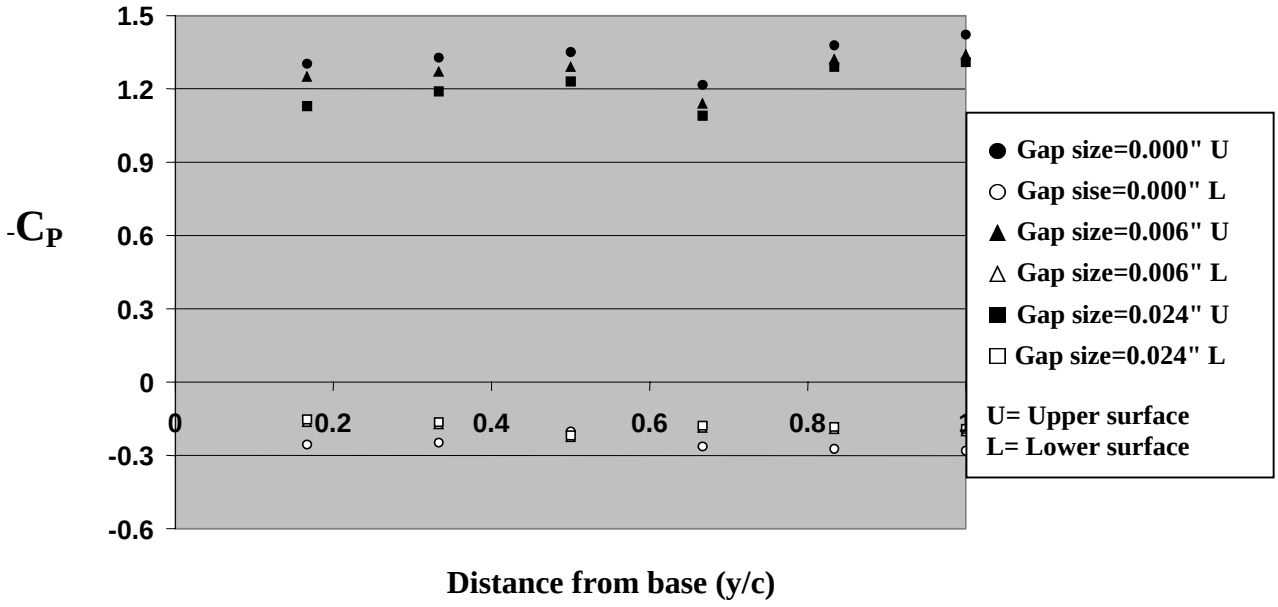

Fig 3. 41 Span wise pressure distribution (NACA 4412) at $\alpha=5^0$, Re=200,000

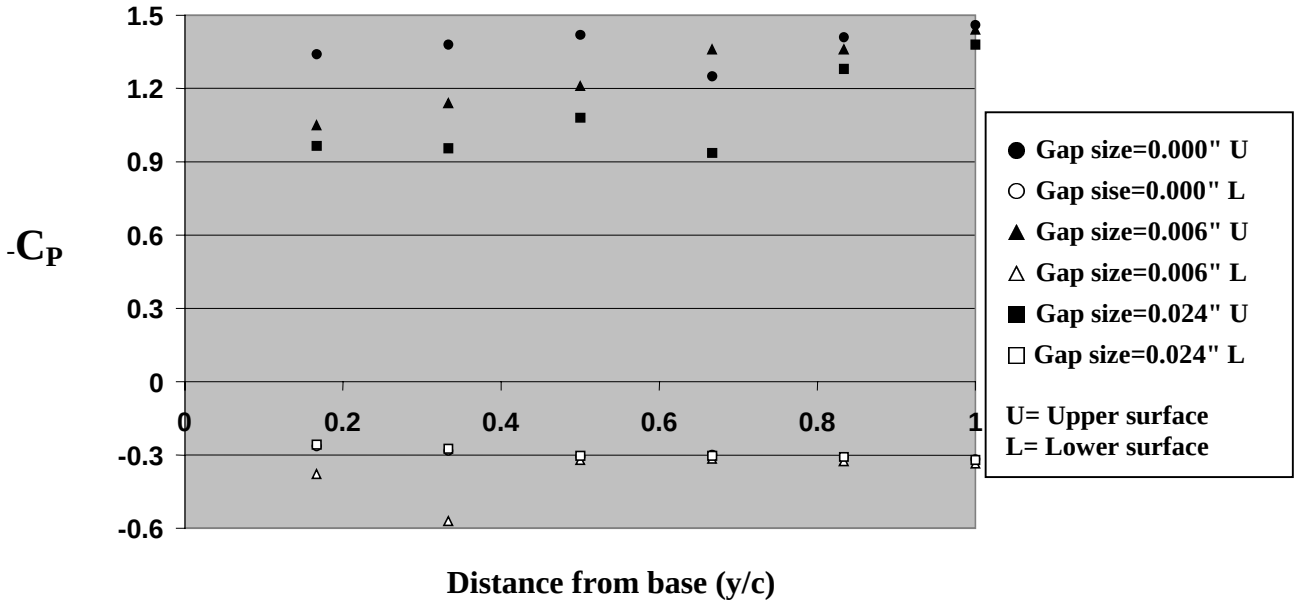

Fig 3. 42 Span wise pressure distribution (NACA 4412) at $\alpha=10^0$, Re=200,000

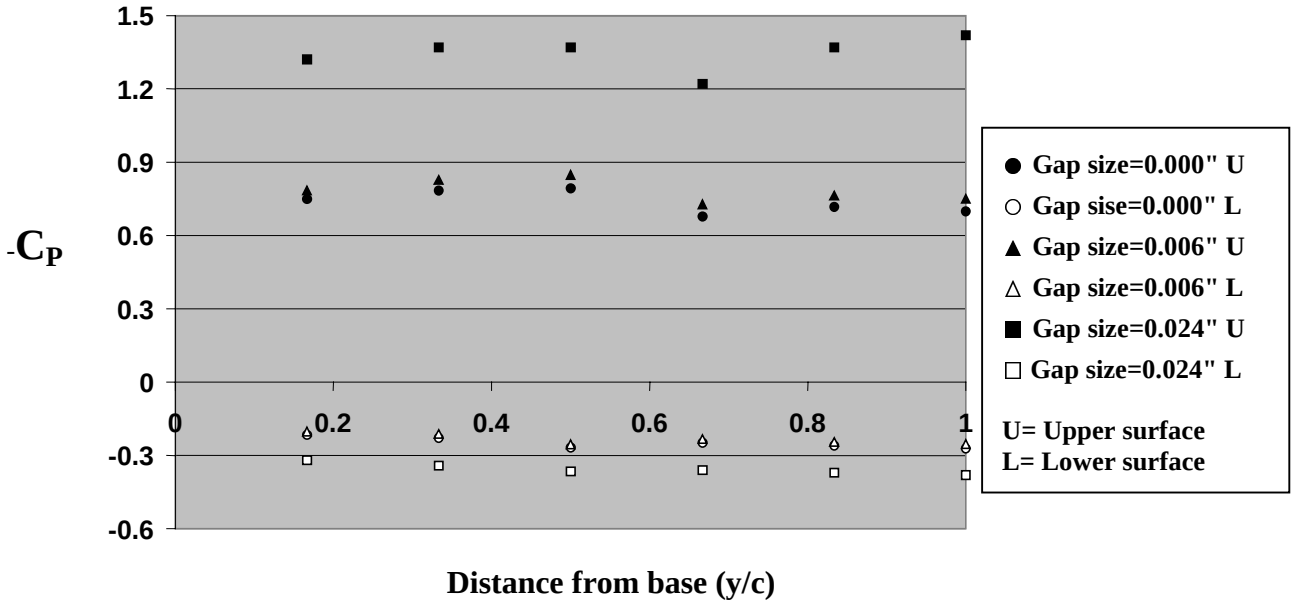

Fig 3. 43 Span wise pressure distribution (NACA 4412) at $\alpha=15^0$, Re=200,000

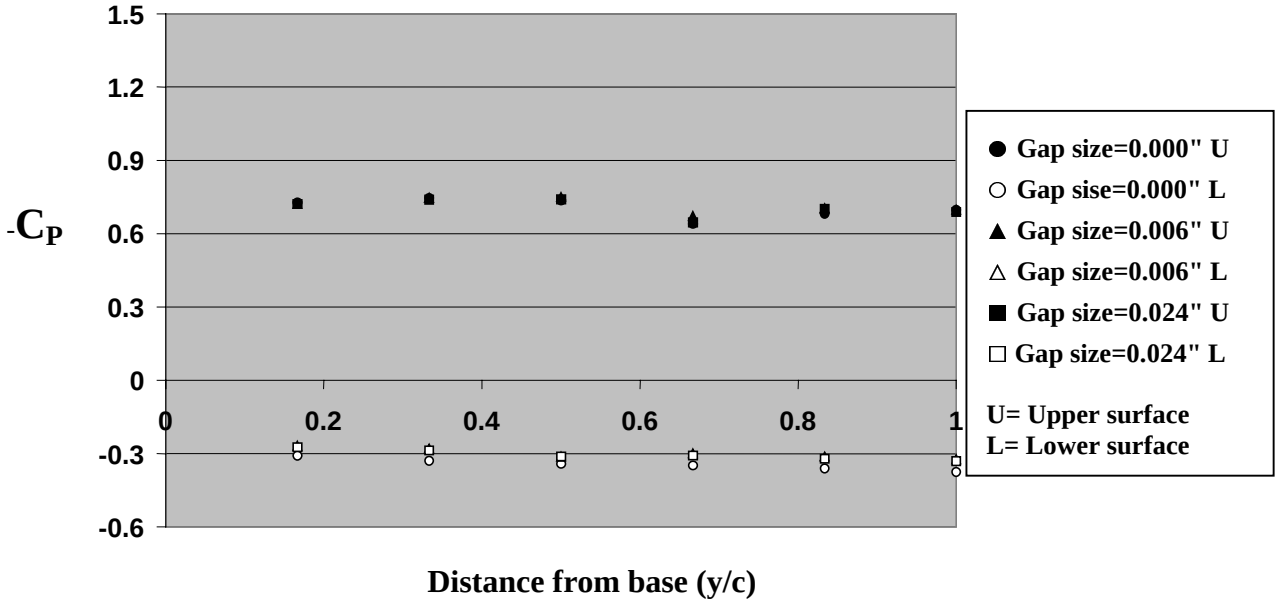

Fig 3. 44 Span wise pressure distribution (NACA 4412) at $\alpha=20^0$, Re=200,000

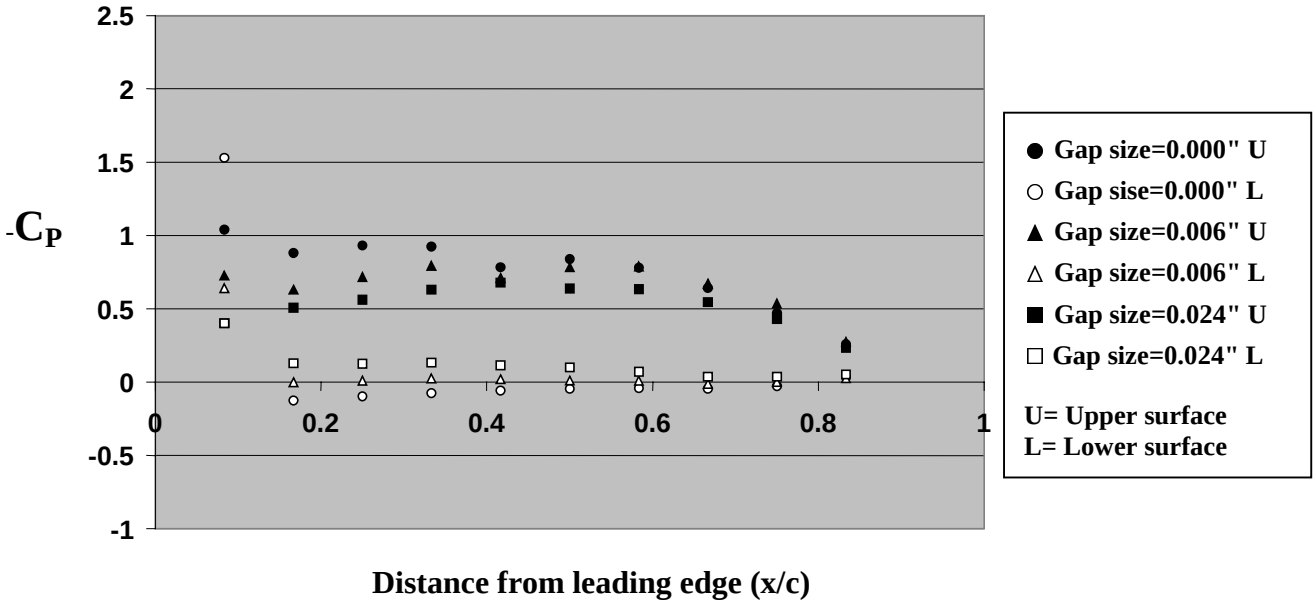

Fig 3. 45 Chord wise pressure distribution (NACA 4412) at $\alpha=0^0$, Re=100,000

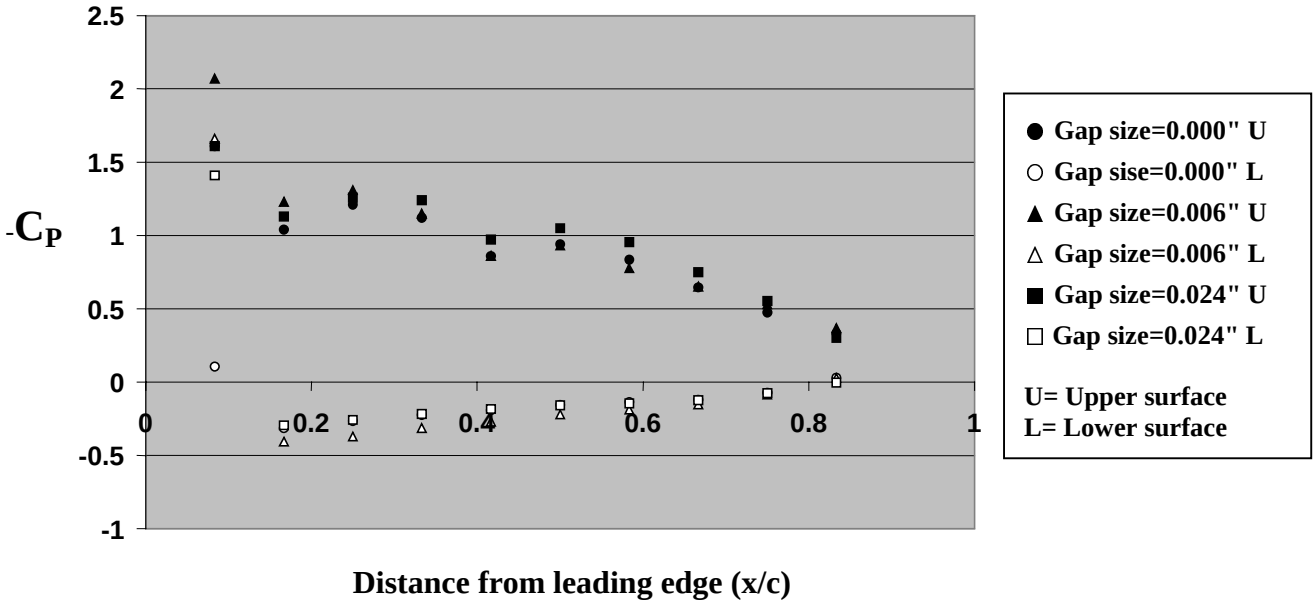

Fig 3. 46 Chord wise pressure distribution (NACA 4412) at $\alpha=5^0$, Re=100,000

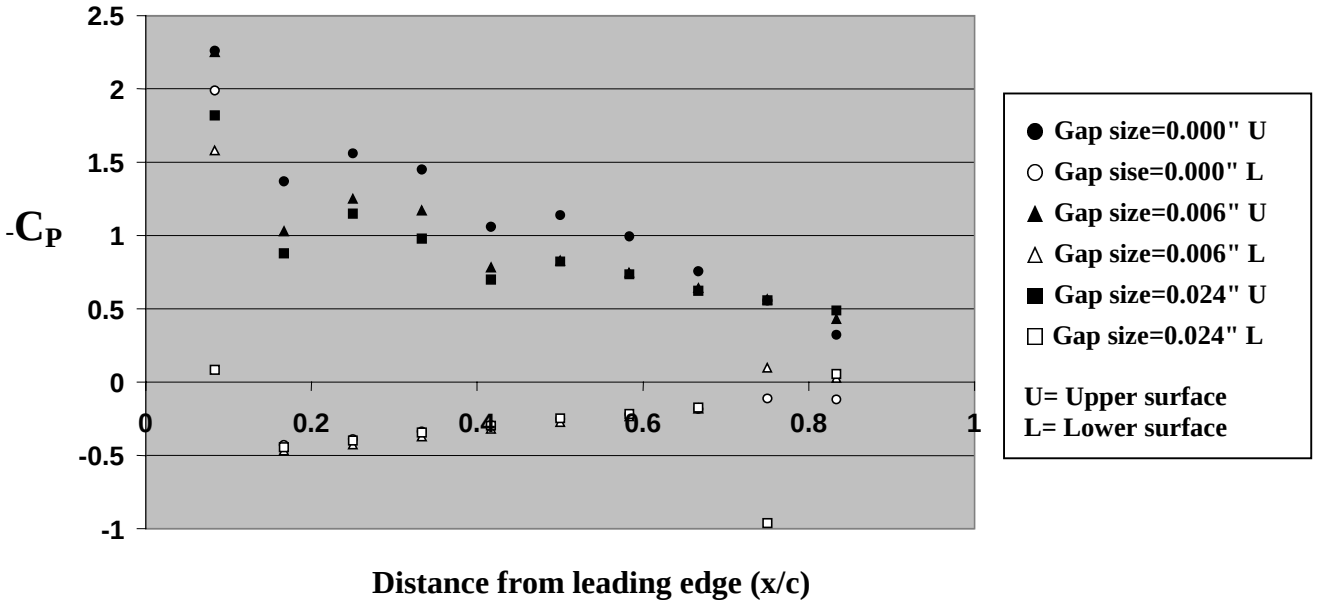

Fig 3. 47 Chord wise pressure distribution (NACA 4412) at $\alpha=10^0$, Re=100,000

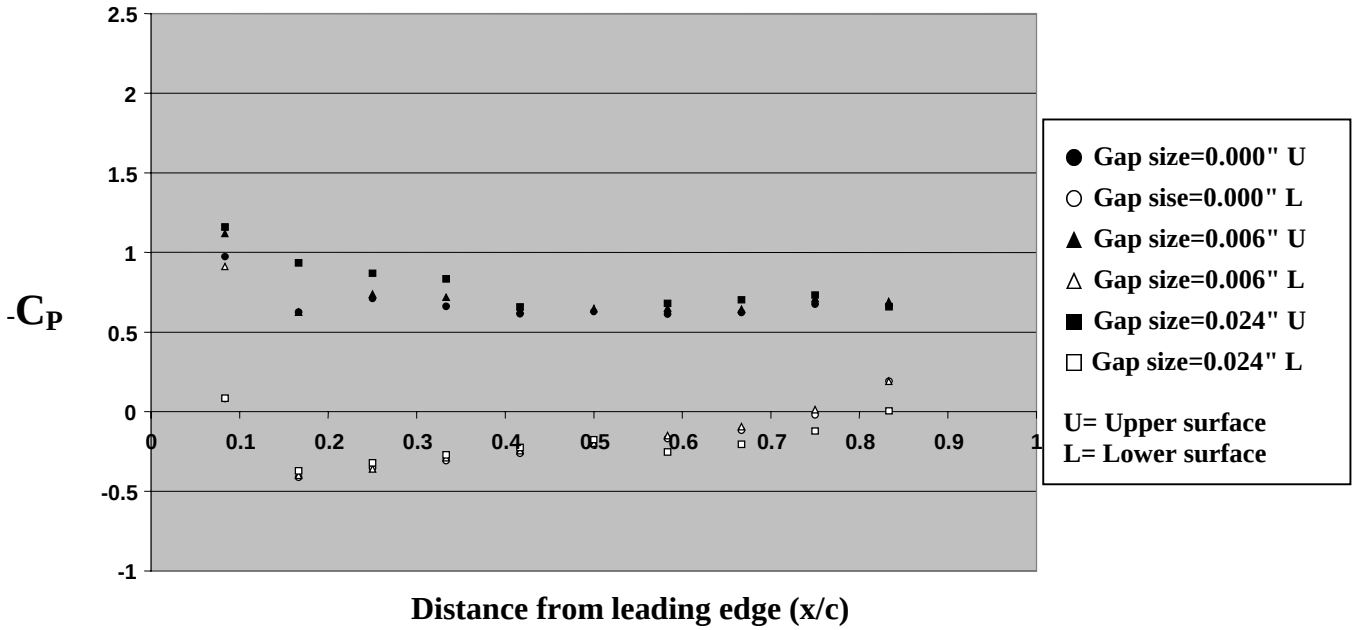

Fig 3. 48 Chord wise pressure distribution (NACA 4412) at $\alpha=15^0$, Re=100,000

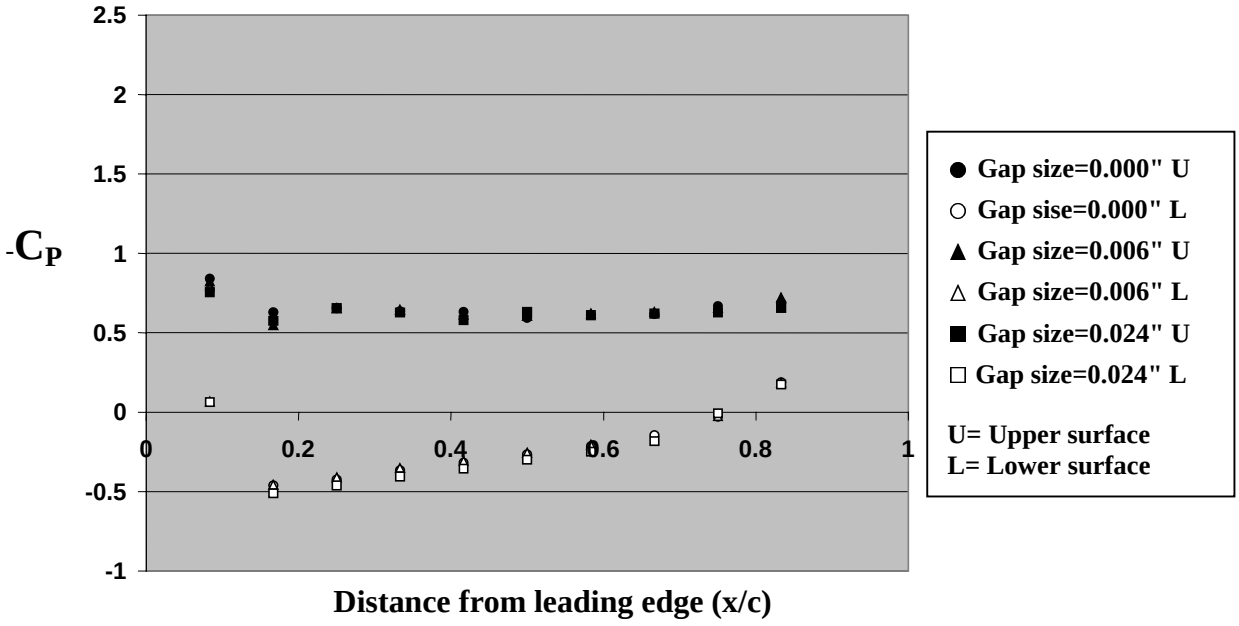

Fig 3. 49 Chord wise pressure distribution (NACA 4412) at $\alpha=20^0$, Re=100,000

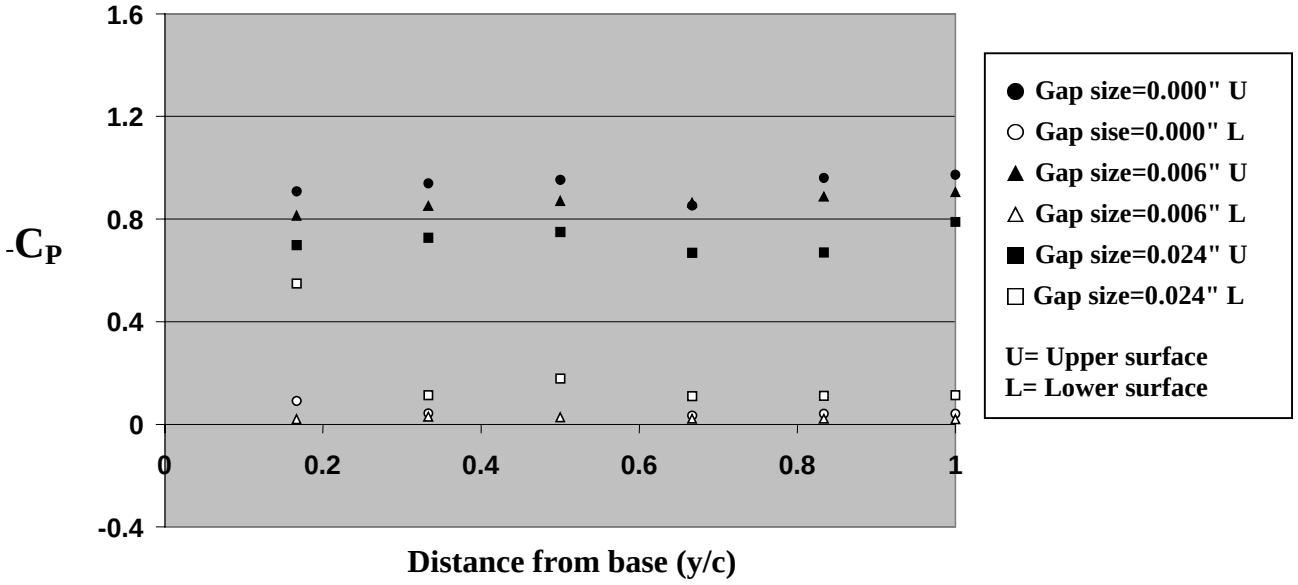

Fig 3. 50 Span wise pressure distribution (NACA 4412) at $\alpha=0^0$, Re=100,000

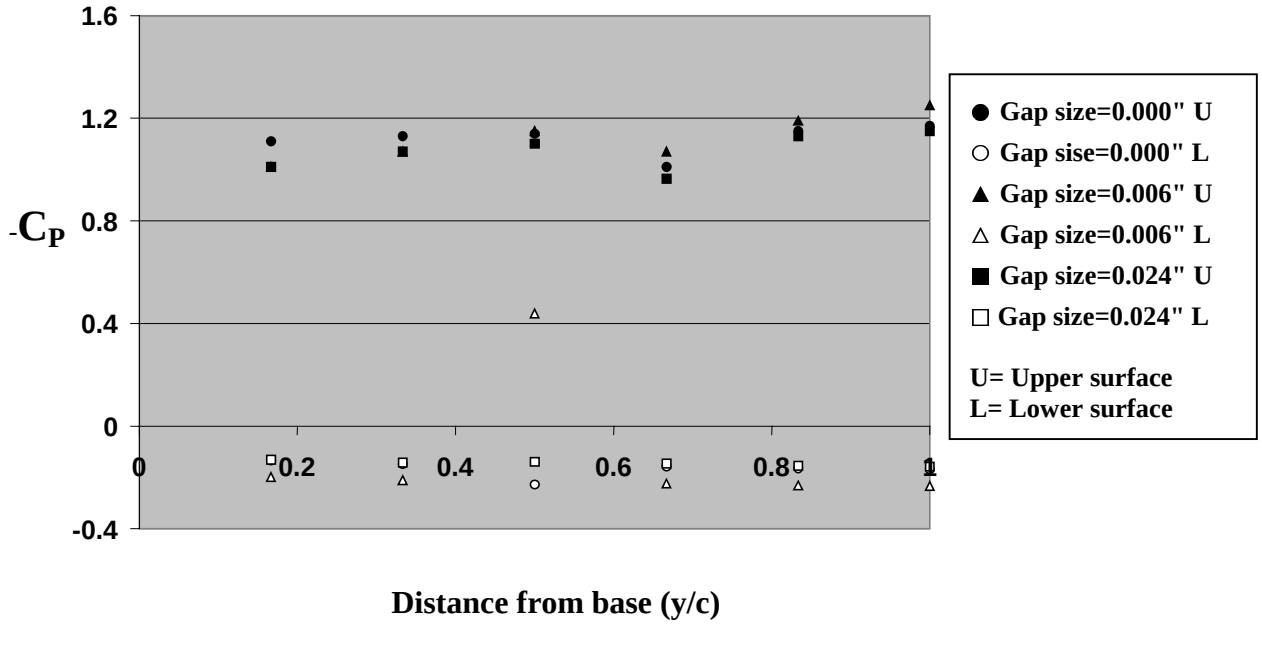

Fig 3. 51 Span wise pressure distribution (NACA 4412) at $\alpha=5^0$, Re=100,000

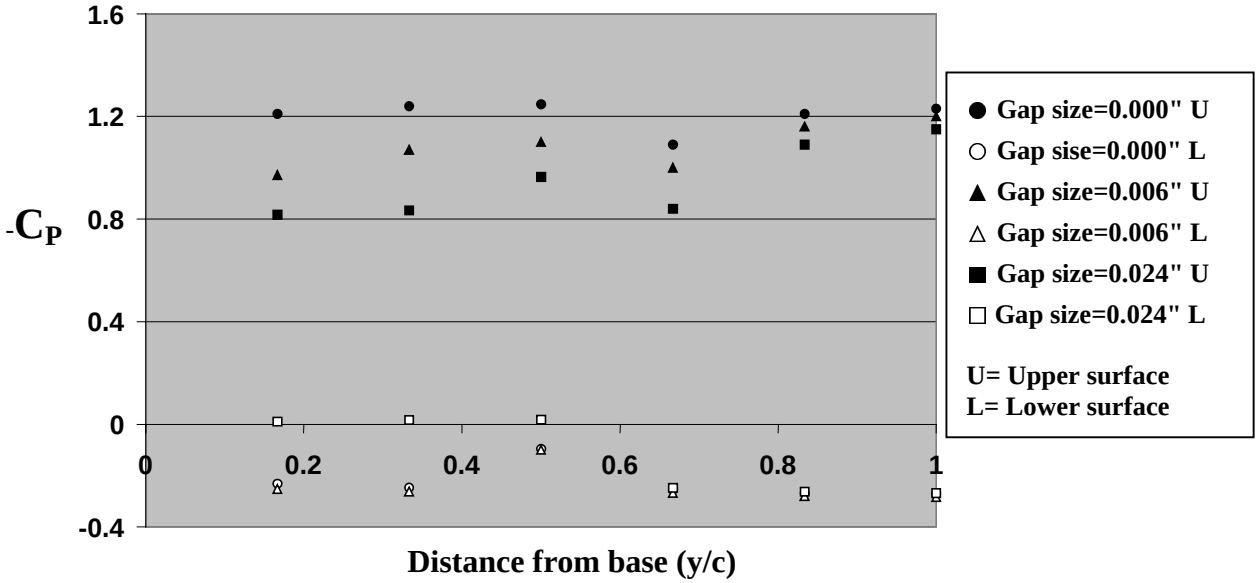

Fig 3. 52 Span wise pressure distribution (NACA 4412) at $\alpha=10^0$, Re=100,000

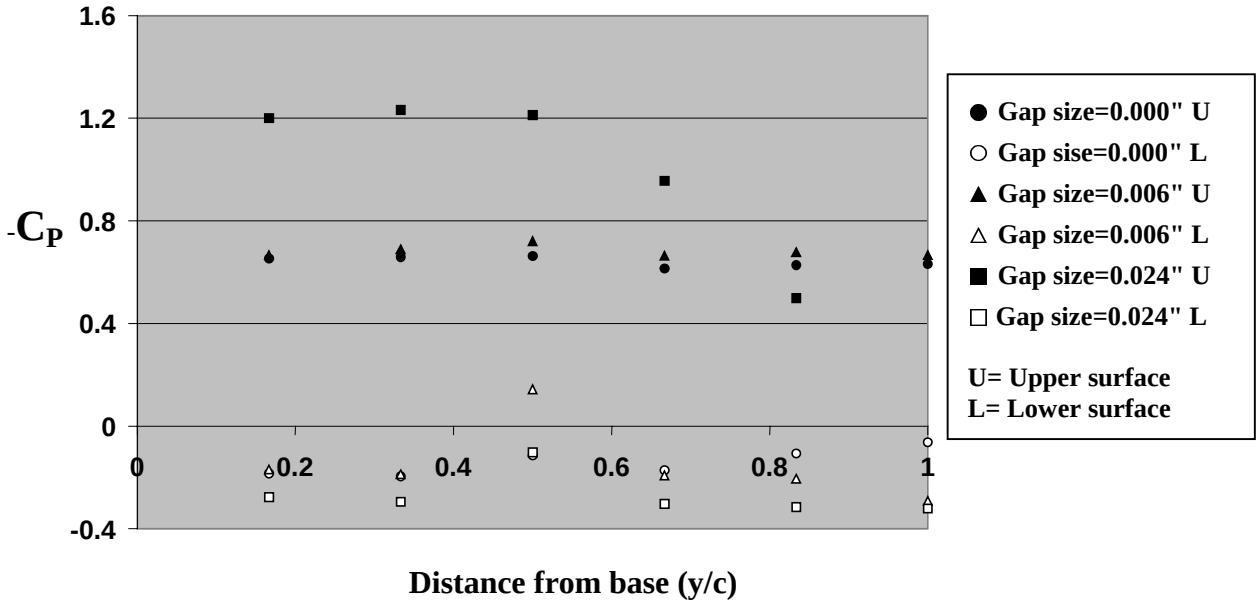

Fig 3. 53 Span wise pressure distribution (NACA 4412) at $\alpha=15^0$, Re=100,000

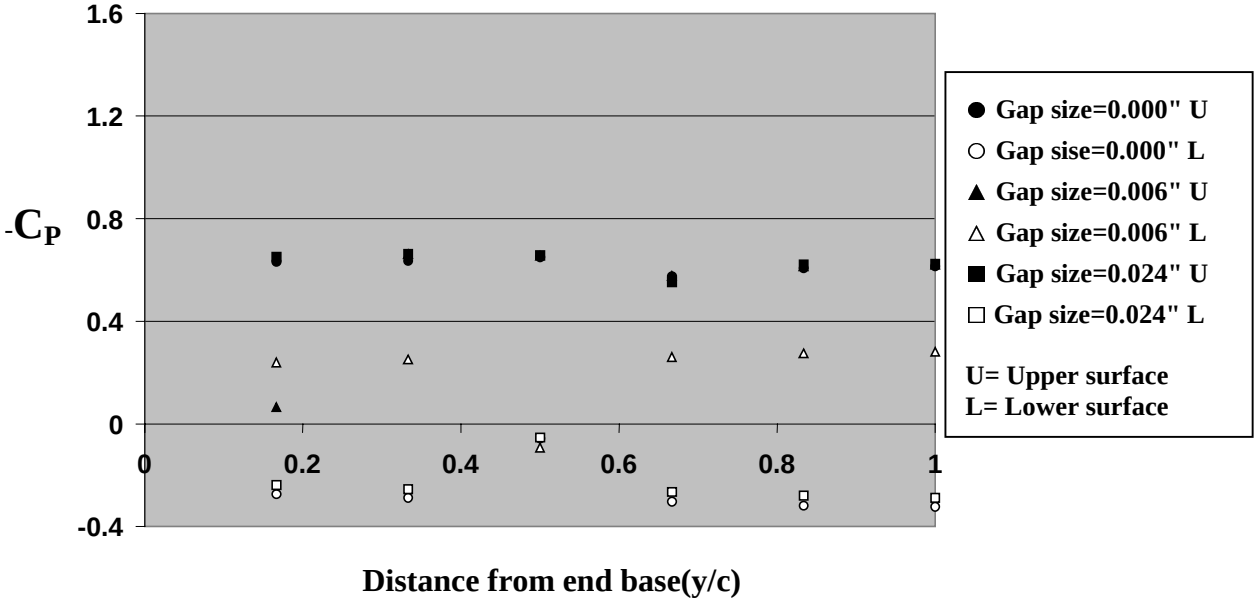

Fig 3. 54 Span wise pressure distribution (NACA 4412) at $\alpha=20^0$, Re=100,000

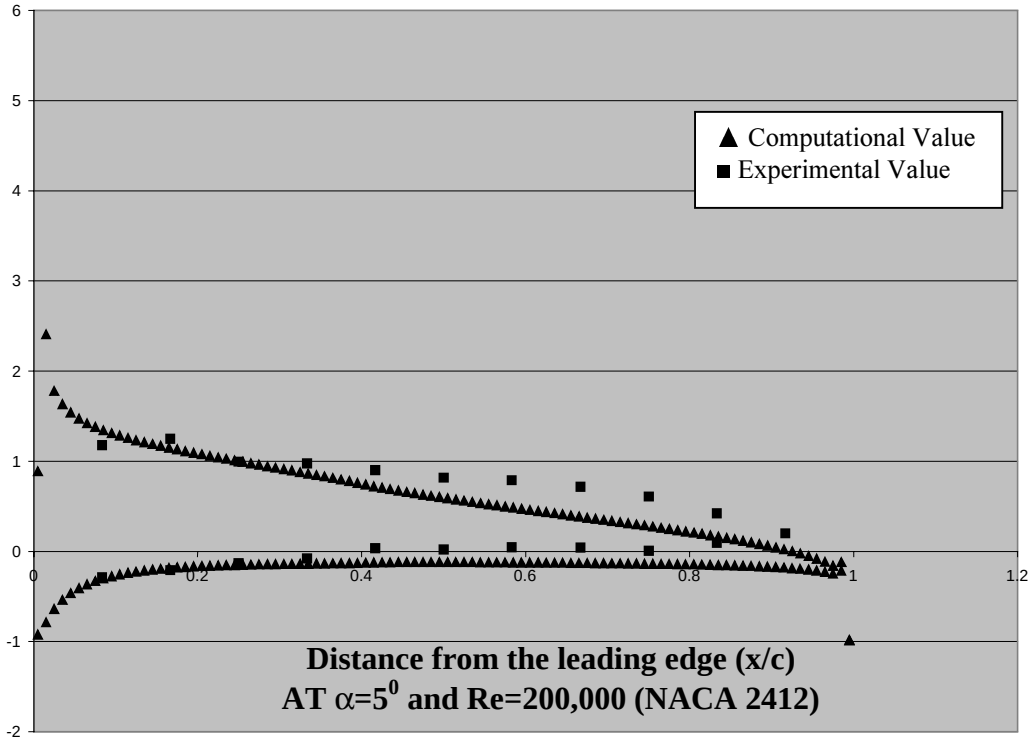

Figure 3.55 Comparison of experimental and calculated pressure distribution

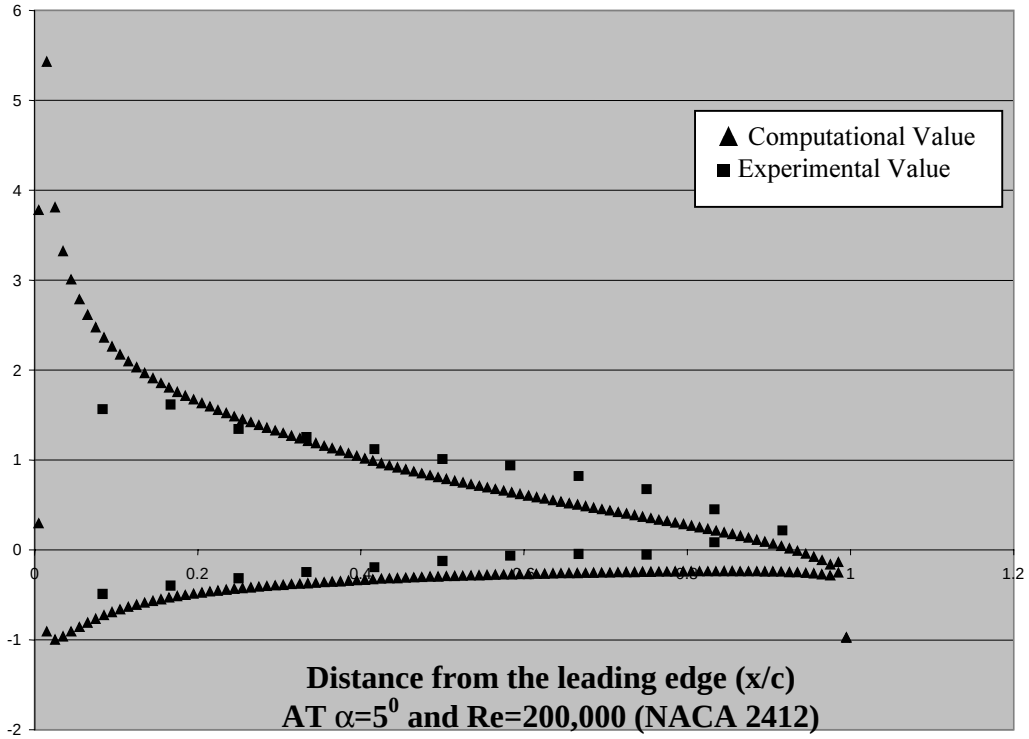

Figure 3.56 Comparison of experimental and calculated pressure distribution

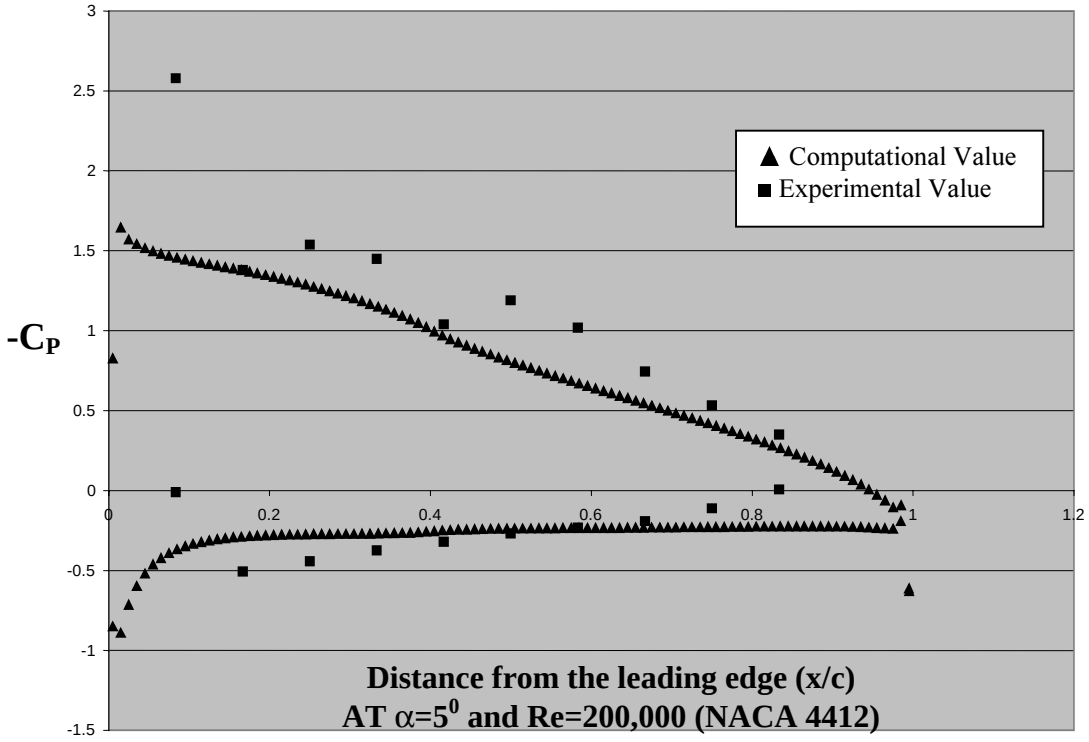

Figure 3.57 Comparison of experimental and calculated pressure distribution

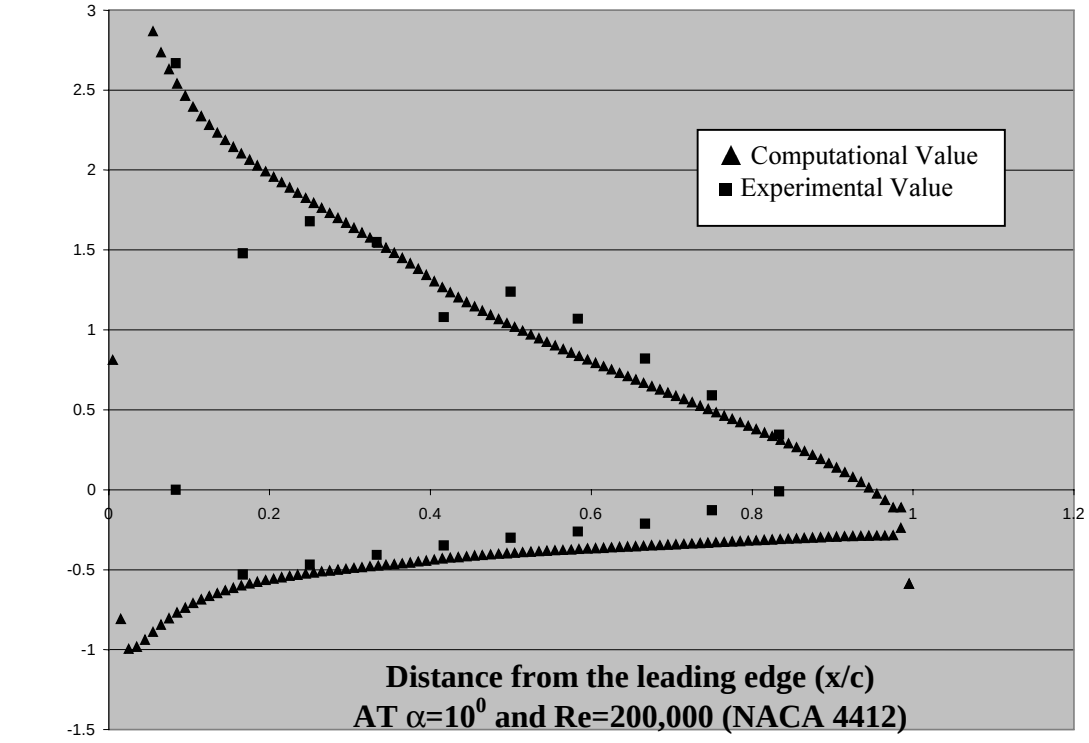

Figure 3.58 Comparison of experimental and calculated pressure distribution

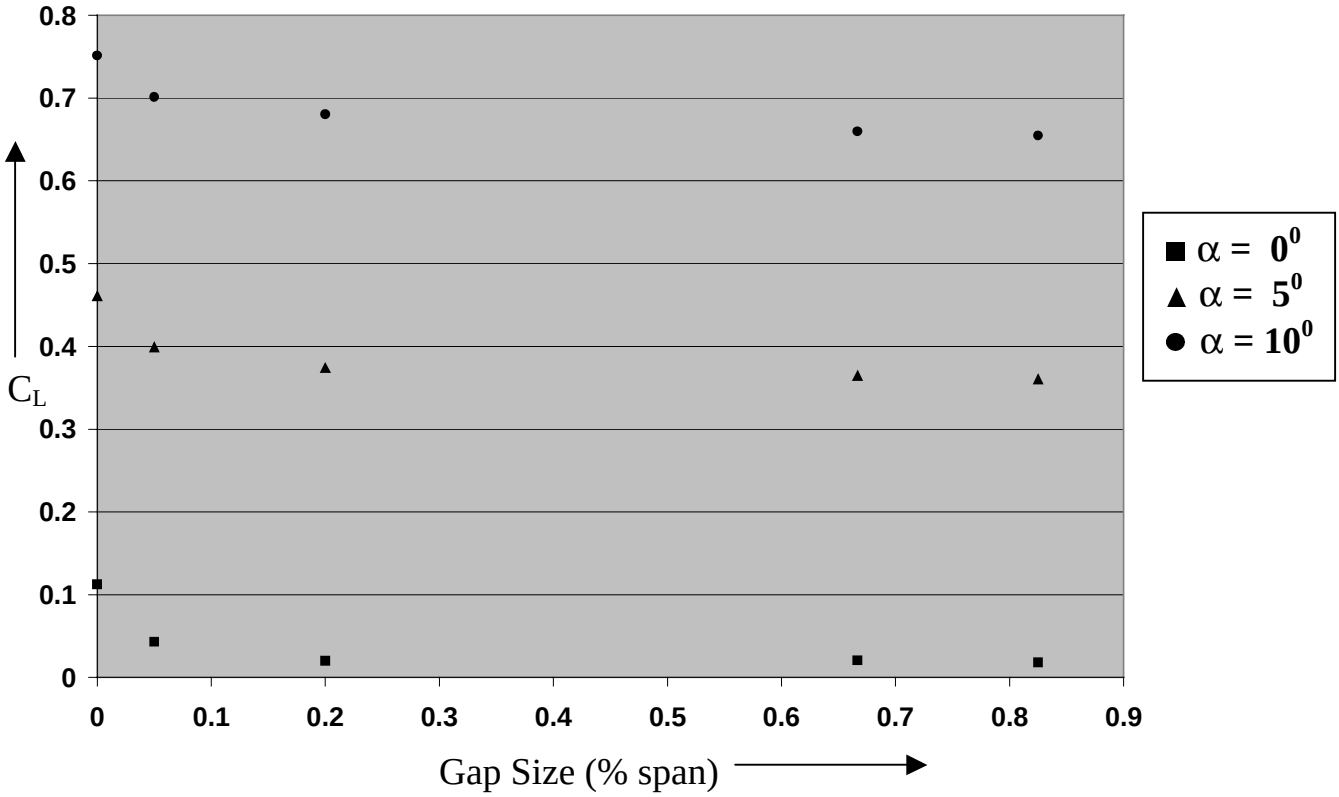

Figure 3.59 Plot for Gap Size vs. C_L at different angle of attack
For Airfoil NACA 1412 at Re = 200,000

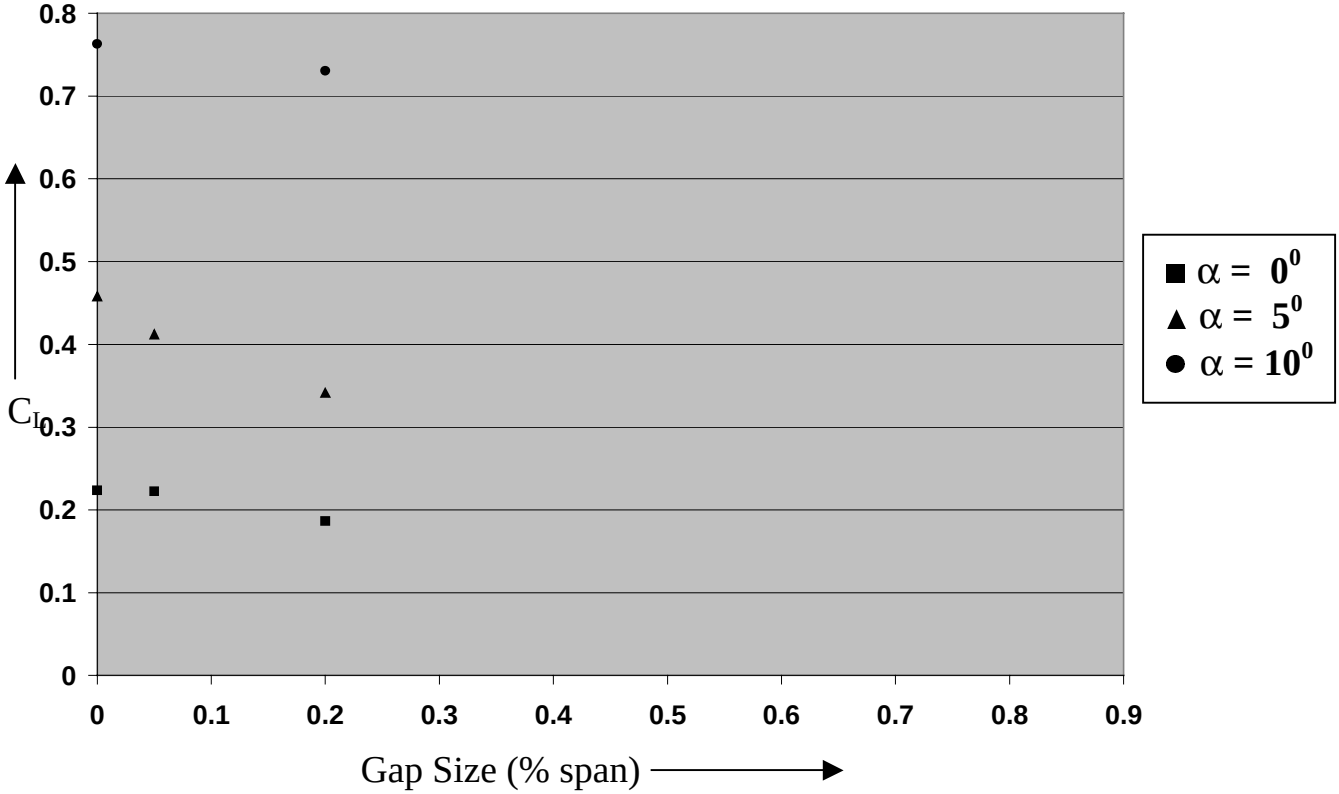

Figure 3.60 Plot for Gap Size vs. C_L (estimated from C_P) at different angle of attack For Airfoil NACA 1412 at Re = 200,000

Vita

Nilanjan Saha was born on December 30th, 1972 in Calcutta, India. Soon after his birth his parents moved to small town named Darjeeling, at the foothills of the Himalayas. He spent his early childhood there and by the time he was almost six his parents moved back to the plains, a town called Chinsurah, by the river Ganges. There he completed his schooling, at Hooghly Collegiate School and joined Indian Institute of Technology, Kharagpur, one of the top five engineering institutes in India, for his Bachelor's degree in Aerospace Engineering in the year 1992. After his graduation in 1996 he joined Hindusthan Aeronautics Limited, the largest aircraft company in India. Next year he decided to pursue his graduate studies in the field of experimental aerodynamics and joined Department of Aerospace and Ocean Engineering, here at Virginia Tech. He intends to continue with his Ph.D. after the completion of his Masters degree.